2008-02-08

Characterizing the Three-Dimensional Behavior of Bistable Micromechanisms

Brian B. Cherry
Brigham Young University - Provo

CHARACTERIZING THE THREE-DIMENSIONAL BEHAVIOR OF BISTABLE MICROMECHANISMS

by

Brian B. Cherry

A thesis submitted to the faculty of

Brigham Young University

in partial fulfillment of the requirements for the degree of

Master of Science

Department of Mechanical Engineering

Brigham Young University

April 2008

BRIGHAM YOUNG UNIVERSITY

GRADUATE COMMITTEE APPROVAL

of a thesis submitted by

Brian B. Cherry

This thesis has been read by each member of the following graduate committee and by majority vote has been found to be satisfactory.

Date	Dr. Larry L. Howell, Chair
Date	Dr. Brian D. Jensen
Date	Dr. Timothy W. McLain

BRIGHAM YOUNG UNIVERSITY

As chair of the candidate's graduate committee, I have read the thesis of Brian B. Cherry in its final form and have found that (1) its format, citations, and bibliographical style are consistent and acceptable and fulfill university and department style requirements; (2) its illustrative materials including figures, tables, and charts are in place; and (3) the final manuscript is satisfactory to the graduate committee and is ready for submission to the university library.

Date

Dr. Larry L. Howell
Chair, Graduate Committee

Accepted for the Department

Matthew R. Jones
Graduate Coordinator

Accepted for the College

Alan R. Parkinson
Dean, Ira A. Fulton College of
Engineering and Technology

ABSTRACT

CHARACTERIZING THE THREE-DIMENSIONAL BEHAVIOR

OF BISTABLE MICROMECHANISMS

Brian B. Cherry

Department of Mechanical Engineering

Master of Science

Compliant bistable micromechanisms have been proposed for use in applications such as switches, relays, shutters, and sensing arrays. Unpublished laboratory testing suggests that off-axis forces may affect the bistable nature of fully compliant bistable micromechanisms (FCBMs). The actuation forces required to snap the FCBM from one stable equilibrium position to another can be altered if the off-axis forces are applied to the mechanism during transition between stable positions. Understanding the three-dimensional characteristics of these mechanisms and the effect of eccentric loading conditions would be helpful in design and analysis of FCBMs.

Two 3-D FEA models were developed for analysis and validation purposes. The 3-D solid element model includes great detail regarding the geometry and boundary conditions of the FCBMs. Including fillets, residual stress, and anchors proved to generate more accurate results. The 3-D beam element model is greatly simplified, and primarily used to validate the results produced by the 3-D solid element model. Both models were validated through comparison to experimental data.

A test suite of FEA runs was constructed to better understand the 3-D behavior of FCBMs. A chief discovery provided by the test suite results was the existence of two phe-

nomenon conditions, defined as Phenomenon 1 and Phenomenon 2. Phenomenon 1 tended to occur when smaller off-axis forces were included in the model. When comparing the two phenomenon, larger pitch rotation, smaller out-of-plane motion, larger reaction forces, and a more consistent bistable mechanism was associated with Phenomenon 1. Phenomenon 2 tended to occur when larger applied forces were included in the model. Once this phenomenon was generated, the FCBM tended to remain in this condition. Reduced reaction forces, larger out-of-plane motion, and a tendency of non-bistability were characteristics of this phenomenon.

The FCBMs could experience much larger in-plane applied forces before transitioning to Phenomenon 2. In contrast, relatively small out-of-plane forces caused the same transition. The FCBMs proved to be well behaved when being pulled into their alternate stable position rather than being pushed. A pushing motion caused the shuttle to roll, pitch and yaw in an inconsistent manner.

ACKNOWLEDGMENTS

I would like to thank Dr. Larry Howell for his consistent guidance and assistance throughout my graduate career. His experience and encouragement helped tremendously in every step of the research and writing process. I would also like to thank my committee members, Dr. Brian Jensen and Dr. Timothy McLain for providing additional guidance and insight to my research in our weekly meetings. Additionally I would like to thank fellow graduate students Quentin Aten and Rob Messenger for their assistance with developing the ANSYS models. To my friends and colleagues in the Compliant Mechanisms Research (CMR) lab, thank you for your advice and help. Additionally, I would like to thank the Fulton Super Computing center at BYU for allowing me to use their facilities.

I would also like to acknowledge my gratitude toward Steven Heffelfinger and Mike Valley at Sandia National Laboratories for making this research possible through funding. Additionally, Jorretta Joseph at the National Physical Science Consortium (NPSC) has been a great help each semester to finalize all the necessary paperwork. The National Science Foundation (NSF) also provided funding to conduct this research.

I would like to thank my wife Alia for all the support and guidance she gave me while conducting my research and writing my thesis. Her encouragement and attitude was a great source of drive for me. To my entire family, thank you for your support. Lastly, I would be ungrateful if I did not thank my Father in Heaven for His unrelenting support through this process.

Table of Contents

List of Tables

List of Figures

Chapter 1

Introduction

1.1 Problem Statement

MEMS (Microelectromechanical Systems) incorporate mechanical structures with microelectronics ranging in size from the micro-scale to millimeters. They are widely used in electronics, process controls, and sensors. Compliant MEMS obtain some of their mobility from the deflection of flexible members rather than traditional pin joints and springs. Bistable mechanisms are devices that tend to remain in one of two stable equilibrium positions. Compliant bistable MEMS have potential use in numerous applications including switches [3], relays [4]–[6], shutters [7], crash sensors [8], latchup testing [9], and micropositioning [10].

Fully compliant bistable micromechanisms have also been proposed for an acceleration sensing array [11]. By altering the shuttle mass of a fully compliant bistable mechanism (FCBM) [12], designated acceleration magnitudes would be required to switch the mechanism from one stable position to another. An acceleration sensing array could be produced by constructing an array of these mechanisms with different switching thresholds, thus providing a system that uses the power from the sensed phenomenon to provide and store the information until it is read and reset.

Unpublished laboratory testing suggests that off-axis forces may affect the bistable nature of FCBMs. The magnitude of the force or acceleration required to transition the FCBM from one stable equilibrium position to another can be altered if these eccentric forces are applied during transition between positions. Understanding the 3-D characteristics of these mechanisms and the effect of eccentric loading conditions would be helpful in design and analysis of the FCBMs for applications such as a sensing array.

Two-dimensional finite element analysis (FEA) models for these FCBMs have already been used in device analysis and design [13], but they do not incorporate three-dimensional forces and neglect some important geometric details. Because the 2-D models are much easier to create and have a fast convergence time, it is valuable to understand if they can provide adequate results. It is important to understand the three-dimensional behavior of the devices and the relative importance of including certain geometric features in the models.

Three-dimensional FEA models were developed to better understand the three-dimensional characteristics of FCBMs. One model includes great detail to the geometry and boundary conditions of the FCBMs, and is constructed of three-dimensional tetrahedral elements. The second is a 3-D beam element model, which is a simplified approach. Both models were validated with comparison to experimental data. An analysis of the effect of actuation location, location of applied eccentric forces, magnitude of eccentric forces, and shuttle size will lead to conclusions regarding the three-dimensional behavior of the FCBMs.

1.2 Objectives

The objectives of this research are to:

1. Evaluate various FCBM finite element models to determine their applicability in accurately analyzing FCBMs.
2. Determine the relative importance of modeling certain geometric features of FCBMs.
3. Characterize the three-dimensional behavior of FCBMs.
4. Evaluate the effects of FCBM behavior of actuation location, location of eccentric forces, magnitude of eccentric forces, and variation in shuttle geometry.

1.3 Background

Previous research [11] showed that using the piezoresistive properties of polysilicon to sense the state of bistable mechanisms eliminates the need for electrical contacts. The

change in resistance between the two stable equilibrium positions is easily measured. This measured change in resistance provides enough signal to adequately determine the state of the bistable mechanism. The geometry from one of Anderson's bistable designs was chosen as the nominal FCBM design in the research (Bistable-A).

The phenomenon of MEMS sensitivity to geometry variation has been recently researched. Methods for uncertainty analysis [14], reliability-based design [15]–[17], robust optimization [18], and sensitivity analysis [19] have already been provided by many researchers. In addition, an uncertainty analysis of bistable micromechanisms has been made available [20]. This information could be used to keep FCBM behavior consistent even after incorporating the variability of the manufacturing process. By introducing the three-dimensional characteristics of FCBMs to the research already conducted, future researchers will have an increased ability to design FCBMs for specific applications.

1.3.1 MEMS

Microelectromechanical systems (MEMS) are the integration of mechanical components, electronics, and transducers (sensors and actuators) on a single silicon substrate. MEMS can range from a micrometer to a millimeter in size. The term "MEMS technology" can refer to a single component within a larger system, an entire system of integrated mechanical and electronic components, and fabrication approaches. It also, at times, embodies a unique machining and manufacturing process which will be briefly described later, and a new format of devices and products [21]. At the micro-scale, the traditional effects of momentum, inertia, and mass do not have the dominating effect that they would have at the macro-scale. Stiction, electrostatic forces, friction, and wetting are far more dominant at this level, and introduce very significant challenges for design engineers.

MEMS technology offers benefits that many macro-scale devices cannot offer. Some of these benefits include:

- Low cost of production per unit
- Small mass and volume
- High sensitivity to noise ratio for sensor application

- Capability of manipulating and actuating at the molecular level
- The ability to go undetected by the human eye (border control/tracking)

Some popular devices that utilize MEMS technology include accelerometers, ink jet printers, toys (Nintendo Wii), gyroscopes, projectors, and optical switching in smartdust technology. Many applications of MEMS are currently being researched and utilized, but will not be discussed in detail [22].

1.3.2 Compliant Mechanisms

A mechanism is a device used to transfer or transform motion, force, or energy [23]. While traditional rigid-body mechanisms utilize links, joints, and rigid segments for transformation, compliant mechanisms rely on the deflection of flexible members for at least a portion of its mobility. While compliant mechanisms offer many benefits, the two main advantages are cost reduction (part count reduction, reduced assembly time, and simple manufacturing processes) and increased performance (precision, reliability, reduced wear, reduced weight, and reduced maintenance).

Networked microsensor technology has been noted as a "key technology" for the future [24], and takes part in one of the most important technologies of the 21st century [25]. Compliant mechanisms at the micro-scale offer great benefits when used in sensor applications. Specifically, the small size for easy placement, lack of traditional joints and hinges for reliability and precision, high sensitivity to noise ratio, and ability to be linked to electronics and feedback control systems for networked communication all make compliant MEMS sensors highly efficient.

1.3.3 Compliant Bistable Mechanisms

Bistable mechanisms are unique mechanisms that tend to remain in one of their two stable positions. Compliant bistable MEMS have potential use in numerous applications, including switches [3], relays [4]–[6], shutters [7], crash sensors [8], latchup testing [9], and micro-positioning [10]. These mechanisms have two stable states of equilibrium, and one unstable state of equilibrium. The equilibrium states of a bistable mechanism can

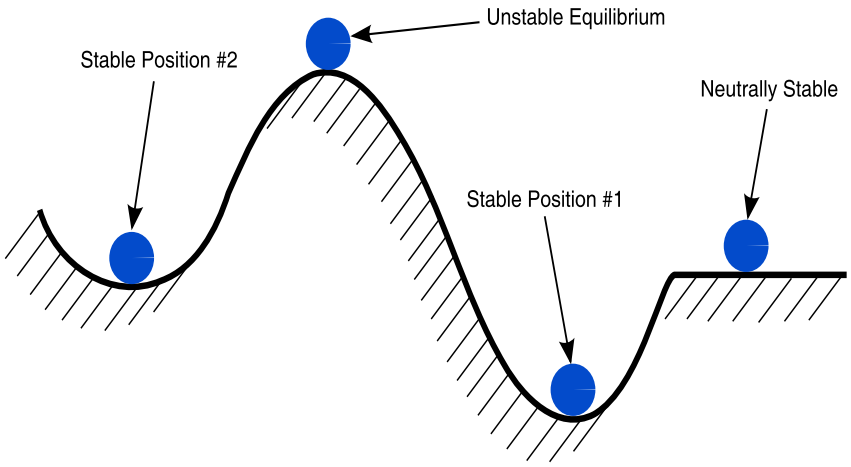

Figure 1.1: Ball on a hill equilibrium analogy.

be further understood through the "ball-on-a-hill" analogy [23], [26]. Figure 1.1 shows the four possible stability scenarios. The first and second stable positions are locations at which the system can be disturbed slightly, and only small oscillations will occur. This is due to the nature of a systems attempt to remain in the lowest energy state possible. When a system is in the unstable equilibrium position, it will be inclined to move toward either the first or second stable position. Thus, when a system is in the unstable equilibrium position, small disturbances will cause large displacements in the system. Finally, if a system is disturbed and remains in that disturbed position (such as the ball that will roll to the left or right, but remain on the plateau), it is in a neutrally stable position.

Compliant bistable mechanisms offer the benefit of storing strain energy in its flexible joints, allowing a system to function without springs or other actuation devices. Springs and onboard actuators will generally raise the chance of failure and decrease precision. Thus, these systems offer a robust method of remaining in a desired state or position without input power or energy.

Some of the greatest challenges of supplying an adequate and feasible power supply for a MEMS device include keeping the power supply size comparable with the devices, assuring the power supply will last long enough for remote location sensing, retaining the memory of the sensed data, and providing enough power to communicate with a network of sensors or communication hub [27]–[29]. While compliant bistable mechanisms may

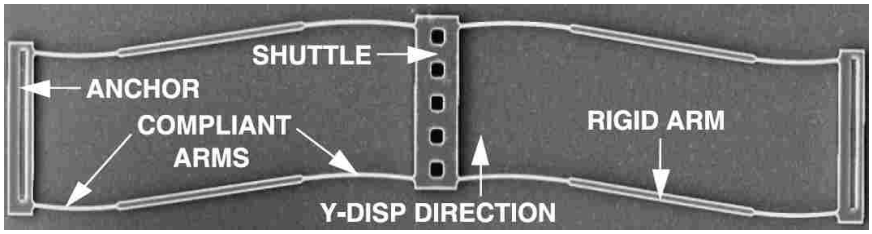

Figure 1.2: The FCBM (Bistable-A) components (SEM).

not solve the problem of communication with networks, they can directly assist with the size, memory, and retaining power over time challenges. By not requiring additional power supply components, the compliant bistable mechanism automatically solves the size challenge. Additionally, the strain energy in the compliant members will not dissipate as a traditional power supply would, allowing the compliant bistable mechanisms to remain in its last position. This provides for non-volatile memory possibilities for sensors.

1.4 Fully Compliant Bistable Mechanism

A scanning electron micrograph of the FCBM (in the second stable equilibrium position) components is shown in Figure 1.2. Figure 1.3 shows the variables important for the parametric design of an FCBM. Variables include rigid arm length (*RAL*), arm width (*AW*), rigid arm width (*RAW*), compliant arm length 1 (*AL*1), compliant arm length 2 (*AL*2), the angle of arm length 1 ($THETA$), the angle of the rigid arm length (*PHI*), the angle of arm length 2 (*ALPHA*), the out-of-plane thickness (T), the shuttle width (*SW*), and the shuttle length (*SL*). The FCBM relies on the deflection of the compliant arms to move to its alternate stable position. $YDISP$ is the actuated shuttle displacement. The Young's Modulus (EX), Poisson's ratio (*PR*), and device thickness are considered constant for a given device.

A specific base design was selected for in depth modeling and to serve as a benchmark. The base design, referred to as "Bistable-A", is defined by the variables listed in Table 1.1. Figure 1.4(a) displays this device in the first stable position, while Figure 1.4(b) displays the device in the second stable equilibrium position. This particular device was selected because it demonstrated good bistable characteristics [11]; there are two distinct

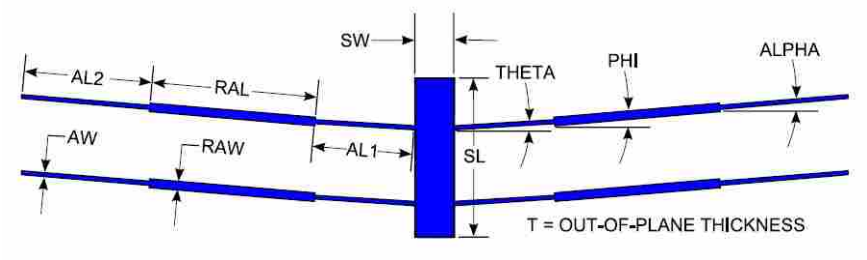

Figure 1.3: Dimensions of the bistable mechanism.

Table 1.1: Bistable-A design

Variable	*Magnitude*
$AL1$ (μm)	75.7
$AL2$ (μm)	57.3
RAL (μm)	126.3
AW (μm)	2.5
RAW (μm)	5.2
$THETA$ (°)	6.4
PHI (°)	5.6
$ALPHA$ (°)	6.6
T (μm)	3.5
EX (GPa)	164
PR	0.22
$YDISP$ (μm)	46

stable positions, the stresses did not exceed critical stress levels, and the numerical model of the device was well behaved.

Figure 1.5 shows the force-displacement relationship for Bistable-A, which is typical of other FCBM designs. Three distinct positions have a zero-force reaction, with the first and third of these positions being the first and second stable equilibrium positions, respectively. The middle zero-force reaction is the location of the unstable equilibrium position. A much larger force of magnitude F_{max} is required to displace the mechanism from the first to the second stable equilibrium position. In reverse, F_{min} is the force that must be applied to displace the mechanism from the second to the first stable equilibrium position.

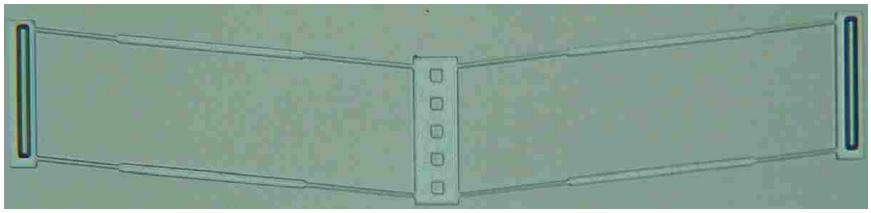

(a) Stable position #1

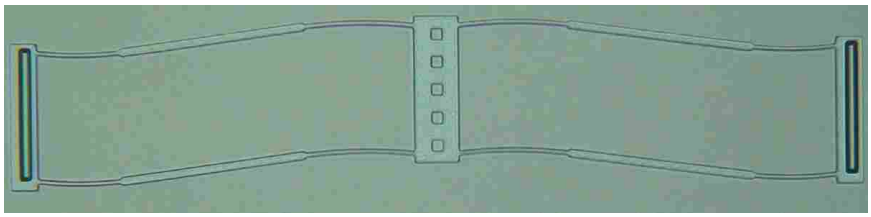

(b) Stable position #2

Figure 1.4: Bistable-A design manufactured with MUMPs.

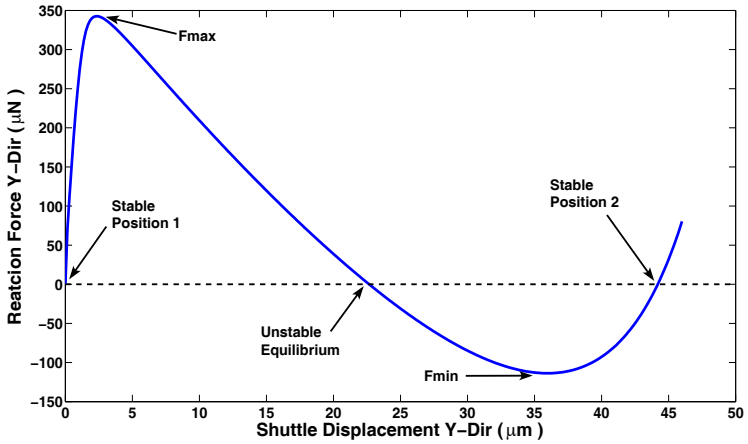

Figure 1.5: Force-displacement plot for the Bistable-A design.

1.5 Threshold Acceleration Sensor Array

The reaction forces required to switch the FCBMs from one stable position to another can be used to calculate what acceleration forces acting on the shuttles are required to produce the same displacement. When calculating the accelerations associated with the forces produced by the FEA model, the assumption was made to only incorporate the mass of the shuttle.

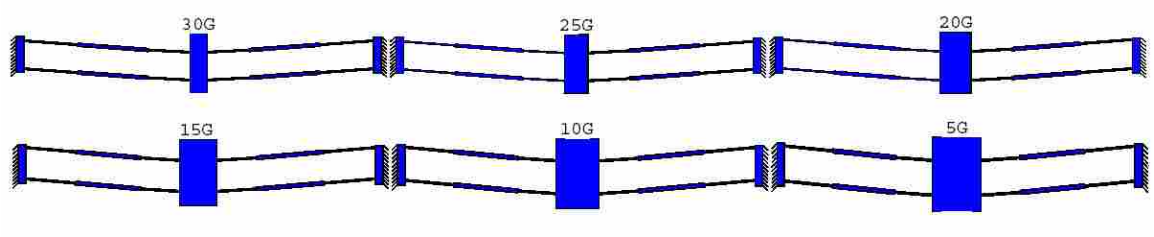

Figure 1.6: FCBM threshold acceleration sensing array example.

Anderson's research suggested that an array of FCBM sensors could be used to determine the magnitude of shock loads [11]. By varying the mass of the shuttle, the accelerations required to switch the bistable mechanism could be controlled. Multiple mechanisms could be placed linearly on a micro chip, with each consecutive FCBM requiring increased increments of acceleration forces before snapping to the alternate stable position (Figure1.6). For example, if one FCBM in the sensing array requiring 25 G's for displacement had snapped into its alternate stable position while the next consecutive mechanism requiring 30 G's for displacement had not snapped into its alternate stable position, it could be deduced that the array of sensors had experienced an acceleration between 25 and 30 G's.

Advantages exist if the FCBM is initially in the second stable position because a much larger force is required to displace the mechanism from its first to its second stable equilibrium position (Figure 1.5). To build an acceptable acceleration array, the sensors must have the capability of sensing a useful range of accelerations. Commercial low-G accelerometers range from 1G to 20 G's, while high-G accelerometers typically range from 20 G's to 250 G's [30]. To meet these acceleration requirements, the reaction forces must remain small, and the mass of the shuttles must be large. Thus, if the FCBM is initially in the second stable equilibrium position, a much smaller force is needed to initiate transition to the first stable equilibrium position. Second, once the FCBM has transitioned to the first stable equilibrium position, it will remain in that state until a much larger acceleration is experienced. It is much harder for the sensor to return to the second stable position, and thus the collected data is retained. This robust, non-volatile memory sensor array offers the benefit of not requiring an onboard power supply.

Chapter 2

FEA Models of the FCBM

Several FEA models of the FCBM were created and compared. The models have varying levels of complexity and capability. The models are described, followed by a comparison of model results, a comparison to experimental data, and the investigation of the relative importance of including various design features in the model.

2.1 Two-Dimensional Models

2.1.1 2-D Plane Element Model

Anderson [11] created two 2-D plane element models of the FCBM. The first was a two-dimensional quarter model based on the symmetric nature of the bistable switch (Figure 2.1). The boundary conditions of this simplified model do not capture the possibility of shuttle rotation. A second 2-D model was created that included all four compliant legs and the shuttle, as shown in Figure 2.2. This more complete 2-D model is used in this work for comparison to other models. In this 2-D model, displacement is applied at a location on the front face of the shuttle, and the resulting reaction forces are recorded at each displacement value. Zero-displacement boundary conditions were assigned to simulate the anchors. The model was created using 4-node plane elements (ANSYS plane2 elements), and the mesh contained approximately 19,500 elements and 42,000 nodes.

2.1.2 2-D 8-Node Quad-Element Model

A fully parametric model was constructed with eight-node quad-elements (ANSYS plane82 elements) to provide more accurate results for automated meshes, and to tolerate irregular shapes without much loss of accuracy (Figure 2.3). The elements can tolerate large deflection, large strain, and stress stiffening. The Bistable-A model resulted in approxi-

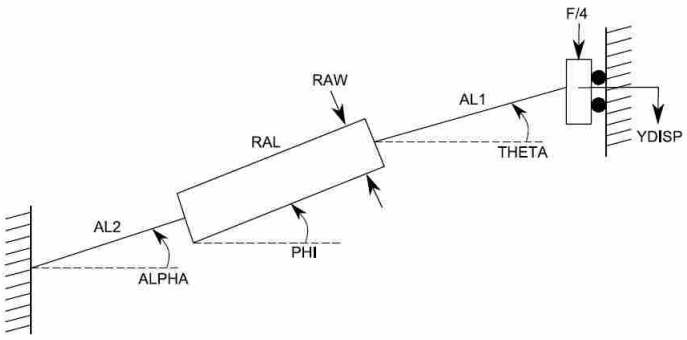

Figure 2.1: 2-D quarter model of the FCBM.

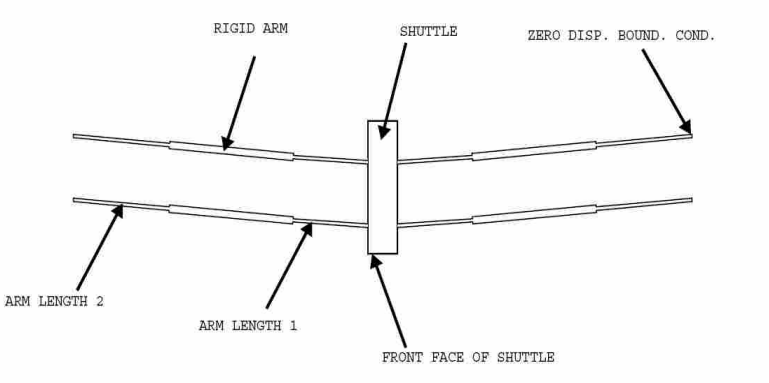

Figure 2.2: 2-D plane element model.

mately 2,500 elements and 6,200 nodes. Displacement was applied to each node on the face of the shuttle, and the reaction force was retrieved as a sum of the nodes on that face. This displacement application method constrained the shuttle to symmetric displacement.

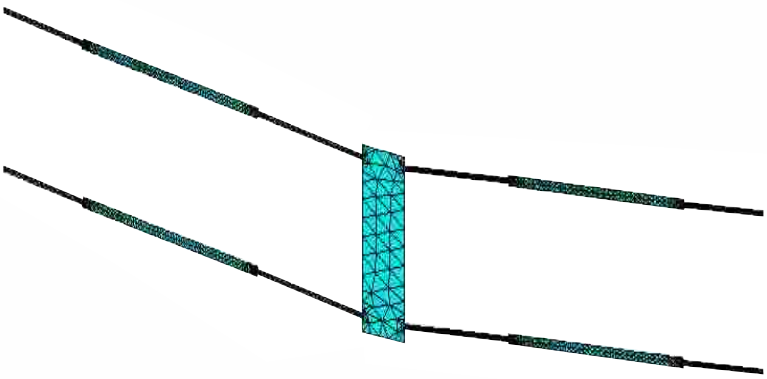

Figure 2.3: Isometric view of the eight-node quad-element model.

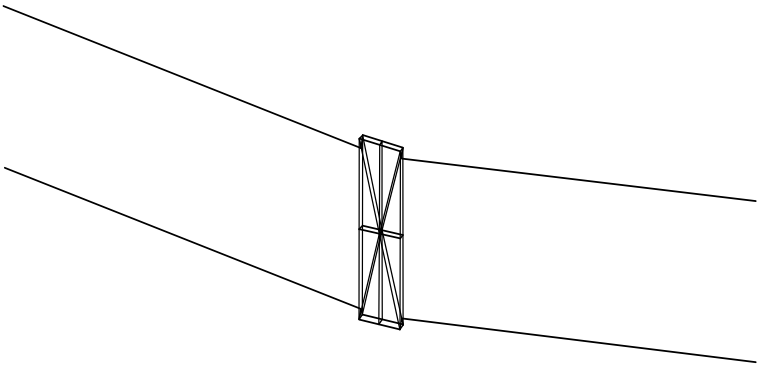

Figure 2.4: Isometric view of the 3-D beam element model.

2.2 Three-Dimensional Models

2.2.1 3-D Beam Element Model

A simplified 3-D beam element model (ANSYS beam4 elements) was created (Figure 2.4). The model is fully parametric, allowing for alternate geometries, material properties, shuttle displacement values, and mesh refinement. To assist with validation of the three-dimensional FCBM characteristics found by the solid element model discussed next, critical node locations were made available for displacement as well as applied off-axis forces.

The beam4 element was chosen for its tension, compression, torsion, and bending capabilities. This element is also capable of dealing with stress stiffening and large strain. The shuttle was constructed with simplified supports to simulate the rigid nature of the shuttle while maintaining the shuttle geometry as shown in Figure 2.5. To maintain rigidity, the shuttle elements were assigned a cross sectional area and moment of inertia that was twice the rigid arms, which in turn was almost two times larger than the compliant arms. Zero displacement boundary conditions were applied at the ends of the compliant arms connected to the anchors. A refined mesh was used in the compliant arm sections, a moderately coarse mesh was assigned to the rigid arms, and a coarse mesh was assigned to the shuttle. The model resulted in approximately 11,600 elements and 11,600 nodes, and converged to a solution in approximately two hours.

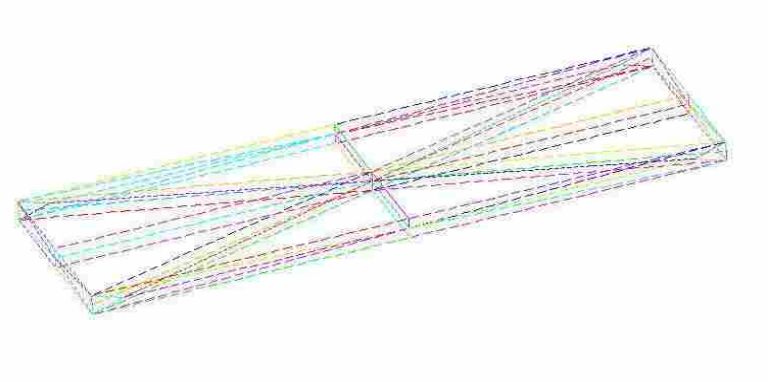

Figure 2.5: Isometric view of the 3-D beam element shuttle.

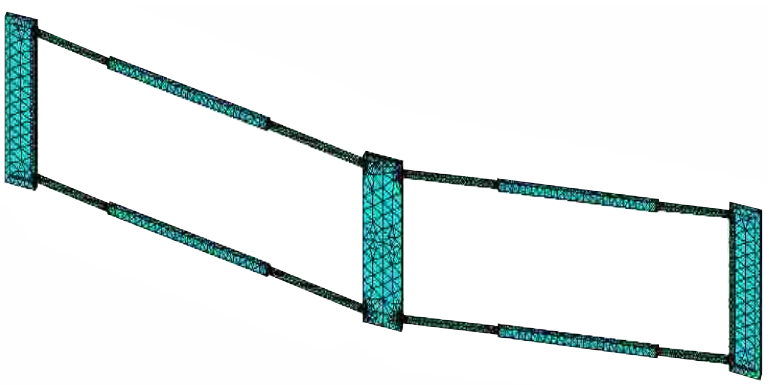

Figure 2.6: Isometric view of the 3-D solid element model.

2.2.2 3-D Solid Element Model

A more complete, 3-D model was created using 3-D solid elements (ANSYS solid95 elements) with the intent of recovering the three-dimensional characteristic of the FCBMs with a high level of accuracy (Figure 2.6). The model requires approximately nine hours to converge to a solution due to a large number of nodes and elements (approximately 21,000 elements and 40,000 nodes). This model incorporated geometric detail that simplified models did not provide. It is fully parametric, allowing for alternate geometries, material properties, and shuttle displacement values. The level of mesh refinement is also parametrically controlled for ease of parallel processing and mesh optimization approaches were employed to efficiently refine the mesh.

One geometric detail included in the model was fillets at each of the compliant arm/rigid arm, compliant arm/shuttle, and compliant arm/anchor intersections. When the

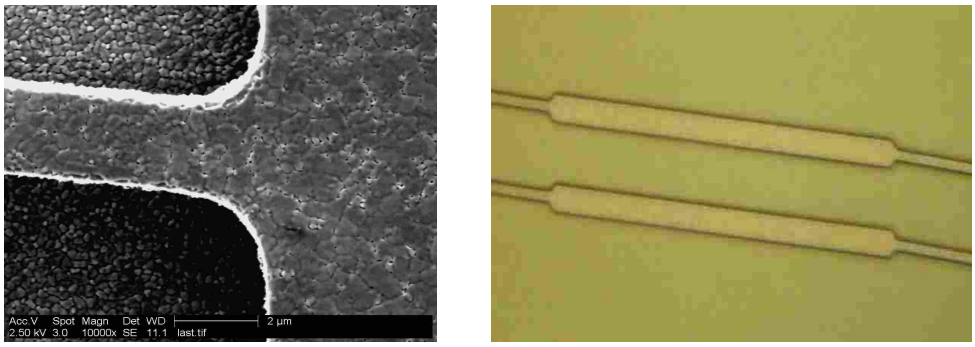

(a) SEM: shuttle fillet (b) Rigid arm fillets

Figure 2.7: Bistable-A fillets.

bistable mechanisms are produced, fillets naturally form at the intersection of two faces. The smaller or sharper the angle between the two faces, the larger the fillet. This is due to multiple applications of low pressure chemical vapor deposition (LPCVD) and etching used in device fabrication. Figure 2.7(a) shows a scanning electron micrograph (SEM) of a compliant arm/shuttle interface fillet, and Figure 2.7(b) displays the fillets created at the compliant arm-rigid arm interface.

Anchor details were also included in the 3-D solid element model. When the anchors are manufactured, a recess exists in the top surface, as can be seen in the 3-D model of the anchor (Figure 2.8(a)). The area contacting the substrate on the bottom of the anchor is equal in size to this recess. The bottom view of the anchor in Figure 2.8(b) shows the resulting overhanging edge. Figure 2.8(c) displays an SEM of the compliant arm/anchor intersection and the clearance between the overhanging edge and the substrate. The recess in the top of the anchor can also be seen in the upper-right corner. While the 2-D plane element model prescribes zero-displacement boundary conditions at the outer edges of the compliant arms, the 3-D solid model prescribes zero-displacement boundary conditions at the entire bottom face of the anchor. Any bending that might occur at the overhanging edge at the compliant arm/anchor intersection may affect the behavior of the FCBM.

The 3-D solid element model also accounts for residual stress. Manufacturing the FCBMs with MUMPs (Multi-User MEMS Processes) [31] creates a uniform residual stress throughout the mechanism. In the case of the FCBMs, a negative or compressive residual stress exists that causes each of the four arms to slightly lengthen, displacing the shuttle

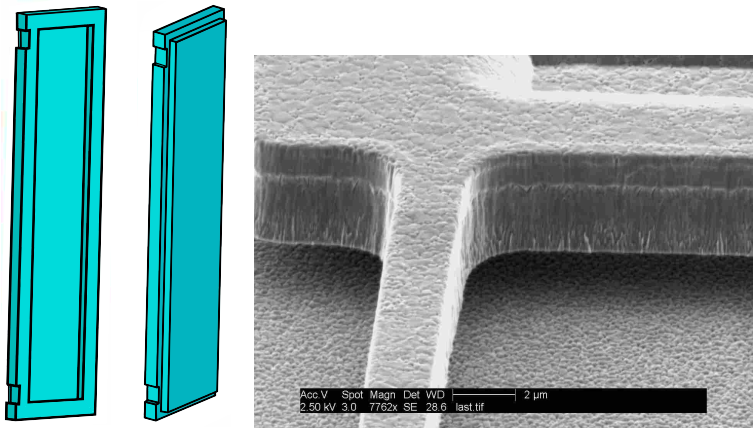

(a) Top (b) Bot. (c) SEM of anchor and fillets

Figure 2.8: FCBM anchors.

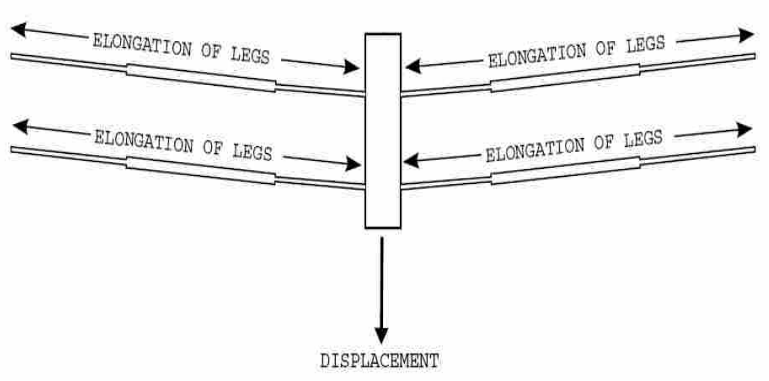

Figure 2.9: Displacement due to compressive residual stress.

in the direction shown in Figure 2.9. Generally, these residual stresses develop due to the temperature difference during the deposition process and application. Thin films are deposited on a heated substrate, and when the substrate is removed from the deposition chamber, the temperature change causes the thin film to expand or contract at a different rate than the substrate [21], [32], [33].

Finally, a mesh optimization technique was used to create a model with the smallest number of nodes and elements possible, while retaining accuracy. As a result, retaining a properly refined mesh in critical areas such as the fillets, compliant arms, bottom surface of the anchor, and all nodes associated with displacement or applied forces was necessary. The model also addressed the challenge of eliminating poorly shaped elements due to the

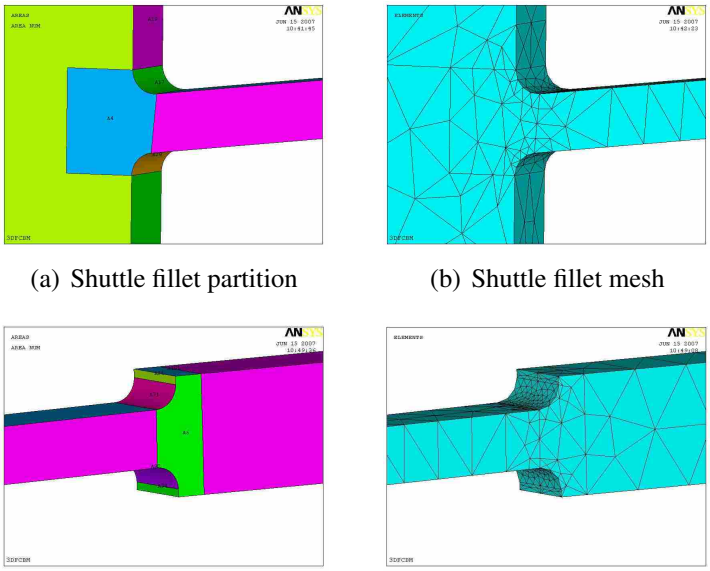

(a) Shuttle fillet partition (b) Shuttle fillet mesh

(c) Rigid/comp. arm partition (d) Rigid/comp. arm mesh

Figure 2.10: Fillet refinement methods (partitioning of volumes).

curved surfaces of the fillets. The 20 node, solid95 tetrahedral element was chosen for its ability to tolerate irregular shapes without much loss of accuracy, and its ability to account for large deflection, large strain, and stress stiffening. The tetrahedral elements are well suited for geometry transitions at fillets and transitions between the contrasting large and small elements surrounding the fillets. Additionally, the tetrahedral form of the solid95 element can be refined and modified using several tools after the initial mesh has been created.

To properly refine the fillets while leaving non-critical areas with a coarse mesh, volumes were defined by partitioning around the curved fillet surface. This allowed for a volume and area refinement immediately around the fillets, and provided options for line element size control to easily transition into the connecting volumes (such as the shuttle, compliant arm, or rigid arm sections) as shown in Figure 2.10.

The reaction forces and displacements of the anchor are only critical on the bottom face where zero displacement boundary conditions were applied, and on the overhanging edge where the compliant arms contact the anchors. Refinement was conducted on each of these areas. This resulted in a refined mesh on the interior and bottom areas of the anchors, leaving a coarse mesh elsewhere (Figure 2.11).

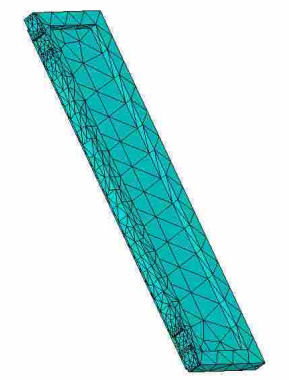

Figure 2.11: Meshed anchor of 3-D solid element model.

Table 2.1: Model comparison of force-displacement values.

Model	F_{max} (μN)	F_{min} (μN)
2-D PLANE ELEMENT	339.3	-111.9
2-D QUAD-ELEMENT	333.2	-108.8
3-D BEAM ELEMENT	343.1	-112.2
3-D SOLID ELEMENT	343.1	-106.4

2.3 Comparison of Models

While the 2-D models have the ability to quickly retrieve the force-displacement data for an FCBM, they lack the ability to recover three-dimensional behavior. The 3-D models were used extensively to recover this three-dimensional data, but were first compared to the 2-D models. The Bistable-A design (Figure 1.2 and Table 1.1) was used in the comparison of models. The same number of loadsteps was used on each device to displace the FCBM shuttle 46.0 μm.

All four models converged to approximately the same stable and unstable equilibrium positions. However, Figure 2.12 shows that the 2-D models produced plots that slightly differed from those predicted by the 3-D models. A graph showing the F_{max} and F_{min} regions of the same force-displacement plot are shown in Figure 2.13 and Figure 2.14, respectively. Table 2.1 lists the F_{max} and F_{min} values calculated by each of the four models. The percent difference between the solid element model and any of the other three models never exceeded 5.45% at F_{max} or F_{min}.

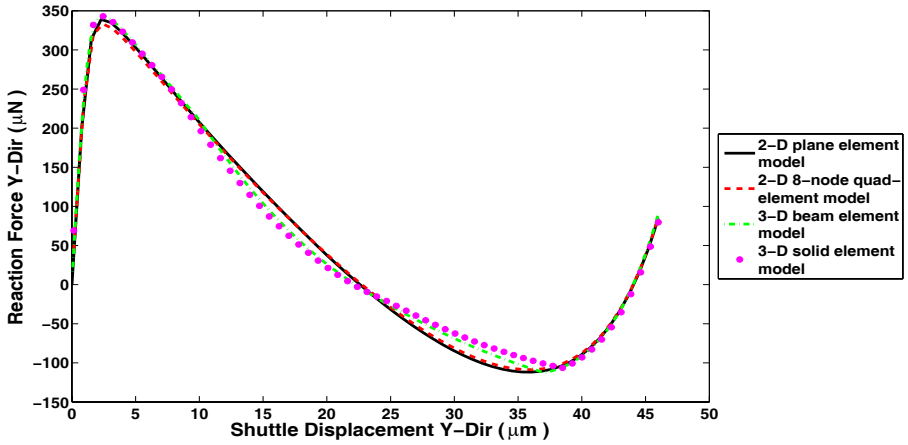

Figure 2.12: Force-displacement comparison of four models.

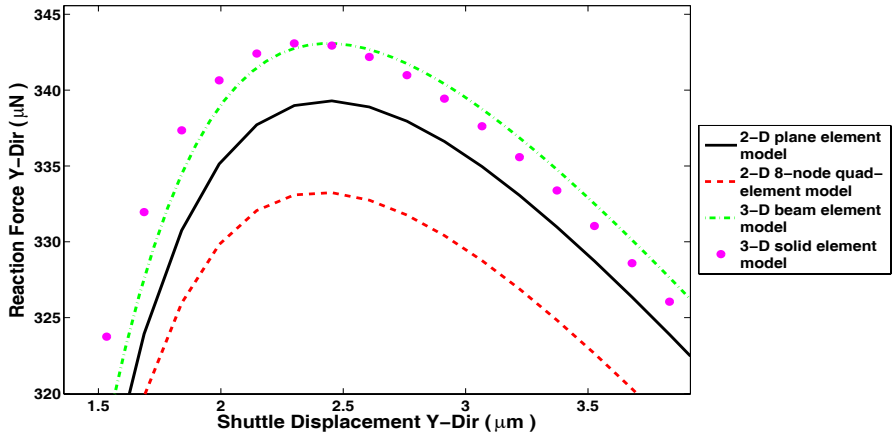

Figure 2.13: F_{max} comparison of four models.

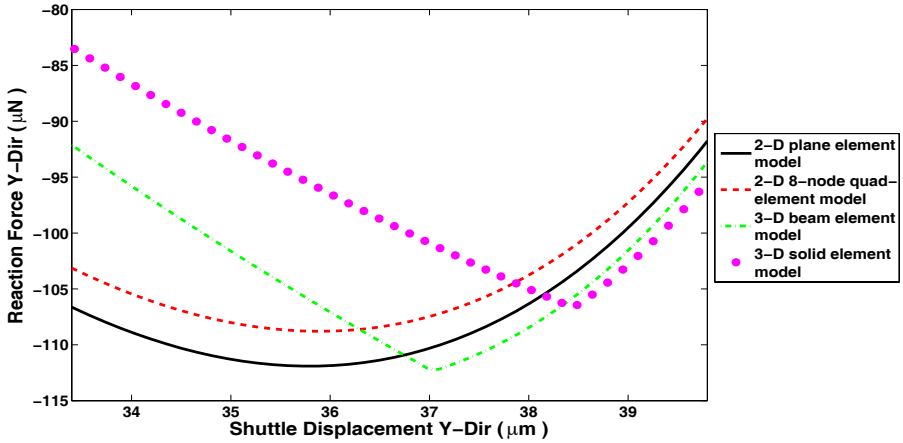

Figure 2.14: F_{min} comparison of four models.

The difference in the general shape of the force-displacement plot between the 2-D and 3-D models suggests that the 3-D models are predicting characteristics that the 2-D models are not. Though this difference did not affect F_{max} or F_{min} greatly for the Bistable-A design, it may affect other three-dimensional characteristics that cannot be shown when only analyzing the force-displacement plot. The ability of the 3-D models to analyze these three-dimensional effects will prove valuable in understanding the behavior of FCBMs.

2.4 ANSYS Batch Code for the Models

Each of the models introduced are available for further research. The ANSYS batch file for the 2-D plane element model is available in Appendix A. The ANSYS batch file providing the 2-D 8-node quad-element model is available in Appendix B. The ANSYS batch file for the 3-D beam element model is available in Appendix C. Finally, the ANSYS batch file for the 3-D solid element model is available in Appendix D.

2.5 Conclusions

Three finite element models were produced for the analysis of FCBMs. These models included the 3-D solid element model, the 3-D beam element model, and the 2-D 8-node quad-element model. A fourth model, the 2-D plane element model, was provided by past research [11] and included in the analysis. The models have varying levels of complexity, and were compared to each other. The 2-D models lacked the ability to recover three-dimensional effects of FCBMs, while the 3-D models were capable of predicting these characteristics. While the force-displacement relationship predictions of each of the models did not differ greatly, it was hypothesized that other three-dimensional characteristics may be affected.

Chapter 3

Influence of Various Design Features

This chapter investigates the effect of including geometric detail and simplified boundary conditions in the 3-D solid element model. The three geometric details include fillets, residual stress caused by the manufacturing process, and the complexity of anchors.

3.1 Fillets

It has been shown that adding fillets will increase the stiffness of the mechanism [34] as well as mitigate the effects of local stress concentrations and local flexibility. This additional geometry slightly increases the predicted values for F_{max} and F_{min}. The 3-D solid element model was used to determine the relative importance of including fillets in the model. A direct comparison of force-displacement data was made when fillets were and were not included in the Bistable-A design. To simplify the comparison, equal displacement was applied to each node on the front face of the shuttle. This constrained the shuttle to zero roll, pitch, and yaw. To isolate the effect fillets had on the force-displacement relationship, no residual stress or anchors were included in the analysis. Zero displacement boundary conditions were applied to the end of the compliant arms to simulate the anchors.

Figure 3.1 shows the results for models with and without fillets. The fillets caused the FCBM to become slightly stiffer, as exemplified by an increase in F_{max} and F_{min}. However, including fillets had little effect on the force-displacement plot at any location other than F_{max} or F_{min}. The fillets have thus affected the peak force magnitudes, but have not altered the general bistable behavior. Although more complete, adding fillets comes at the price of increasing the number of nodes and elements in the model, thus increasing solution times. Including fillets in the Bistable-A model increased F_{max} by 2.4%, and increased F_{min} by 3.7% (Table 3.1).

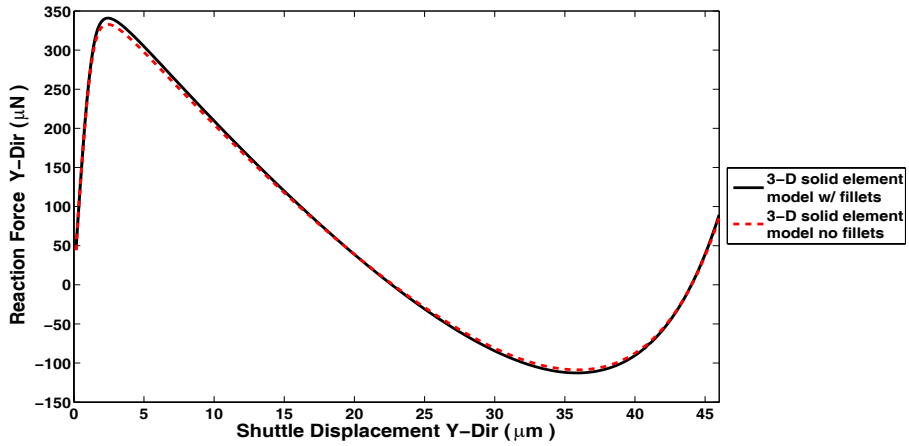

Figure 3.1: Force-displacement plot for comparing fillets.

Table 3.1: Analysis of the effect of fillets.

Model	*Fmax (μN)*	*Fmin (μN)*
FILLETS	340.9	-112.7
NO FILLETS	332.9	-108.7
% DIFFERENCE	2.4	3.7

3.2 Residual Stress

The effect of including residual stress in the 3-D solid element model was also analyzed. As mentioned before, an initial stress was applied to the entire mechanism to simulate the compressive residual stress induced by the manufacturing process. A stress of negative 10 MPa was used, matching the published data available through MUMPs [31]. No off-axis forces were included in the model, and the shuttle was displaced by pulling a node on the back face of the shuttle. The only locations on the force-displacement curve that were affected by the prestress were F_{max} and F_{min}, and these were only slightly different. Figure 3.2 and Figure 3.3 displays the F_{max} and F_{min} regions of the force-displacement plot, respectively.

Table 3.2 lists the values recorded at the critical points on the force-displacement plot. By including residual stress in the model, F_{max} increased by 0.7%, while F_{min} increased by 1.0%. Though it did not make a large difference in the results, it also did not add much complexity to the model or significantly increase the convergence time.

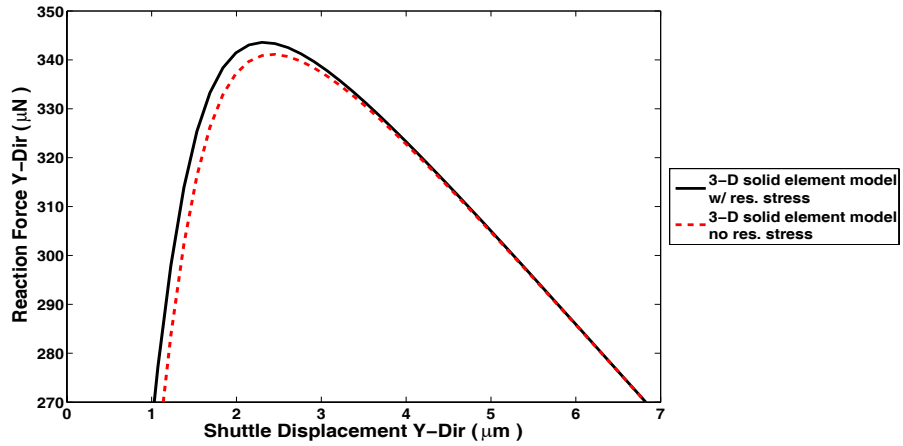

Figure 3.2: Force-displacement plot for comparing residual stress (F_{max}).

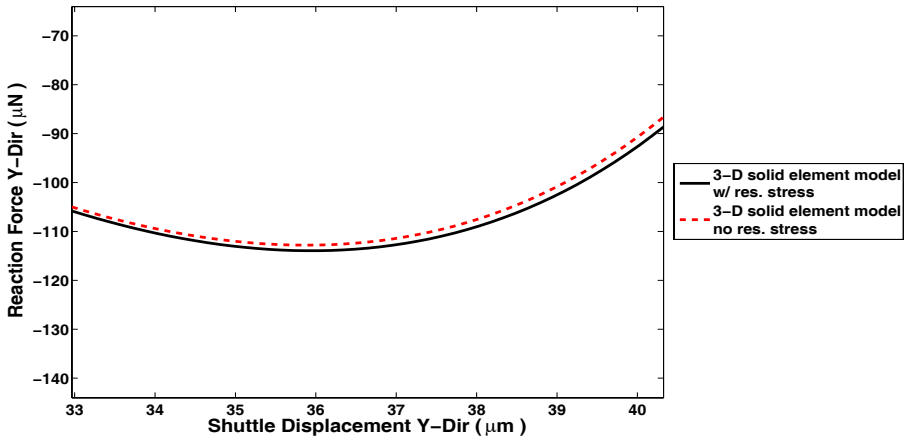

Figure 3.3: Force-displacement plot for comparing residual stress (F_{min}).

3.3 Anchors

The effect of including anchors in the 3-D solid element model was also analyzed. One version of the model included the full geometry of anchors, while the other simulated the anchors through zero displacement boundary conditions at the ends of the compliant arms. Fillets and residual stress were included in each of the models.

Figure 3.4 shows that including anchors altered the characteristic of the FCBM force-displacement plot. The reaction forces between F_{max} and F_{min} were the most affected. When anchors were included, the slope of the plot was more steep near the region to the left

Table 3.2: Analysis of the effect of residual stress.

Model	*Fmax* (μN)	*Fmin* (μN)
RESIDUAL STRESS	343.6	-113.9
NO RESIDUAL STRESS	341.1	-112.8
% DIFFERENCE	0.7	1.0

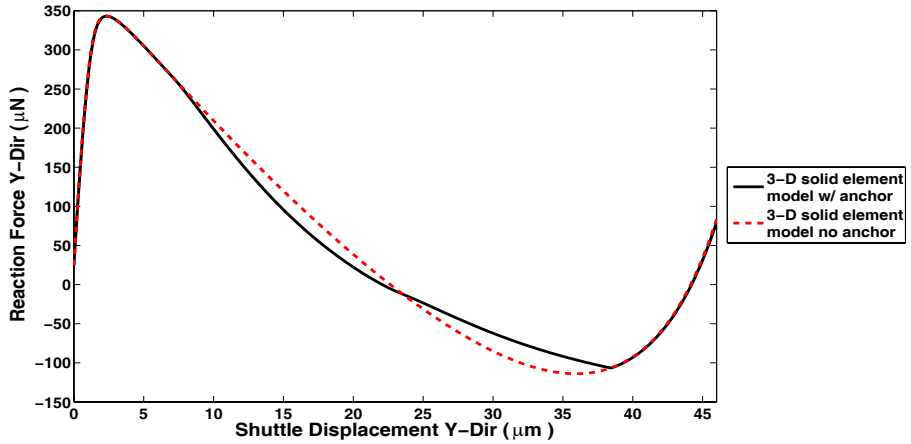

Figure 3.4: Force-displacement plot for comparing anchors.

of the unstable equilibrium position, and more shallow near the region to the right of the unstable position. This plot strayed from its original path at a location to the right of F_{max}, then snapped sharply back onto the original path to the right of the original F_{min}, defining a new reduced F_{min}. While F_{max} decreased slightly, F_{min} decreased a significant amount.

Table 3.3 shows the critical reaction force values for the force-displacement plot in Figure 3.4. While F_{max} decreased by only 0.1%, F_{min} decreased by 7.0% when anchors were included. By including the geometric detail of anchors, the three-dimensional characteristic and critical point magnitudes were altered. Though this will increase the model complexity and solution time, it is necessary to properly characterize the three-dimensional nature of FCBMs.

3.4 Conclusions

Including fillets, residual stress, and anchors in the 3-D solid element model resulted in a model that could more accurately predict the force-displacement relationship

Table 3.3: Analysis of the effect of anchors.

Model	*Fmax (μN)*	*Fmin (μN)*
ANCHORS	343.1	-106.4
NO ANCHORS	343.6	-113.9
% DIFFERENCE	-0.1	-7.0

of an FCBM. Including fillets increased the reaction forces significantly, while including residual stress had a similar but smaller effect. Including the geometric detail of anchors resulted in an altered force-displacement relationship. The general shape of the force-displacement plot changed, and the reaction forces were decreased significantly.

Chapter 4

Comparison to Experiment

Two sets of devices were designed, fabricated, and tested. Two fabrication methods were used. These devices, their results, and the comparison to predicted results are described next. Additionally, to further validate the 3-D solid element model, efforts were made to ensure that the model would naturally converge to the second stable equilibrium position. This was accomplished by displacing the FCBM shuttle to a position beyond the second stable equilibrium position, then removing the assigned displacement to allow the model to converge to a displacement solution. Figure 4.1 shows that the model naturally converged to a Y-displacement value of 44.21 μm after being forced to 46.0 μm. This matched the predicted zero magnitude reaction force generated by the force-displacement plots in the 3-D solid element model.

4.1 SUMMiT V Device

The FCBM geometry listed in Table 4.1 was created using Sandia National Laboratory's SUMMiT V manufacturing process [35]. Reaction forces were recorded at various displacement values using a surface micro-machined force gage [36].

Three sets of experimental data were taken [1], [2], each representing an FCBM of identical geometry, but located at alternate locations on the same SUMMiT V die. The force measurements were limited to displacements approaching F_{max} on the force-displacement plot when displacing the FCBM from the first stable equilibrium position to the second, and approaching F_{min} when displacing the FCBM from the second to the first stable equilibrium position. Because the FCBM transitioned to the alternate stable position after reaching F_{max} or F_{min}, several reaction forces approaching F_{max} and F_{min} were recorded, but few values could be recorded between F_{max} and F_{min}.

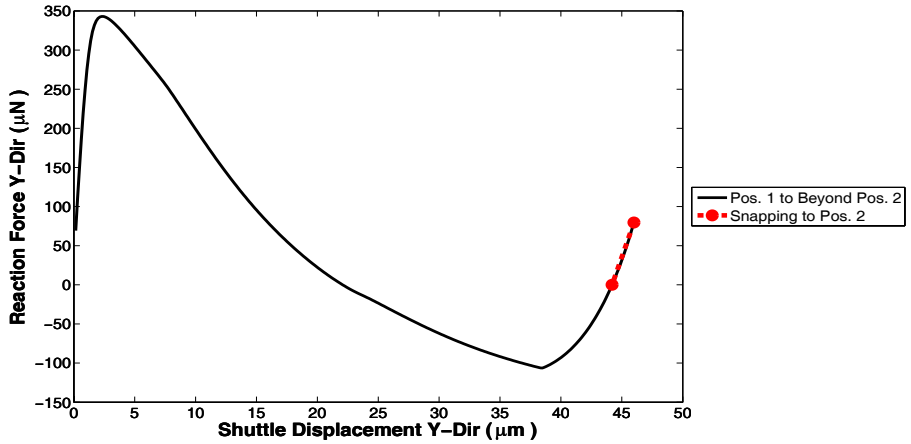

Figure 4.1: Force-displacement plot showing that the 3-D solid element model naturally converges to the second stable equilibrium position.

Table 4.1: Geometry of the SUMMiT V device design.

Variable Description	*Magnitude*
*AL*1	13.7 μm
*AL*2	13.7 μm
RAL	103.3 μm
AW	1.4 μm
RAW	6.2 μm
THETA	2.44 °
PHI	2.44 °
ALPHA	2.44 °
T	4.75 μm
EX	164 GPa
PR	0.23
YDISP	11 μm

To account for the fact that the model and experiment do not have results at the same displacement values, a high-order polynomial was fit to the model results. Each polynomial matched the model result with a minimum R^2 value of 0.9997 (Table 4.2). The equation of the polynomial was then used to calculate the reaction forces at the experimental displacement values. Figure 4.2 compares the model predictions to the average experimental data. A comparison of F_{max} and F_{min} results are listed in Table 4.3. Each of the models matched the region to the left of F_{max} on the force-displacement plot well. The models underestimated the value of F_{min} and the region to the right of F_{min} slightly, but followed the trend

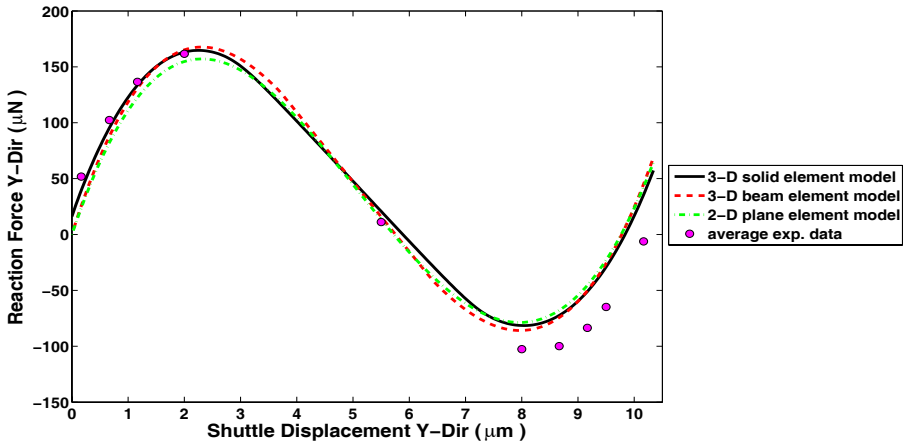

Figure 4.2: Model comparison to experimental data [1], [2] for the SUMMiT V device.

Table 4.2: R^2 values for the polynomial fit.

Model	*R^2 Fit to Experimental Data Set 1*	*R^2 Fit to Experimental Data Set 2*	*R^2 Fit to Experimental Data Set 3*
2-D PLANE ELEMENT	0.9753	0.9927	0.9955
3-D BEAM ELEMENT	0.9794	0.9927	0.9961
3-D SOLID ELEMENT	0.9918	0.9963	0.9972

well. Graphs showing how well the models matched each of the experimental data sets are provided in Figures H.1 through H.3 (Appendix H).

Table 4.3: Comparison of F_{max} and F_{min} for model validation.

Model	*Experimental F_{max}/F_{min} (μN)*	*Predicted F_{max}/F_{min} (μN)*	*%Error F_{max}/F_{min}*
2-D PLANE ELEMENT	163.2/ -99.07	154.8/ -78.67	-5.4/ 25.9
3-D BEAM ELEMENT	163.2/ -99.07	165.2/ -85.87	1.2/ 15.4
3-D SOLID ELEMENT	163.2/ -99.07	163.2/ -81.44	0.0/ 21.6

4.2 MUMPs Device

A second comparison of the 3-D solid element model predictions to experimental data was made for further validation of the model. While the first validation was conducted using an FCBM manufactured with the SUMMiT V process, this validation was achieved through comparison to an FCBM manufactured with MUMPs. The geometry of the FCBM matched the Bistable-A device listed in Table 1.1.

A force gage and probe guide was attached to the FCBM shuttle to retrieve all necessary reaction force and displacement data, as shown in Figure 4.3. To retrieve the force-displacement data, the tip of a probe was placed in the probe guide, and moved in the direction necessary to cause a transition between stable equilibrium positions [1]. The force gage was customized for the expected magnitudes of force and displacement it would experience while retrieving data from the theoretical force-displacement plot. Because the probe guide and force gage are rigidly attached, one end of the force gage is displaced the same amount as the probe guide. The side of the force gage attached to the FCBM shuttle is then displaced a magnitude that is dependent on the stiffness of the force gage. A vernier designed to provide displacement values for each side of the force gage is shown in Figure 4.4. The vernier motion is recorded with a video camera through a microscope, and the displacements are retrieved from the vernier. By knowing the stiffness and displacement of each end of the force gage, the reaction forces were determined.

A coupling between the force gage and FCBM shuttle was designed to allow the capture of force data between the stable equilibrium positions. The coupling mechanism was constructed with beams that translated parallel to each other, as shown in Figure 4.5. Three of the beams are rigidly attached to the force gage, while two beams are rigidly attached to the FCBM shuttle. Stops 1 and 3 are rigidly attached to the force gage, and stops 2 and 4 are attached to the FCBM shuttle. As the FCBM is pulled from the first stable equilibrium position to the second, stop 3 pulls stop 2 to the right. As the force gage pushes the FCBM shuttle back into the first stable equilibrium position, stop 3 pushes stop 4 to the left. The distance between each stop allows the FCBM to freely transition to its alternate stable position relatively unrestrained. Including the coupling mechanism reduced

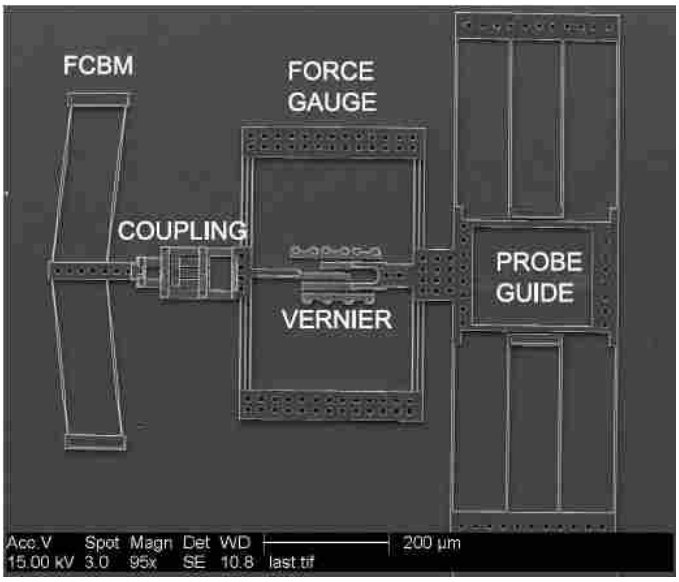

Figure 4.3: Test device used in MUMPs experimental data comparison (SEM).

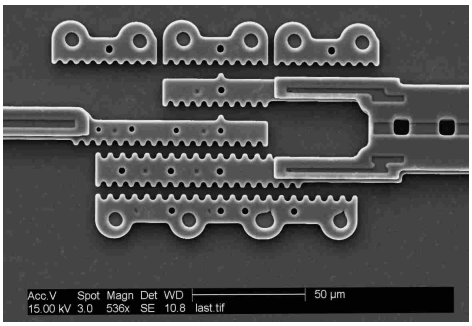

Figure 4.4: The force gage vernier (SEM).

the constraint of the force gage on the FCBM. The coupling design also allowed the FCBM shuttle some freedom to roll, pitch, and yaw.

Two FCBMs were chosen for testing, each on a separate MUMPs die. The first die was chemically released, then tested approximately twenty-four hours later. This is referred to as Device 1. The second die was released separately, and the FCBM was tested immediately afterward (Device 2). It can be assumed that both Device 1 and Device 2 have the same geometry and material property values. Figure 4.6 shows one iteration of the experimental results for Device 1. The data labeled “Device 1: 1-2” and “Device 1: 2-1” were retrieved from the transition from the first to second and second to first stable

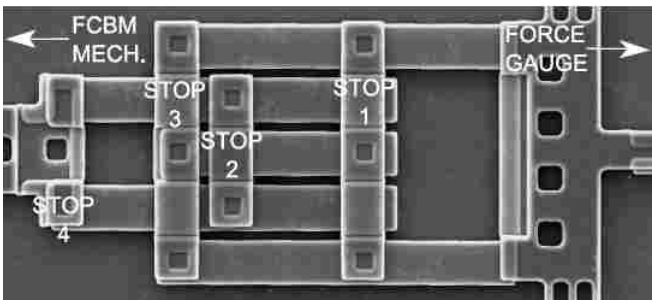

Figure 4.5: The coupler mechanism (SEM).

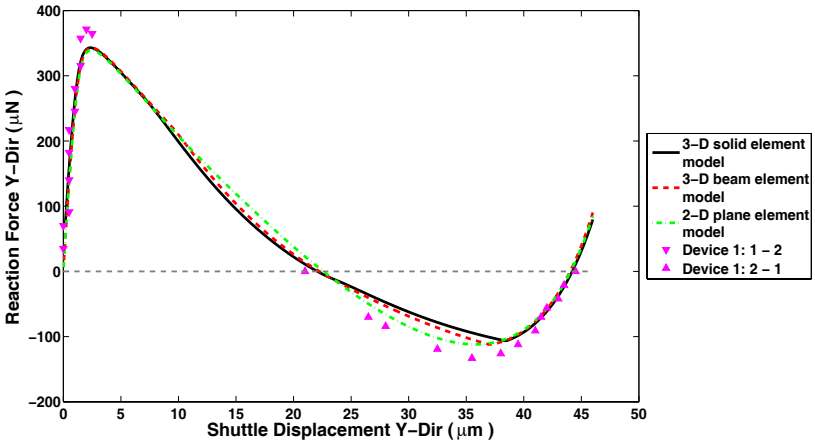

Figure 4.6: Validation of models using MUMPs Device 1 experimental data.

equilibrium positions, respectively. The models predicted the measured trend as expected from testing the SUMMiT device.

Figure 4.7 shows the surprising result for Device 2. The data labeled "Device 2: 1-2" and "Device 2: 2-1" are the experimental results for Device 2. Device 1 also proved capable of producing results similar to those for Device 2 shown next, but produced the results similar to those in Figure 4.6 more frequently. Device 2 also proved capable of producing results similar to those for Device 1, but more often produced results similar to those in Figure 4.7. For simplicity here, the form of force-displacement curve of Figures 4.6 and 4.7 will be associated with Device 1 and Device 2, respectively, but results later in the paper will provide insight on why both curves can occur.

Although Device 1 and Device 2 are essentially identical, they could experience radically different plots. The peak reaction force for Device 2 is only a third of that for

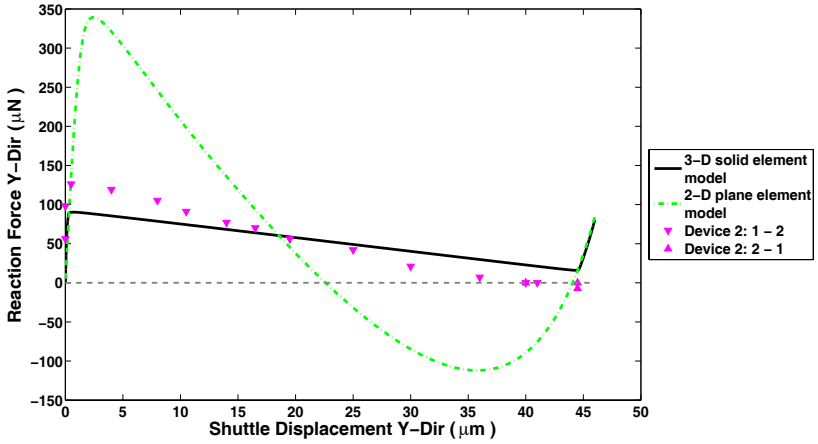

Figure 4.7: Validation of models using MUMPs Device 2 experimental data.

Device 1. Device 2 is also barely bistable, as evidenced by the very small experimental F_{min} value. The change in behavior is not accounted for by stiction or similar phenomena because the trends are opposite of what would be predicted for those behaviors (i.e. the reaction forces would increase to account for both the elastic energy stored in the flexible beams and friction). These findings lead to interesting discoveries about the behavior of FCBMs. The results for each device are discussed next, with the result of Device 2 leading to particularly revealing conclusions regarding the three-dimensional behavior of FCBMs.

4.2.1 Discussion of Results for Device 1 - Phenomenon 1

Overall, model predictions agreed with the experiment in both trend and magnitude for Device 1. Behavior similar to the force-displacement plot predicted by the 3-D models will be referred to as Phenomenon 1. The measured forces are still slightly larger than the predicted forces, and there are several possible causes. First, the material properties of the physical FCBM differs from the FEA model slightly. If the modulus of elasticity in the model were smaller than the actual value, the model predictions would produce smaller reaction forces. Additionally, the geometry of the physical FCBM may slightly differ from the geometry defined in the models. Any one of the dimensions used to fully define the FCBM in the model may be slightly inaccurate due to uncertainties in the manufacturing

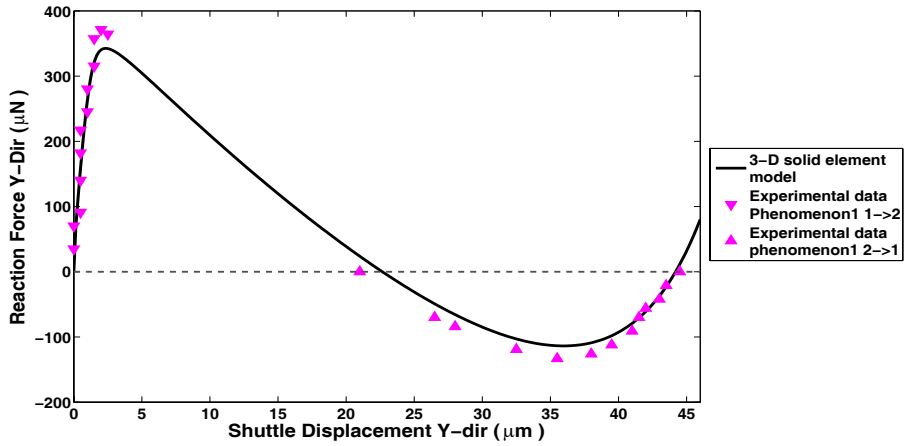

Figure 4.8: Effect of applying displacement at the face of the shuttle to simulate the coupling mechanism.

process. Friction between the FCBM shuttle and the substrate could also be a contributing factor.

The inability of the shuttle to roll, pitch, or yaw will affect the experimental force-displacement values. To account for the constraint caused by the coupling mechanism, the 3-D solid element model was modified to prescribe the displacement at each node on the front face of the shuttle rather than a single node (thus constraining the roll, pitch, and yaw of the shuttle). This force-displacement plot, and the experimental data for Phenomenon 1 is provided in Figure 4.8. When prescribing displacement at the face of the shuttle, F_{min} increases. The same trend can be seen in the experimental data when being compared to the FEA prediction in Figure 4.6. Though the coupling mechanism provides some freedom for out-of-plane motion, it does not allow the shuttle to freely roll, pitch, or yaw as it displaces. Therefore, it is plausible that the coupling mechanism is influencing the force-displacement data by smoothing out and increasing the magnitude of the F_{min} region.

4.2.2 Discussion of Results for Device 2 - Phenomenon 2

The behavior similar to the force-displacement plot associated with Device 2 will be referred to as Phenomenon 2. The results of the experiment showed a radical unexpected departure from the plot associated with Device 1. This force-displacement plot has much lower peak reaction forces, and is nearly linear between F_{max} and F_{min}. The results initially

appeared to follow the plot produced by Device 1, but strayed from the expected path before reaching the expected F_{max}. Though the reaction forces were greatly reduced, the force-displacement plot still suggested that the mechanism was bistable.

It is hypothesized that the cause of such characteristics is due to the 2-D effects associated with the FCBMs. Many of the past 2-D models assumed that perfect symmetry was associated with the FCBM geometry and applied force location. However, the FCBM shuttle is free to roll, pitch, and yaw as it is moving to its alternate stable equilibrium position. The FCBM's ability to displace out-of-plane can also affect the behavior of the mechanism, including the reaction forces of the force-displacement plot.

The 3-D solid element model is capable of incorporating the non-linear three-dimensional behavior of FCBMs in the analysis. To better understand this 3-D behavior, eccentric loading conditions and off-axis forces were introduced to the mechanism during analysis. Several locations on the FCBM shuttle were chosen for the mechanism's displacement, and several more locations were chosen for off-axis force application. As a result, the 3-D solid element model proved to have the ability to predict the Phenomenon 2 trends observed during experimentation, as seen in Figure 4.7. To produce these results, the FCBM was displaced from a node on the back face of the shuttle. An off-axis force was also applied in the negative Z-direction, perpendicular to the top surface of the shuttle, and located at the shuttle's center of mass. With these loading conditions, the model predicted the Phenomenon 2 trends, including reduced peak reaction forces, and a nearly linear region in the force-displacement curve. The discrepancy between the experimental data and model prediction are the result of three-dimensional effects. The 3-D model results showed that Phenomenon 1 occurred when no off-axis or eccentric loads were applied, or when the magnitude of those forces were lower. Phenomenon 2 occurred when larger off-axis or eccentric loading conditions occurred.

4.3 Conclusions

The 3-D solid element model, the 3-D beam element model, and the 2-D plane element model predictions were compared to experimental data for validation. FCBMs that were manufactured using two different manufacturing methods were used for the source of

this experimental data. The first was the SUMMiT V method provided by Sandia National Laboratories, and the second was MUMPs provided by MEMSCAP. Each of the models predicted the SUMMiT V results adequately, with the 3-D solid element model matching the experimental data slightly better than the others. Two FCBMs , Device 1 and Device 2, were manufactured with MUMPs and used for testing. Each of the models predicted the Device 1 results well. However, Device 2 produced drastically different and unexpected experimental results. The two types of behavior associated with Device 1 and Device 2 were defined as Phenomenon 1 and Phenomenon 2, respectively. The 3-D solid element model was capable of predicting both Phenomenon 1 and Phenomenon 2, while the 2-D model was not.

Chapter 5

3-D Model Inputs and Metrics

A test suite of FEA runs was constructed to better understand the three-dimensional behavior of FCBMs using Bistable-A as the nominal design. The input for all analysis was a Y-direction displacement of the FCBM shuttle ($YDISP$). Several input locations were selected to simulate eccentric loading conditions. Off-axis forces of various magnitudes were applied at several locations on the shuttle. The output also was a metric set chosen to organize the comparison of FCBM three-dimensional characteristics. These output metrics included the following:

1. F_{max} magnitude (Figure 5.1).
2. F_{min} magnitude (Figure 5.1).
3. The roll of the shuttle (Figure 5.2(a)).
4. The pitch of the shuttle (Figure 5.2(b)).
5. The yaw of the shuttle (Figure 5.2(c)).
6. The Z-displacement of the shuttle (Figure 5.2(d)).

Each of these metrics provided a value for comparison. Videos of the predicted displacement were also used to visualize the three-dimensional characteristics of the FCBM as it was displaced. Pictures and videos taken with a microscope of the manufactured FCBMs as they were being displaced provided further understanding.

5.1 Locations of Displaced Nodes

Four locations on the FCBM shuttle were chosen for prescribing displacements. Figure 5.3 shows a diagram of these locations on the FCBM shuttle. The back-center node

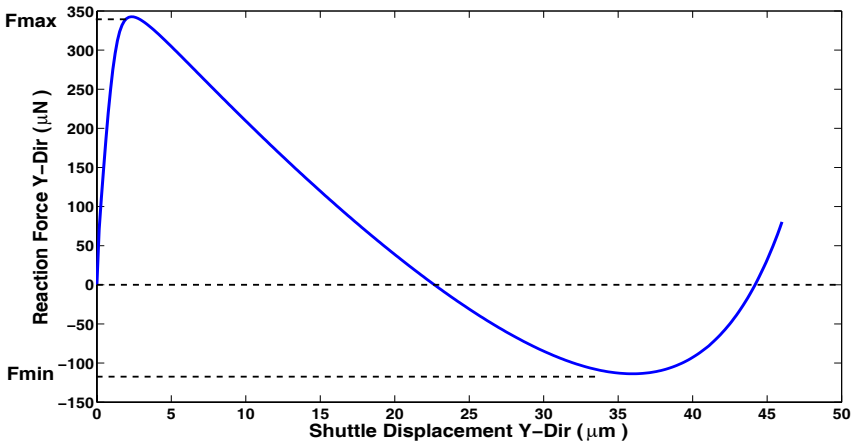

Figure 5.1: A graphical definition of F_{max} and F_{min}.

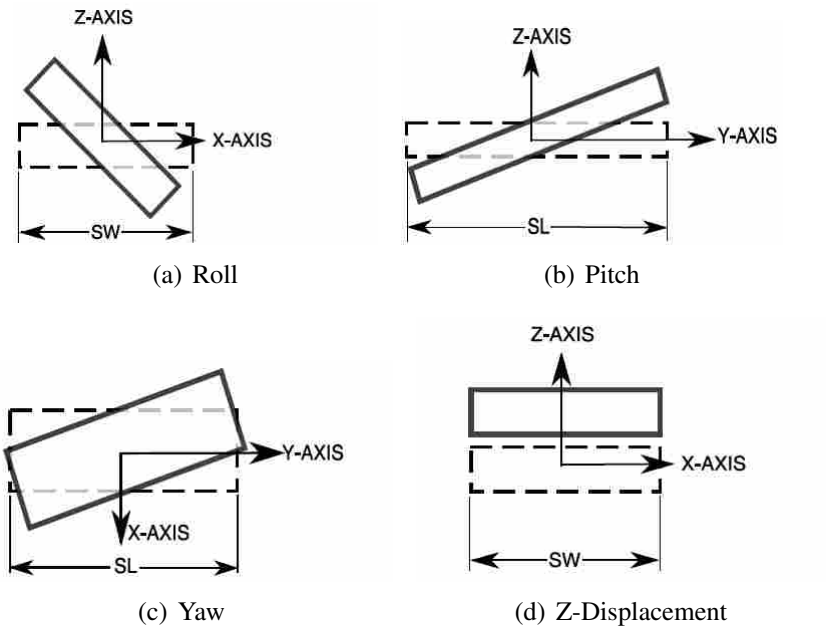

(a) Roll (b) Pitch

(c) Yaw (d) Z-Displacement

Figure 5.2: An illustration of the rotation and displacement metrics.

is centered in the X and Z direction, and is located on the back face of the shuttle. By prescribing a displacement here, the shuttle is being pulled into the second stable equilibrium position. The back-side node is located on the top right corner of the shuttle, and is centered in the Z direction. The center-side node is located on the right side of the shuttle, and is centered in the Y and Z direction. Finally, the front-side node is located on the bottom

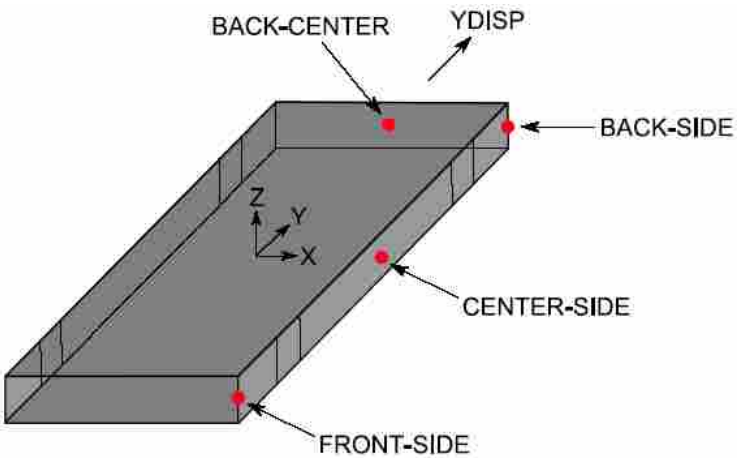

Figure 5.3: Location of displaced nodes on the FCBM shuttle.

right corner of the shuttle, and is centered in the Z direction. Due to symmetry across the YZ plane, there was no need for displacement locations on the left side of the shuttle.

By displacing the shuttle from the side nodes (back-side, center-side, and front-side nodes), the offset introduces a Z-axis torque to the mechanism. This offset simulates methods of displacement that are not perfectly centered on the shuttle face or back. For example, when testing the FCBMs for bistability, a probe can be used to push the FCBM shuttle to its alternate stable position. The large size of the probe in contrast to the small size of the shuttle makes it difficult to apply a force centered on the shuttle face, thus creating a Z-axis torque.

5.2 Off-Axis Forces

Six locations on the shuttle were selected for possible off-axis force application (Figure 5.4). The center-top node is centered on the top surface of the shuttle. The front-center-top node is located at the corner of the front face and top surface of the shuttle, and is centered in the X-direction. The back-center-top node is located at the corner of the top surface and back face of the shuttle, and is also centered in the X-direction. The back-side, center-side, and front-side nodes are the same nodes described previously. Due to symmetry, off-axis loads are applied only to one side of the shuttle. The selected nodes are located as far from the center of gravity of the shuttle as possible, maximizing the three-dimensional effects.

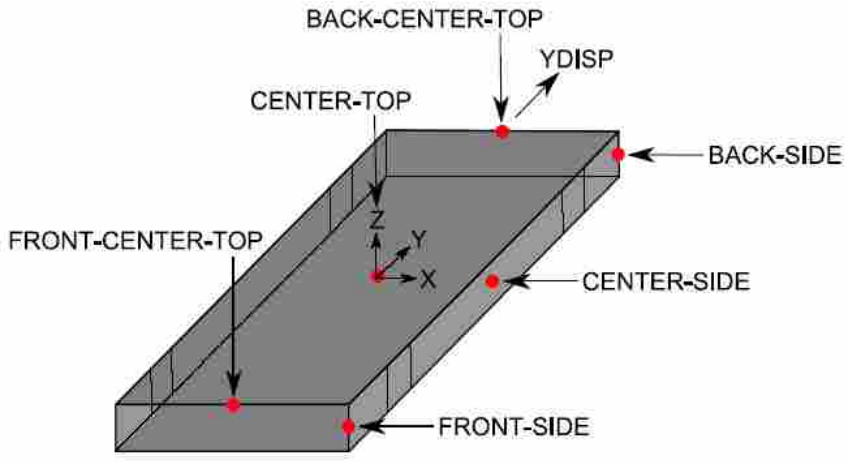

Figure 5.4: Locations of off-axis forces on the FCBM shuttle.

The off-axis forces applied to the front-center-top, center-top, and back-center-top nodes were applied in the negative Z-direction, while the off-axis forces applied at the front-side, center-side, and back-side nodes were applied in the negative X-direction. No additional force was applied in the Y-direction because a Y-direction displacement was already assigned to the shuttle.

Any magnitude of force can be applied to the available nodes. Because one application for the FCBMs is an acceleration sensing array, the unit of force used in the 3-D solid element and 3-D beam element model is equal to the force of gravity on the mass of the shuttle. This magnitude of force is defined as "g". Thus, 1000 g's is a force 1000 times the shuttle weight. To correlate g's with the magnitude of reaction force used in the force-displacement plots, 1 g is equal to 0.00024 μN. This approach is useful because the shuttle mass will be much larger than the mass of the legs when used in a sensing array.

5.3 Roll, Pitch, and Yaw

The roll, pitch and yaw of the shuttle were retrieved from the models at each time step of the analysis. These rotations were calculated using the X, Y, and Z displacement values retrieved from six critical nodes shown in Figure 5.5. These nodes were: back-side node (TR), front-side node (BR), front-side-l node (BL), back-side-l node (TL), back-center node (BC), and the front-center node (FC). The displacements of these nodes were used to calculate the roll, pitch, and yaw rotations of the shuttle at each time step. The

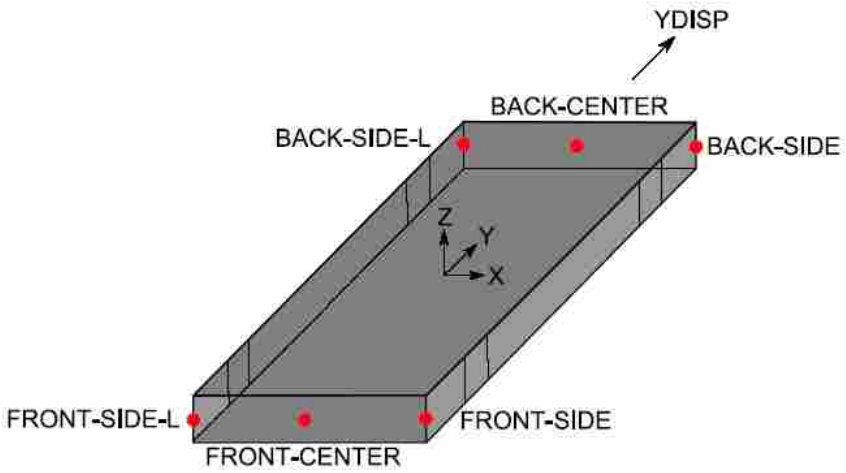

Figure 5.5: Roll, pitch, and yaw rotations of the FCBM shuttle.

equations are provided as equations 5.1 through 5.3. The subscripts of the variables in the equations represent the location of the node for a specific axis. For instance, TR_x represents the X-direction location of the TR node.

$$\text{Roll Rot.} = (\frac{180}{\pi}) \times sin^{-1} \frac{(TL_z - TR_z)}{\sqrt[2]{(TR_x - TL_x)^2 + (TR_z - TL_z)^2}} \tag{5.1}$$

$$\text{Pitch Rot.} = (\frac{180}{\pi}) \times sin^{-1} \frac{(BC_z - FC_z)}{\sqrt[2]{(BC_y - FC_y)^2 + (BC_z - FC_z)^2}} \tag{5.2}$$

$$\text{Yaw Rot.} = (\frac{180}{\pi}) \times sin^{-1} \frac{(BC_x - FC_x)}{\sqrt[2]{(BC_x - FC_x)^2 + (BC_y - FC_y)^2}} \tag{5.3}$$

5.4 Z-Displacement of Shuttle

The final metric for comparing and analyzing the three-dimensional behavior of the FCBMs is the Z-displacement of the shuttle. This information is particularly important because it was expected that the out-of-plane displacement of the mechanism is highly correlated to the force-displacement relationship. The Z-direction displacement of the shuttle center of gravity was recorded at each time step, and plotted as a function of the Y-displacement.

Table 5.1: Geometry variation designs.

Variable	*Bistable-A*	*Bistable-B*	*Large SL*	*Small SL*	*Large SW*	*Small SW*
$AL1$ (μm)	75.7	115.7	75.7	75.7	75.7	75.7
$AL2$ (μm)	57.3	97.3	57.3	57.3	57.3	57.3
RAL (μm)	126.3	166.3	126.3	126.3	126.3	126.3
AW (μm)	2.5	2.5	2.5	2.5	2.5	2.5
RAW (μm)	5.2	5.2	5.2	5.2	5.2	5.2
$THETA$ (°)	6.4	7.4	6.4	6.4	6.4	6.4
PHI (°)	5.6	5.6	5.6	5.6	5.6	5.6
$ALPHA$ (°)	6.6	6.6	6.6	6.6	6.6	6.6
T (μm)	3.5	3.5	3.5	3.5	3.5	3.5
EX (GPa)	164	164	164	164	164	164
PR	0.22	0.22	0.22	0.22	0.22	0.22
$YDISP$ (μm)	46	71	46	46	46	46
SL (μm)	100	100	150	75	100	100
SW (μm)	30	30	30	30	50	10

A positive displacement is defined as a displacement in the positive Z-direction, according to the notation in Figure 5.2(d). It should be noted that the 3-D solid element and 3-D beam element models do not include the substrate that the mechanisms are produced on. While not affecting the displacement in the positive Z-direction, the models can provide shuttle displacement data in the negative Z-direction larger than would be allowed by the substrate. Because of the resulting input forces and friction, contact with the substrate is usually undesirable and it is advantageous to avoid it. The results analysis can be used to determine if contact with the substrate may be a problem under certain conditions.

5.5 Geometry Variation

It was desired to understand how alternate geometries would affect the 3-D characteristic of FCBMs. A pilot test was run on seventeen designs that were selected using a fractional factorial statistical approach, and one of these designs, Bistable-B, was selected as an alternate design for further study. The dimensions of this new design are listed in Table 5.1.

Design Bistable-B offered alternate values for $AL1$, $AL2$, RAL, $THETA$, PHI, and $ALPHA$. The thickness (T), modulus of elasticity (EX), and Poisson's ratio (PR) remained

constant. Due to the different length of the compliant and rigid legs, the Bistable-B model was capable of displacing a larger distance when moving to its alternate stable equilibrium position. When comparing the original Bistable-A design to the Bistable-B design, only two conditions were considered. First, no off-axis forces were applied, then and an off-axis force was applied at the center-top node in the negative Z-direction. In the latter case, several magnitudes of force were used, each resulting in a separate analysis.

Another subset of the test suite was created by altering the shuttle geometry of the Bistable-A design. In this case, each of the variables remained the same as the Bistable-A design except for *SW* (shuttle width) and *SL* (shuttle length). The purpose of this test was to understand how the geometry of the shuttle affected the stability of the device. The nominal size of the shuttle being tested thus far was $SL = 100\ \mu$m and $SW = 30\ \mu$m. To alter the geometry, a new high and low value for each of the two dimensions was provided. Four new shuttle geometry conditions were created, and are listed in Table 5.1.

The last subset of the test suite included increasing the thickness of the mechanism. Altering the thickness was highly beneficial because it provided rotational stiffness data, and yet was still very simple to adjust. The largest out-of-plane thickness that can be obtained using MUMPs is 3.5 μm, and this value was used in the previous models. To provide as much stability to the mechanisms as possible, this value was nominally used in each of the models. To investigate the effects of thickness, a model with a thickness of 7.0 μm was used, with all other variables the same as for the Bistable-A design.

5.6 Solution Behavior

An attempt was made to keep the model inputs as consistent as possible while being used in the test suite. However, due to the non-linear nature of the 3-D solid element and beam element models, some designs would not converge to a solution. To remedy this, several methods were used. First, the number of time steps was increased. One cause of non-convergence was that the model attempted to displace the FCBM shuttle too far each time step. By increasing the number of time steps while keeping the *YDISP* variable constant, the resolution of the model was increased. This method was successful a large majority of the time. However, if this method did not assist with model convergence, the

second method was to manually adjust the convergence tolerances. The tolerance was only tightened, providing a model that could produce higher resolution results. The typical values used when tightening the convergence tolerance for both displacement (u) and force (f) was 0.000001, with a minimum tolerance of 0.01. At times, a combination of both methods was used to assist with model convergence.

Sometimes, however, the model did not converge to a solution. This was typical when the applied forces were large, and very commonly near the region around F_{max} or F_{min} on the force-displacement plot. An attempt was made to manually control the increments of time steps throughout the entire theoretical force-displacement plot. The regions near F_{max} or F_{min} were refined, while the regions before F_{max}, after F_{min}, or between the two were coarsened. This model was very ill-behaved, and would not converge to a solution even when inputs that had previously proved successful were included.

5.7 Conclusions

A test suite of ANSYS runs was constructed to better understand the 3-D nature of FCBMs, including Phenomenon 1 and Phenomenon 2. A nominal FCBM design, Bistable-A, served as the benchmark for comparison. An analysis of the effects of various eccentric loading conditions and off-axis applied forces was a large majority of the test suite. The off-axis forces were applied to several locations on the FCBM shuttle, and at incrementally increasing magnitudes. To assure that the general results of the test suite were not restricted to a specific FCBM geometry, an FCBM with different dimensions than Bistable-A was included in the analysis. The effects of increased out-of-plane thickness and altered shuttle dimensions were also included in the test suite. Six metrics were chosen for the comparison of each analysis.

Chapter 6

Model Results

6.1 The 3-D Effects of the Models

The three-dimensional behavior of FCBMs is dependent on the method of displacement, as well as the location and direction of off-axis applied forces. This was supported by results that differed when displacing the back-center node, and when equally displacing each node on the back face of the shuttle. When displacing the shuttle from a single node, the shuttle was free to roll, pitch, and yaw. In contrast, when prescribing displacement to several nodes on a face, the shuttle was constrained from this motion. These results suggest that the three-dimensional effects of FCBMs may vary, depending on their loading condition. While Figure 4.8 was initially used to explain the difference between the experimental MUMPs data and model predictions, it supports this idea as well. A 2-D analysis lacked the ability to predict the three-dimensional effects, while the 3-D analysis provided additional insight to the behavior of the FCBMs. The following sections provide the results of the test suite, helping to characterize this three-dimensional behavior.

6.2 Locations of Displaced Nodes

Figure 6.1 shows the force-displacement curves of the FCBM for applied displacements at various nodes. Table 6.1 lists the peak reaction forces for these curves. The force-displacement plots were nearly identical when the back-center or back-side nodes were displaced. Under these conditions, the magnitude of F_{max} was largest. When displacement was applied to the center-side node, a similar shaped force-displacement plot was produced, but with smaller peak reaction forces. When the shuttle was displaced from the front-side node, the general shape of the force-displacement plot changed. The segment

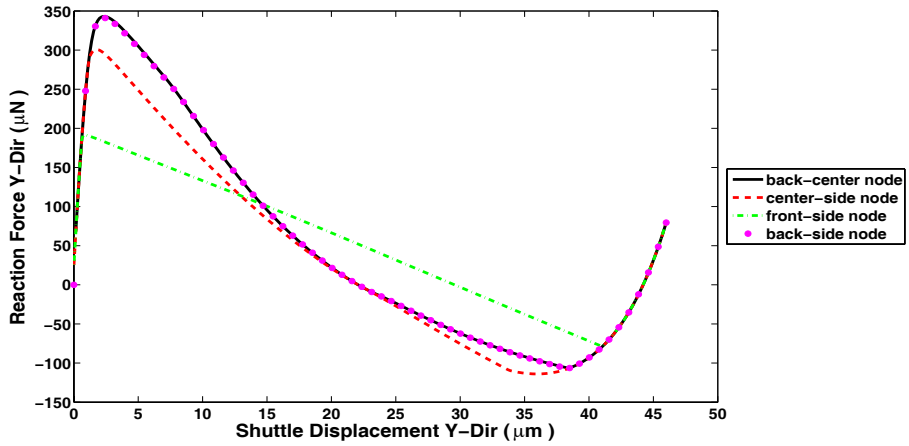

Figure 6.1: Comparison of displacement locations produced by the 3-D solid element model when no off-axis forces was applied.

Table 6.1: Results for applied displacement at various nodes.

Displaced Node	F_{max} (μN)	F_{min} (μN)
BACK-CENTER NODE	343.1	-106.5
CENTER-SIDE NODE	300.8	-113.9
FRONT-SIDE NODE	191.4	-78.3
BACK-SIDE NODE	341.1	-107

of the plot between F_{max} and F_{min} became nearly linear, and the magnitudes of F_{max} and F_{min} decreased.

It is understandable that the force-displacement plot produced when prescribing displacement at the back-center node is similar to the plot for the back-side node. In both cases, the FCBM is being pulled into its alternate stable position. The system is consistently well behaved when being pulled rather than pushed. To illustrate this behavior, consider pulling a trailer behind a vehicle while traveling. The vector of the trailer's travel will likely remain nearly equal to that of the vehicle pulling it due to the force displacement at the front of the trailer. Now, consider pushing the trailer with the same vehicle. Slight modifications of the vehicle force vector could dramatically affect the trailer's displacement vector. However, the motion may be very different when the FCBM is pushed from the front-side node, resulting in a force-displacement relationship with a lower peak reaction force. An intermediate behavior may be produced as well, as is the case when the center-

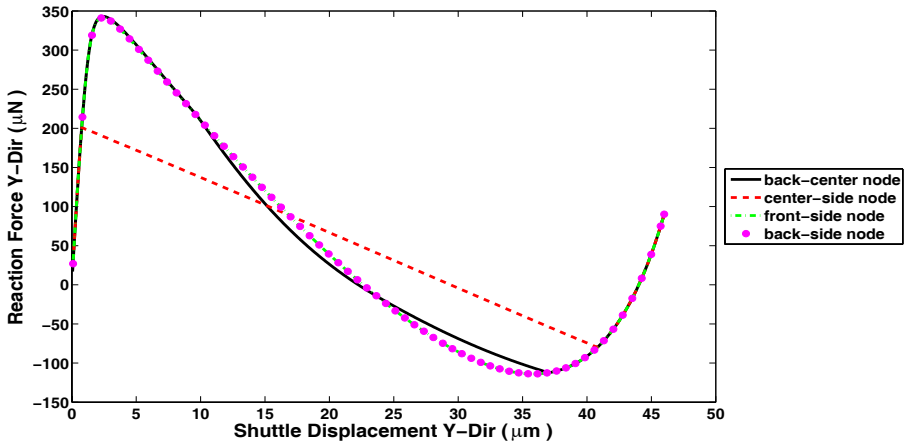

Figure 6.2: Comparison of displacement locations produced by the 3-D beam element model when no off-axis force was applied.

side node was displaced. These characteristics suggest that the location of the displaced nodes in the Y-direction is a large factor affecting the force-displacement relationship. In contrast, the small difference in the force-displacement curves when the back-center and back-side nodes were displaced suggests that the location of the displaced nodes in the X-direction does not have as large of an effect on the force-displacement relationships.

The results of the 3-D beam element model are additionally shown in Figure 6.2. Two of the trends produced by the 3-D solid element model are repeated. First, the magnitude of F_{max} is largest when either the back-center node, or back-side nodes are displaced. The magnitude of these reaction forces are similar, supporting the idea of well behaved systems being produced when pulling the FCBM to its alternate stable position. Second, there does not appear to be a significant correlation between the X-direction location of the displaced node and the force-displacement plots. Displacing the back-center, front-side, or back-side nodes result in similar F_{max} and F_{min} values.

6.3 Off-Axis Forces

Results were calculated for models incorporating various locations and magnitudes of applied off-axis force (Figure 5.4). Though the six off-axis force conditions were incorporated in each of the four displacement conditions, only the results associated with displacement at the back-center node are shown here. A summary of the results will be

given first, followed by an explanation of the three-dimensional trends. Many intermediate magnitudes of applied force were analyzed, but only a few illustrative plots are provided here.

Figure 6.3 displays the results of displacing the shuttle at the back-center node while applying a Z-direction off-axis force at the center-top node for various magnitudes of applied force. As expected, applying a 1 g load did not have a significant effect on the force-displacement plot relationship. The same was true for force magnitudes up to and including 750 g's, which is equivalent to 0.18 μN. However, a significant difference in the force-displacement plot was produced when a magnitude of 850 g's was applied, which is equivalent to 0.204 μN. The general trends of these two force-displacement plots will be referred to as Phenomenon 1 (similar to the plots produced when 1 through 750 g's was applied), and Phenomenon 2 (similar to the plot produced when 850 g's was applied). The magnitude of applied force causing a transition from Phenomenon 1 to Phenomenon 2 will be defined as "F_{tr}". Thus, F_{tr} for this analysis is between 750 and 850 g's. The force-displacement plots generated by applying forces greater than 850 g's reacted in the same manner as the 850 g's condition, and were excluded from Figure 6.3. The transition from a Phenomenon 1 condition to a Phenomenon 2 condition caused F_{max} to decrease from 343.0 μN to 90.7 μN. In addition, the reaction forces associated with Phenomenon 2 remained positive as the mechanism was displaced (the value of F_{min} increased from -106.3 μN to 15.6 μN), which means the mechanism was not bistable.

Applying off-axis forces to the front-center-top and back-center-top nodes produced similar trends, as shown in Figures 6.4 and 6.5. The transition force ranges, F_{tr}, are listed in Table 6.2. As was the case when force was applied to the center-top node, an increase in applied force beyond F_{tr} did not alter the force-displacement plots significantly, and are not shown in the figures. In both cases, F_{max} and F_{min} were approximately 343.0 and -106.0 μN, respectively when Phenomenon 1 occurred. When the Phenomenon 2 transition occurred, the peak reaction forces of F_{max} and F_{min} decreased to 90.6 and 15.9 μN, respectively.

Further understanding of the three-dimensional behavior was gained when the back-center node was displaced, and X-direction off-axis forces were applied to the center-side node. A similar Phenomenon 1 plot was produced, but it was maintained for applied forces

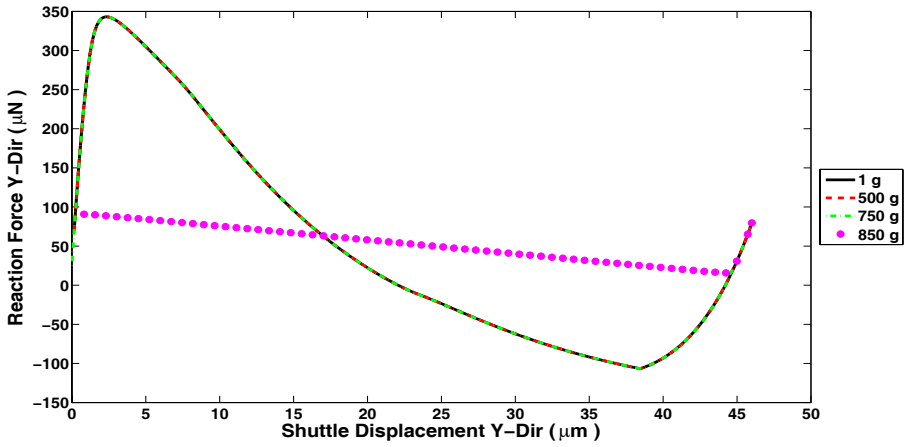

Figure 6.3: Comparison of force-displacement plots when the back-center node was displaced, and a Z-direction off-axis force was applied to the center-top node.

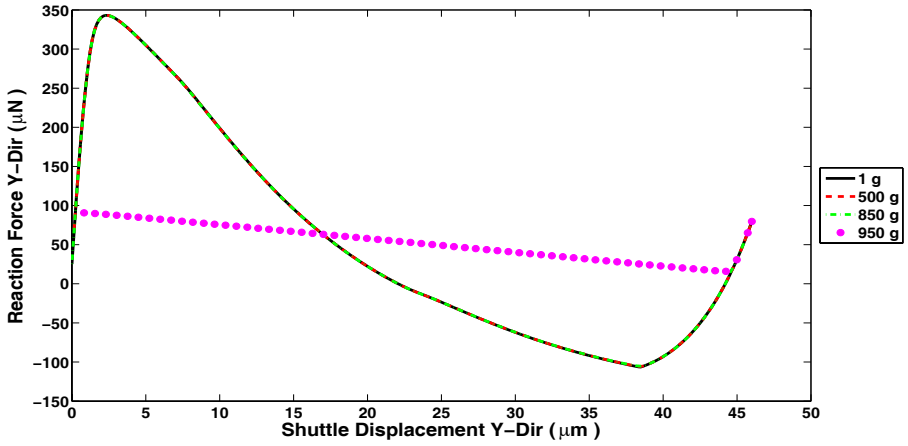

Figure 6.4: Comparison of force-displacement plots when the back-center node was displaced, and a Z-direction off-axis force was applied to the front-center-top node.

Table 6.2: F_{tr} magnitudes for Phenomenon 1 and 2 when the back-center node was displaced.

Force Location	*Force Direction*	*Transition Force (F_{tr}) (g's)*
CENTER-TOP NODE	-Z	$750 < F_{tr} \leq 850$
FRONT-CENTER-TOP NODE	-Z	$850 < F_{tr} \leq 950$
BACK-CENTER-TOP NODE	-Z	$350 < F_{tr} \leq 450$
CENTER-SIDE NODE	-X	$1{,}250{,}000 < F_{tr} \leq 1{,}500{,}000$
FRONT-SIDE NODE	-X	$950{,}000 < F_{tr} \leq 1{,}000{,}000$
BACK-SIDE NODE	-X	$950{,}000 < F_{tr} \leq 1{,}000{,}000$

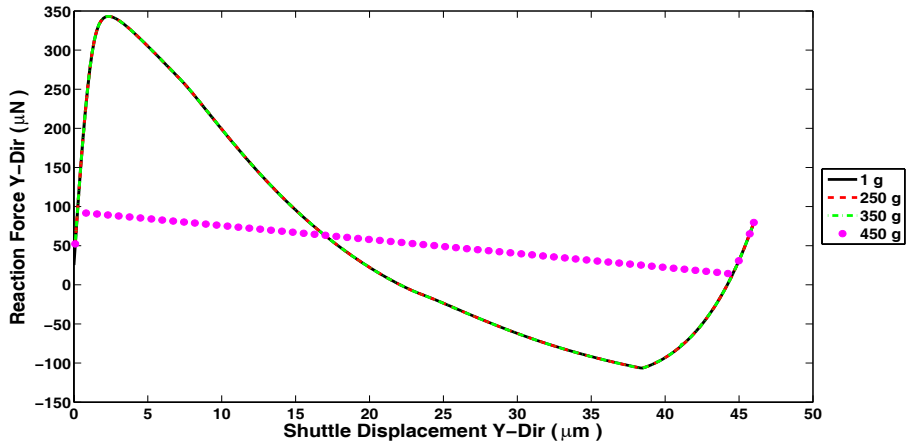

Figure 6.5: Comparison of force-displacement plots when the back-center node was displaced, and a Z-direction off-axis force was applied to the back-center-top node.

several orders of magnitude larger. Figure 6.6 shows that increases in applied force up to and including 1.25 x10^6 g's (equivalent to 300.0 μN) consistently produced a Phenomenon 1 force-displacement plot. Unlike applied forces in the Z-direction, applied X-direction forces caused a shift in F_{max} for increasing applied forces. When the X-direction applied force reached 1.5 x10^6 g's (equivalent to 360.0 μN), Phenomenon 2 results were produced, but the resulting F_{max} and F_{min} magnitudes were nearly twice as large as those generated when the off-axis forces were applied in the Z-direction. Unlike conditions caused by Z-direction forces, when forces were applied in the X-direction, the system remained bistable. Similar characteristics were generated when forces were applied to the front-side and back-side nodes (Figure 6.7, Figure 6.8). The F_{tr} results from applying an off-axis force in the X-direction are also listed in Table 6.2.

Several important characteristics were learned from this analysis. First, inconsistent force-displacement plots result when two phenomenon conditions exist. Phenomenon 1 provided a force-displacement plot that was similar to model predictions excluding applied off-axis forces. The peak reaction forces were largest when this phenomenon occurred, with Phenomenon 2 peak reaction forces sometimes being only a third of the Phenomenon 1 values. A Phenomenon 2 force-displacement plot followed the Phenomenon 1 plot initially, but soon transitioned into a nearly linear force-displacement path toward the second stable

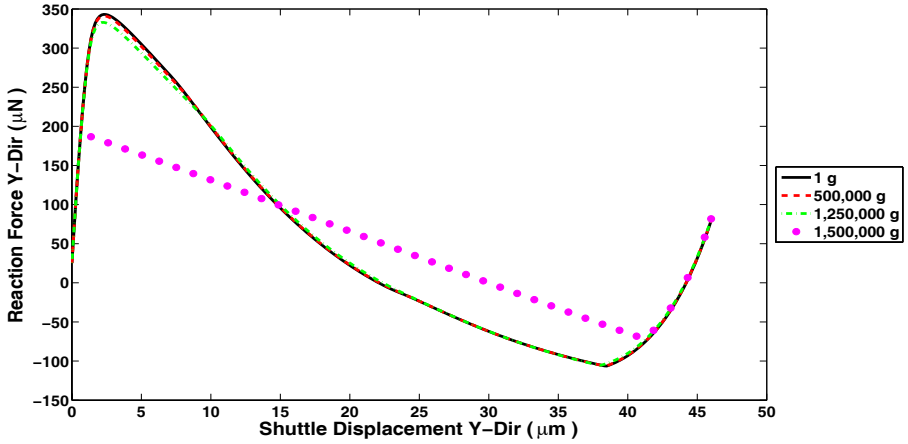

Figure 6.6: Comparison of force-displacement plots when the back-center node was displaced, and a X-direction off-axis force was applied to the center-side node.

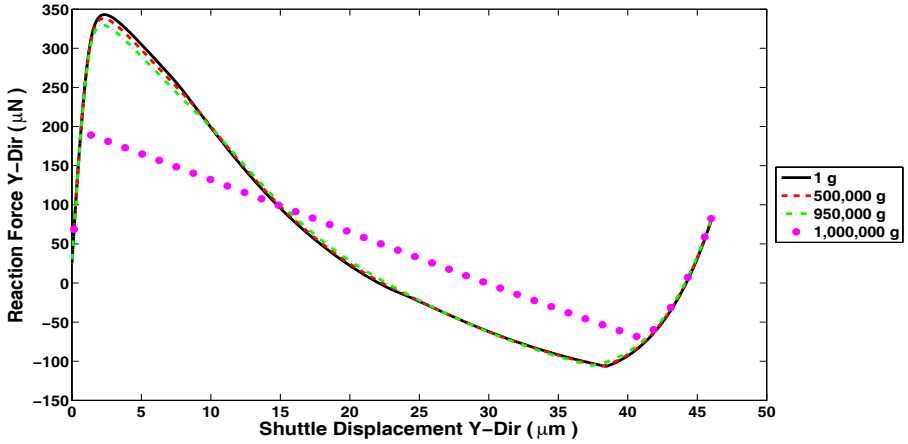

Figure 6.7: Comparison of force-displacement plots when the back-center node was displaced, and a X-direction off-axis force was applied to the front-side node.

position. This linear path eventually intersected the Phenomenon 1 force-displacement plot near the F_{min} region.

A device that is bistable under Phenomenon 1 conditions may not be bistable under Phenomenon 2 conditions. When a Phenomenon 2 force-displacement plot remained bistable, the magnitude of F_{min} would frequently be small, and only slightly negative. FCBMs that generate these types of force-displacement characteristics tend to lack a high level of bistable consistency. For instance, the uncertainty in FCBM geometry due to the manufacturing process [2] could shift the force-displacement curve to smaller magnitudes.

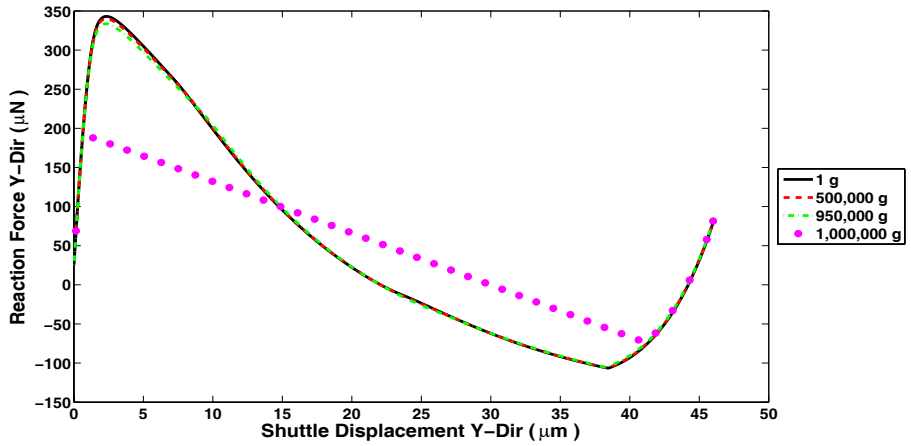

Figure 6.8: Comparison of force-displacement plots when the back-center node was displaced, and a X-direction off-axis force was applied to the back-side node.

This uncertainty could affect a mechanism's bistability. Thus, devices undergoing Phenomenon 2 behavior have more unpredictable results.

Table 6.2 shows that F_{tr} magnitudes greatly differ when comparing the X-direction and Z-direction applied force conditions, with those in the X-direction being at least 1000 times larger than for the Z-direction. It can be deduced that the FCBMs are less sensitive to X-direction accelerations than acceleration in the Z-direction. Comparing F_{tr} magnitudes to F_{max} shows that F_{tr} is about three orders of magnitude smaller than F_{max} for Z-direction forces, and F_{tr} and F_{max} have similar orders of magnitude for X-direction forces.

6.4 Roll, Pitch, and Yaw

A correlation between the roll, pitch, and yaw rotations was revealed for Phenomenon 1 and Phenomenon 2 conditions. This section primarily provides results for displacement at the back-center node when a Z-direction off-axis force was applied to the center-top node, and displacements at the back-center node when a X-direction off-axis forces was applied to the center-side node. These conditions are shown because the resulting general trends were characteristic of most other conditions.

Figure 6.9 displays the roll rotation results when displacements were applied to each of the four designated displacement locations without off-axis forces. Displacing the shuttle at either the back-center node, center-side node, or back-side node produced

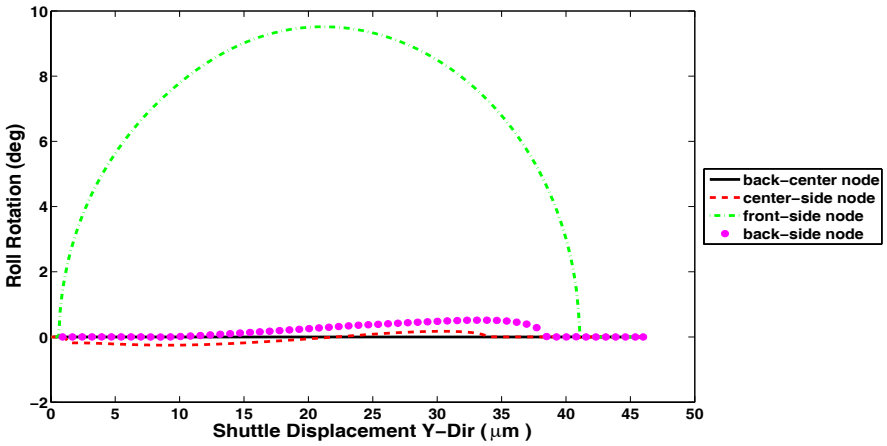

Figure 6.9: Comparison of roll rotation plots when no off-axis force was applied.

small roll rotations. It is not surprising that displacing the back-center node would produce nearly zero roll, while displacing the center-side and back-side nodes would produce slightly larger roll values. A Y-axis torque is introduced to the FCBM shuttle when displacing the mechanism from these nodes. In contrast, no moment exists when pulling the shuttle from the back-center node. The instability caused by pushing the shuttle from the front-side node produced largely different roll rotation results, increasing the roll to nearly 9.5 °.

Figure 6.10 shows that displacing the shuttle from the back-center, center-side, or back-side nodes produced similar peak pitch magnitudes of nearly 20 °. However, displacing the front-side node generated a pitch of only 5 °, a quarter of that for the other three conditions. This can once again be explained by the inconsistent behavior associated with pushing rather than pulling the FCBM into its second stable equilibrium position.

The yaw rotation plot in Figure 6.11 shows that each of the four displacement conditions produce nearly zero yaw. There are slight differences in the shapes of the plots, but none of the four conditions exceed 0.25 °. The slightly negative values are an effect of a Z-axis torque caused by displacing the right side of the shuttle. In contrast, by pulling the shuttle from the back-center node, no torque is applied, and the shuttle does not yaw.

Including off-axis applied forces to the model revealed important characteristics as well. The results of displacing the back-center node, while applying Z-direction off-axis

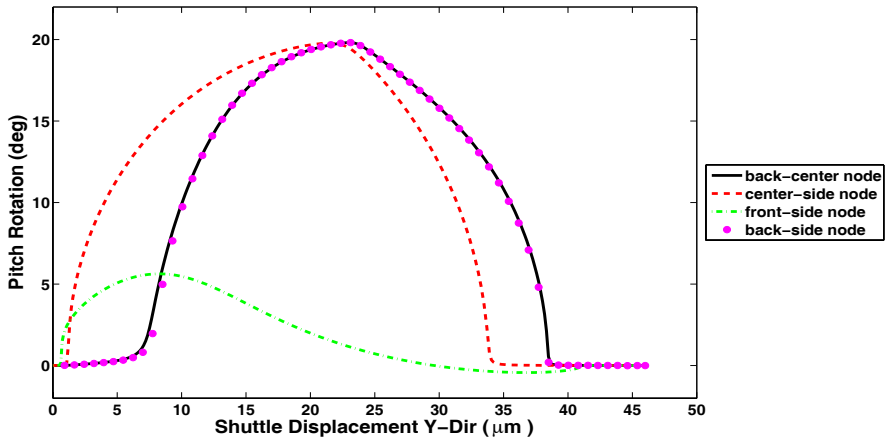

Figure 6.10: Comparison of pitch rotation plots when no off-axis force was applied.

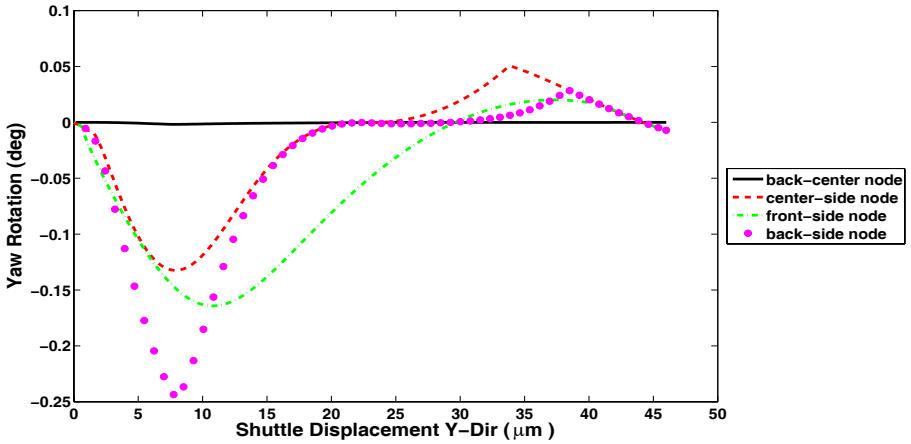

Figure 6.11: Comparison of yaw rotation plots when no off-axis force was applied.

forces to the center-top node are used to describe the general results. The transition forces, F_{tr}, listed in Table 6.2 also apply to the roll, pitch, and yaw results. Figure 6.12 shows the roll rotation associated with Phenomenon 1 and Phenomenon 2. Neither phenomenon produced significant roll. Figure 6.13 shows the pitch data for the two phenomenon. Large pitch rotations correlate with Phenomenon 1, while Phenomenon 2 conditions result in nearly zero pitch. Figure 6.14 shows that the yaw values were also nearly zero for both phenomenon conditions, but with different trends for Phenomenon 1 and Phenomenon 2. The same general trends continued when displacement was applied to the back-center node, and an X-direction off-axis force was applied to the center-side node.

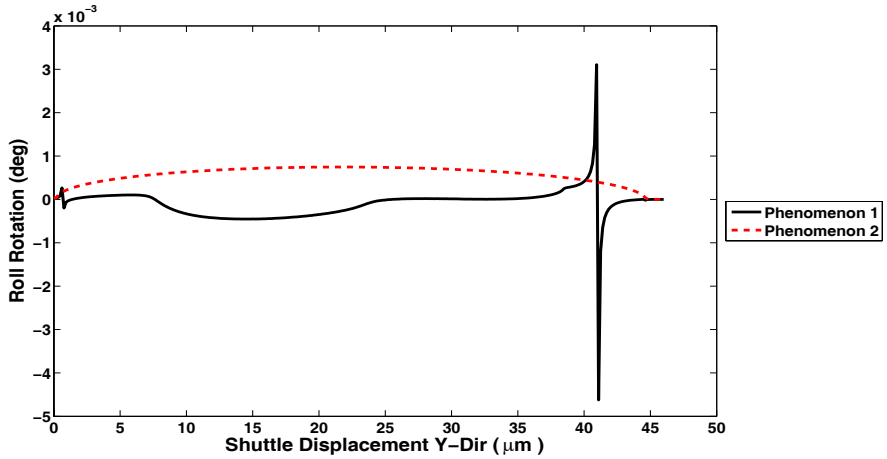

Figure 6.12: Comparison of roll rotation when the back-center node was displaced, and a Z-direction off-axis force was applied to the center-top node.

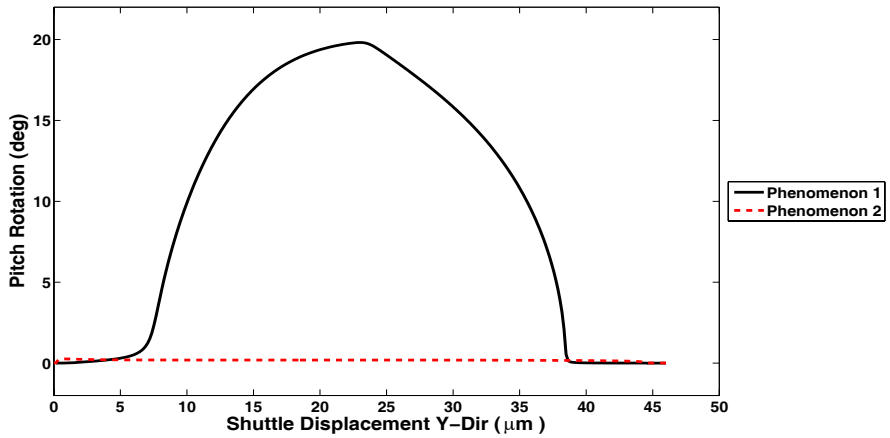

Figure 6.13: Comparison of pitch rotation when the back-center node was displaced, and a Z-direction off-axis force was applied to the center-top node.

Figure 6.15 correlates with Figures 6.12 through 6.14, and shows the FCBM when displaced approximately 23 μm while experiencing Phenomenon 1 and Phenomenon 2 conditions. When displaced this distance, Phenomenon 1 predicted the largest pitch, and nearly zero roll or yaw, while Phenomenon 2 predicted nearly zero roll, pitch, or yaw.

To assist the visualization of the three-dimensional motion, videos were created to show the motion while moving from the first to the second stable equilibrium position. Figure 6.16 displays seven positions of the device motion undergoing Phenomenon 1 motion. Notice that the roll and yaw are nearly zero, while the pitch increases to nearly 20 °.

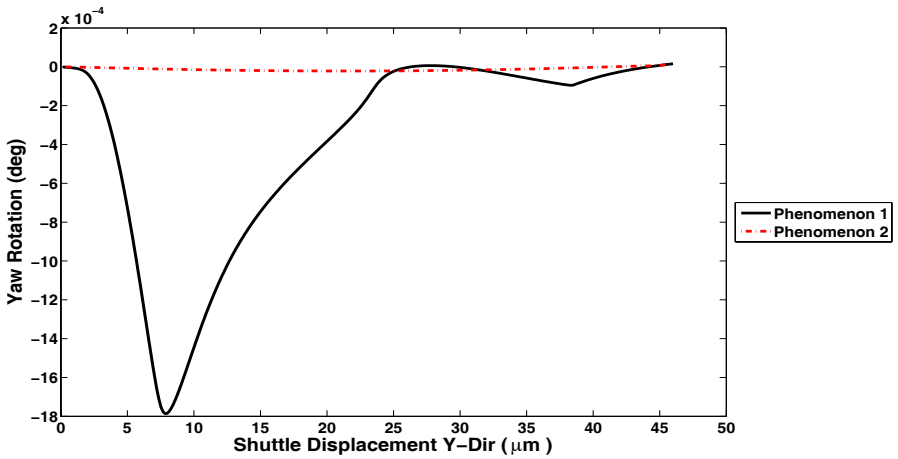

Figure 6.14: Comparison of yaw rotation when the back-center node was displaced, and a Z-direction off-axis force was applied to the center-top node.

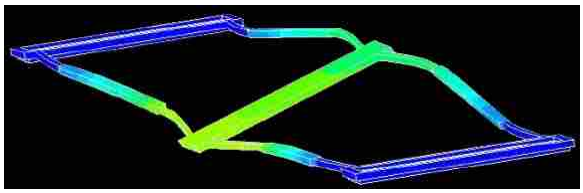

(a) Phenomenon 1

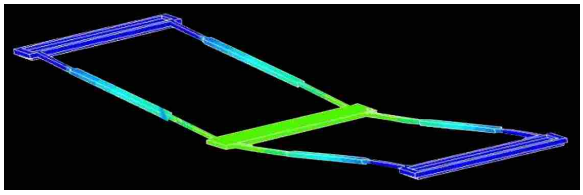

(b) Phenomenon 2

Figure 6.15: The Phenomenon 1 and Phenomenon 2 FCBM predictions when displaced 23 μm.

Figure 6.17 displays the motion when a Z-direction off-axis force greater than F_{tr} was applied, causing Phenomenon 2. This resulted in nearly zero pitch, and greatly increased the out-of-plane motion.

The same general trends continued when displacement was applied to the back-center node, and an X-direction off-axis force was applied to the center-side node. Figure 6.18 shows that the roll rotation is small for Phenomenon 1 conditions. Once the applied force exceeded F_{tr} and Phenomenon 2 conditions existed, the roll rotation increased to nearly 9.5 °.

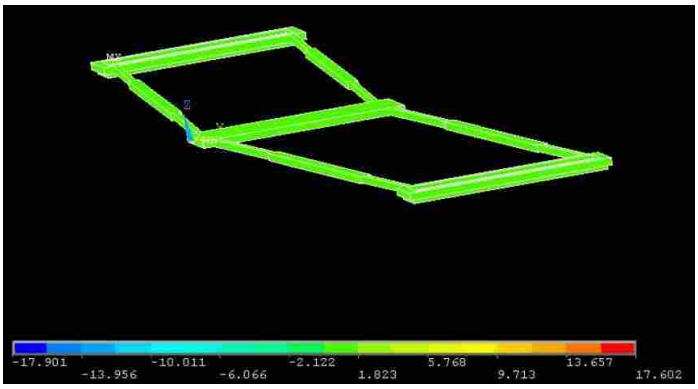

(a)

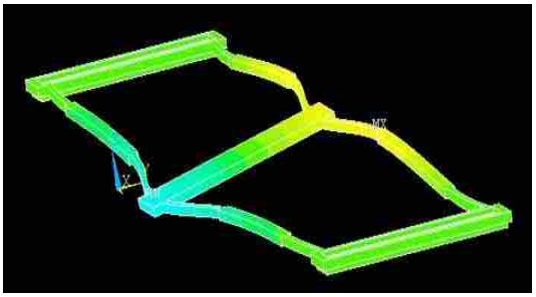

(b)

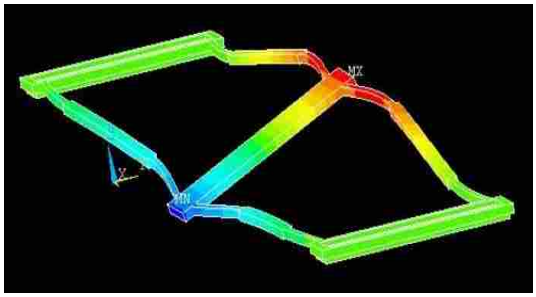

(c)

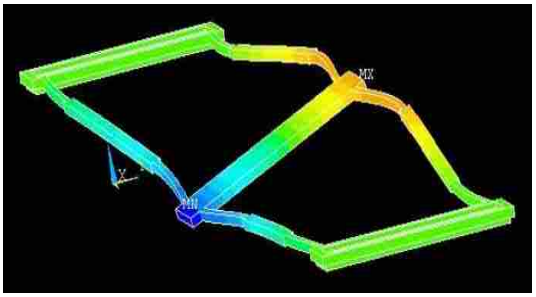

(d)

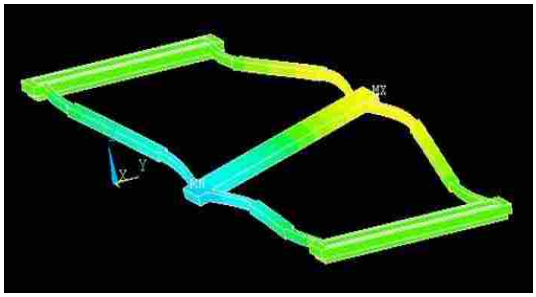

(e)

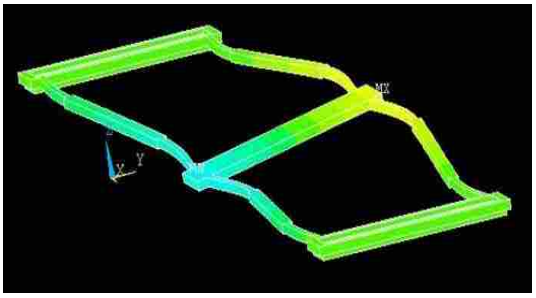

(f)

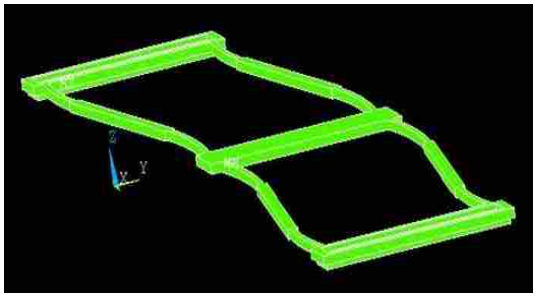

(g)

Figure 6.16: Seven positions of a device undergoing Phenomenon 1 motion.

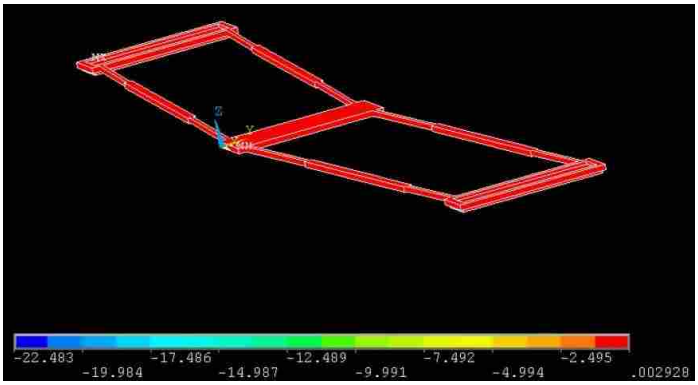

(a)

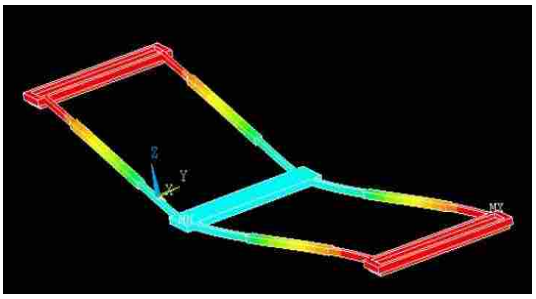

(b)

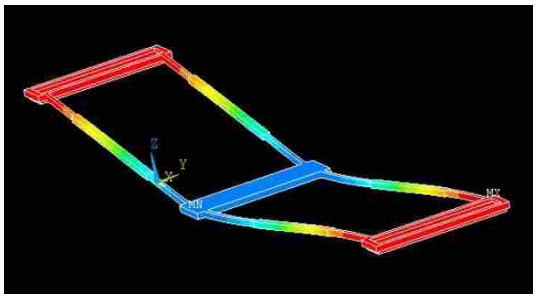

(c)

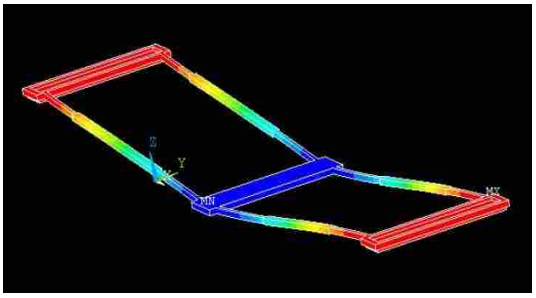

(d)

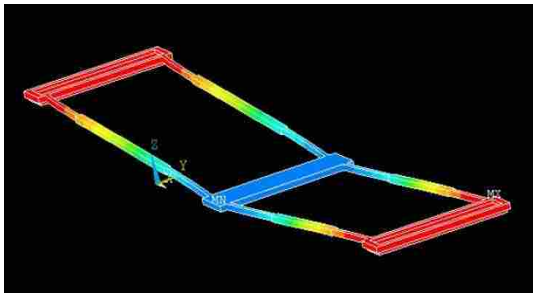

(e)

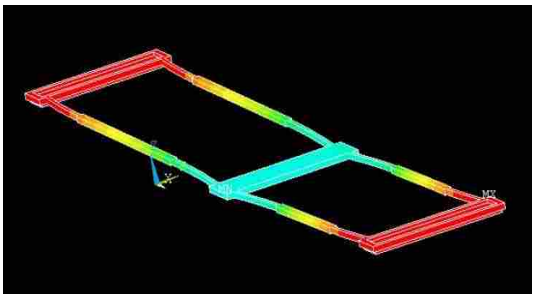

(f)

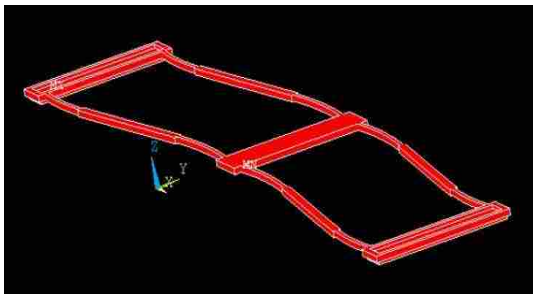

(g)

Figure 6.17: Seven positions of a device undergoing Phenomenon 2 motion.

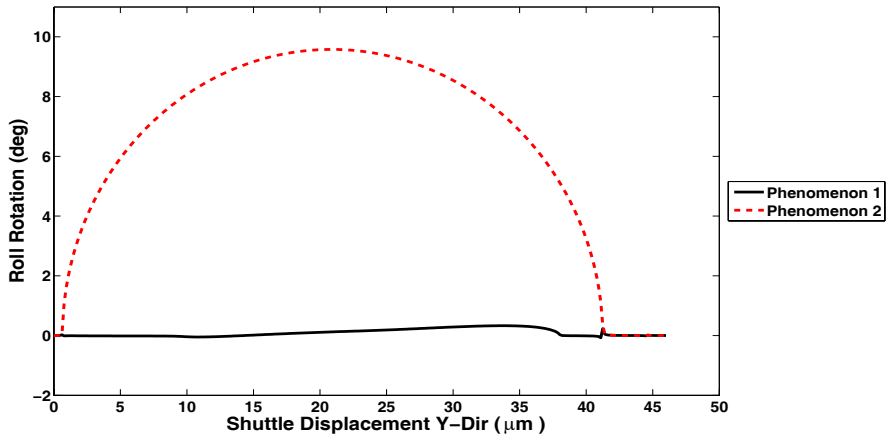

Figure 6.18: Comparison of roll rotation plots when the back-center node was displaced, and a X-direction off-axis force was applied to the front-side node.

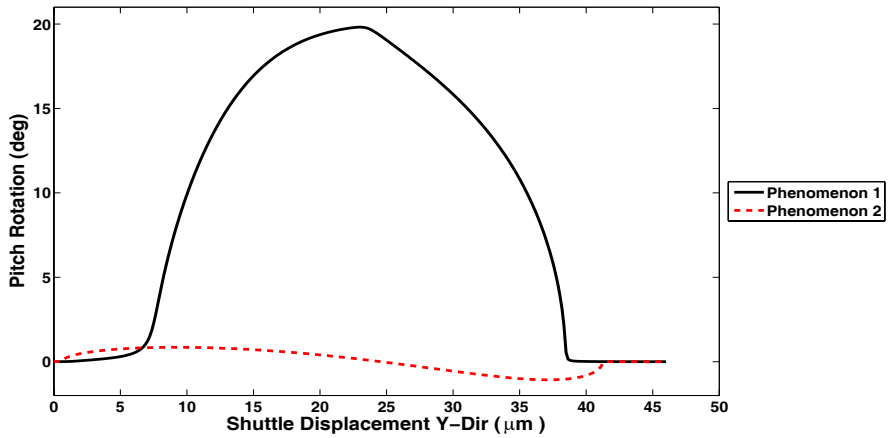

Figure 6.19: Comparison of pitch rotation plots when the back-center node was displaced, and a X-direction off-axis force was applied to the front-side node.

Figure 6.19 shows that the pitch rotation was larger for Phenomenon 1. The peak magnitudes of pitch decreased slightly as the applied forces increased, but continued to remain near 20 °. Once the applied force caused a transition to Phenomenon 2, the pitch rotation was reduced to approximately 1 °.

The trends continue when analyzing the yaw rotation plots. Figure 6.20 shows that the yaw rotation is small for both phenomenon conditions. The yaw rotations associated with Phenomenon 1 tended to slightly increase as the applied forces increased. In this

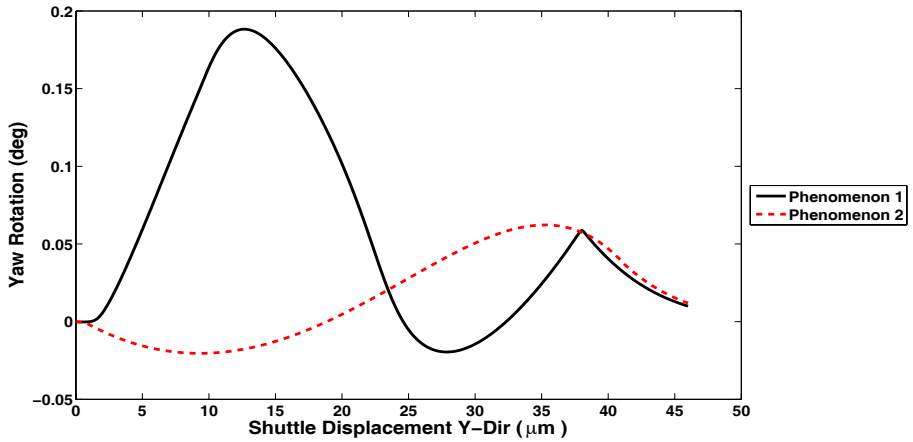

Figure 6.20: Comparison of yaw rotation plots when the back-center node was displaced, and a X-direction off-axis force was applied to the front-side node.

case, a maximum yaw rotation of approximately 0.2 °is reached before transitioning to approximately -0.025 °for Phenomenon 2.

6.5 Z-Displacement of Shuttle

An examination of the Z-displacement of the shuttle provides additional insight to the three-dimensional characteristics of FCBMs. Figure 6.21 displays the Z-displacement results when displacements were applied to each of the four designated displacement locations without off-axis forces. Prescribing displacement at the back-center and back-side nodes once again generated similar results. Displacing the shuttle from the center-side node produced larger Z-displacements. In each of the three cases, the plots show that the shuttle tends to displace in the positive and negative direction before reaching the second stable equilibrium position. When pushing the shuttle at the front-side node, the Z-displacement remains positive and smaller than the other three conditions.

Z-displacement data was collected and analyzed when applying increasing off-axis forces. Figure 6.22 displays the results of displacing the back-center node, and applying a Z-direction off-axis force to the center-top node. Phenomenon 2 behavior has approximately a 20 μm greater Z-displacement than the Phenomenon 1 condition. These displacements are also shown in Figures 6.16 and 6.17. Applying Z-direction off-axis forces to the front-center-top and back-center-top nodes produced similar results. These results

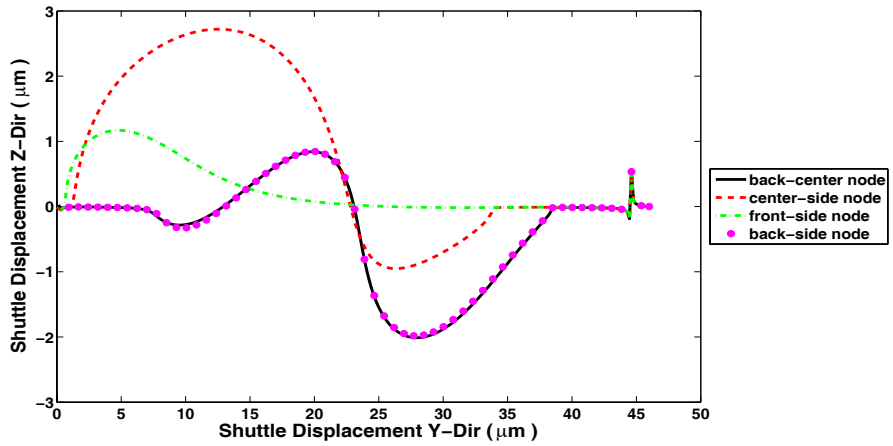

Figure 6.21: Comparison of Z-displacement plots when several nodes were displaced, and no off-axis force was applied.

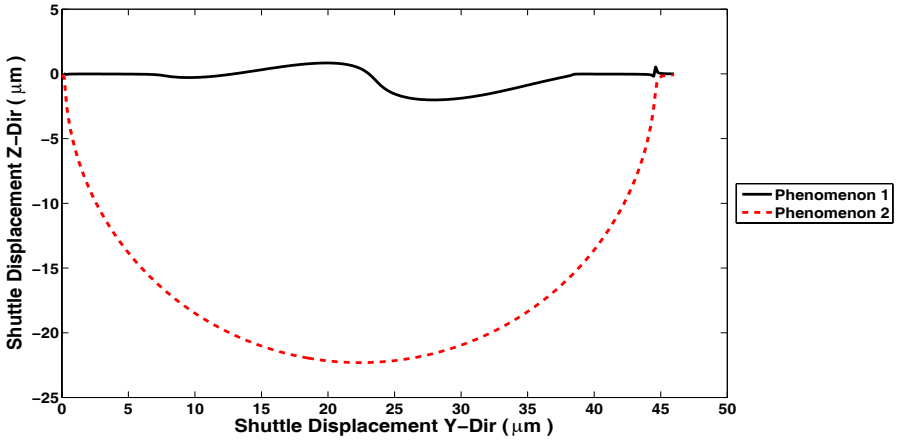

Figure 6.22: Comparison of Z-displacement plots when the back-center node was displaced, and a Z-direction off-axis force was applied to the center-top node.

suggest that Phenomenon 1 tends to produce similar and small values of Z-displacement when a Z-direction off-axis force is applied, while Phenomenon 2 results tend to produce larger Z-displacements. Displacing the back-center node while applying X-direction forces produced similar results as well (Figure 6.23).

Phenomenon 1 characteristics tend to generate smaller Z-displacements, and the plots tend to have multiple peaks and troughs. In contrast, Phenomenon 2 characteristics tend to generate larger Z-displacements with a unimodal relationship with the Y-displacement. The models would occasionally predict a shift in Z-displacement direction,

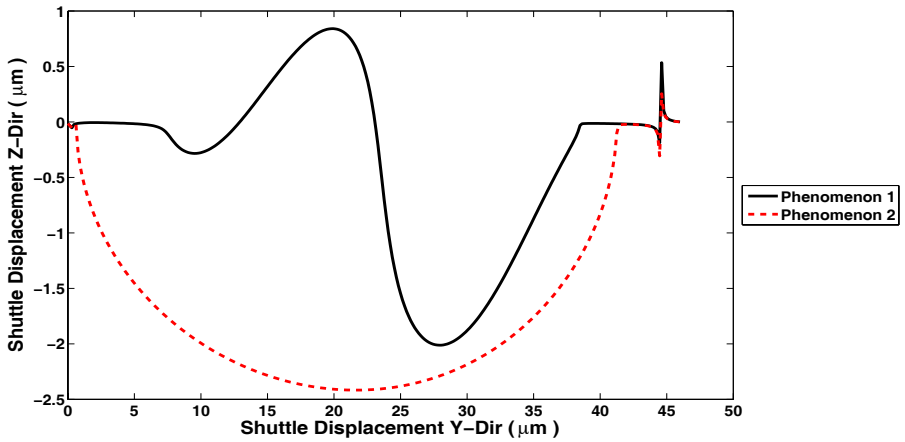

Figure 6.23: Comparison of Z-displacement plots when the back-center node was displaced, and a X-direction off-axis force was applied to the front-side node.

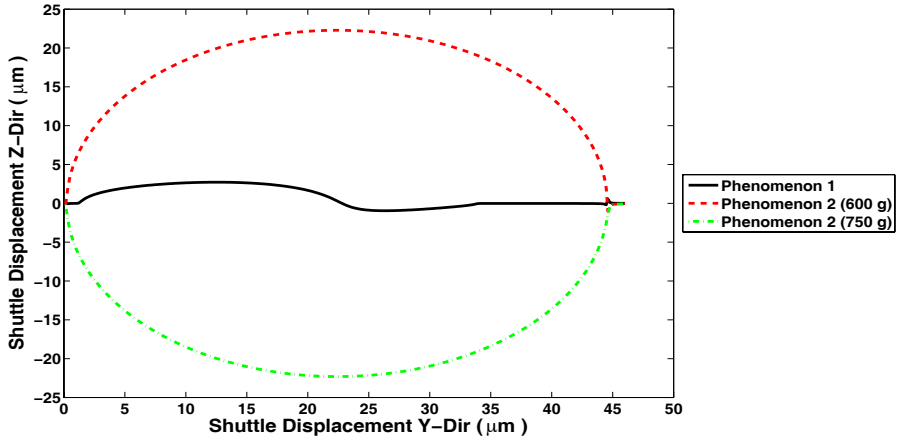

Figure 6.24: Example of the Z-displacement plot shifting direction when the center-side node was displaced, and a Z-direction off-axis force was applied to the front-center-top node.

suggesting that the FCBM shuttle could displace in the positive Z-direction at times, and in the negative Z-direction at others. An example of this is shown in Figure 6.24. Here, the Z-displacement is approximately 22.5 μm when a 600 g force was applied. When 750 g's was applied, the shuttle displaced -22.5 μm. However, when the FCBMs are manufactured, they are anchored to a substrate that would not allow negative Z-displacement.

The results of the finite element analysis showed that the three-dimensional FCBM behavior can have significant changes in both force-displacement characteristics and bistable behavior. These characteristics are dependent on the phenomenon conditions that occur.

Phenomenon 1 behavior occurred when no off-axis forces were applied, and when the shuttle was pulled to the alternate stable equilibrium position rather than being pushed. It also occurred for off-axis forces below the transition force, F_{tr}. Phenomenon 2 behavior occurred for off-axis forces of F_{tr}, and higher, or when the shuttle was pushed to its stable equilibrium position.

Some general comparisons of Phenomenon 1 and Phenomenon 2 are:

- Phenomenon 1 has larger F_{max} and F_{min} magnitudes than Phenomenon 2.
- Phenomenon 1 has a non-linear force-displacement curve with a smooth or rounded peak at the F_{max} and F_{min} regions while Phenomenon 2 has nearly linear force-displacement plots between the F_{max} and F_{min} peak reaction forces.
- Phenomenon 2 has larger roll than Phenomenon 1.
- Phenomenon 1 has larger pitch than Phenomenon 2.
- Phenomenon 1 has larger yaw than Phenomenon 2.
- Phenomenon 2 has larger shuttle Z-displacement than Phenomenon 1.
- Phenomenon 1 occurs when no off-axis forces are applied, or when these forces are below F_{tr}. Phenomenon 2 occurs when the off-axis forces meet or exceed F_{tr}.
- The magnitude of the off-axis force required for transition between Phenomenon 1 and Phenomenon 2 is dependent on the location and magnitude of the force, and the geometry of the FCBM.

6.6 Geometry Variation

The 3-D behavior of the FCBM was further investigated by analyzing the effect of certain changes to the FCBM geometry. This included the analysis of the behavior of a different design, Bistable-B, and variation on shuttle dimensions and overall thickness for the Bistable-A design. These are discussed next.

6.6.1 Bistable-B Design

A 3-D solid element model of the Bistable-B design was analyzed for comparison to Bistable-A. The parameters for both designs are listed in Table 5.1. In this comparison, the back-center node was displaced, and a Z-direction off-axis force was applied to the center-top node. It was discovered that the Bistable-B model generated many of the same trends discussed regarding the Bistable-A design. As a brief summary, both phenomenon characteristics surfaced. Phenomenon 1 characteristics continued to generate the largest reaction forces, the regions near F_{max} and F_{min} were relatively smooth, and the mechanism remained bistable. Phenomenon 2 characteristics generated reduced peak reaction forces, and linear force-displacement relationships between F_{max} and F_{min}. The pitch rotation increased when correlating with Phenomenon 1, and decreased to nearly zero when associated with Phenomenon 2. Finally, the Z-displacements correlating with Phenomenon 1 remained small, and significantly increased when Phenomenon 2 occurred.

There were some differences in the model comparison as well, but this can be expected since there were significant differences in the FCBM geometries. First, the Bistable-B model predicted that the Phenomenon 2 characteristics occurred at different magnitudes of applied force. In addition, the Bistable-B model did not follow the Phenomenon 1 pitch rotation trend generated by the Bistable-A model. This suggests the trends are somewhat dependent on the FCBM design.

6.6.2 Shuttle Dimensions

Another subset of models was created to analyze how changes in the shuttle dimensions would affect the three-dimensional characteristics of the FCBM. After conducting these tests, several correlations were discovered between the shuttle length or width, and the two phenomenon characteristics. As before, the nominal shuttle dimensions were SL = 100 μm and SW = 30 μm. Comparing the results of the four shuttle geometry conditions to the nominal geometry helped to evaluate the effects of shuttle dimension variation.

Figure 6.25 shows the force-displacement results when no off-axis forces were included in the model. By increasing the shuttle length to 150 μm, the model predicted a Phenomenon 2 transition without an applied off-axis force while the model with nominal

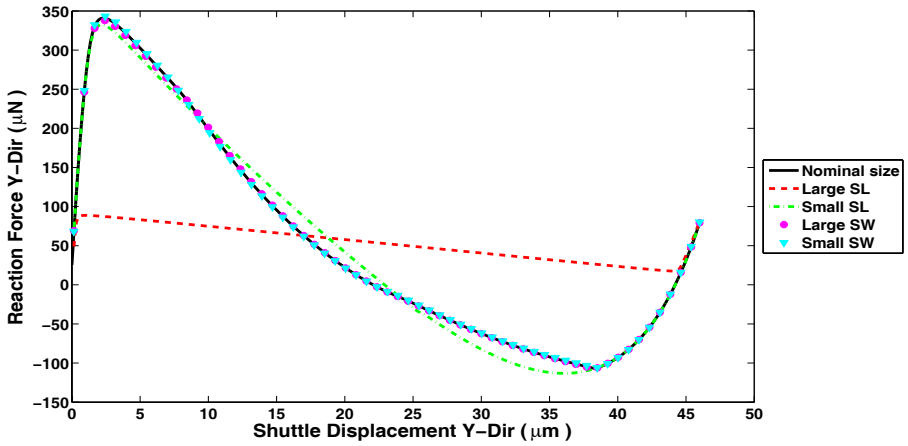

Figure 6.25: The force-displacement plots generated by various shuttle designs when the back-side node was displaced, and no off-axis forces were applied.

shuttle dimensions required a 800 g force before transitioning to Phenomenon 2. While most of the previously defined trends were replicated, decreasing the shuttle length produced slightly different results. When the force-displacement, roll, and yaw plots displayed Phenomenon 1 characteristics, the trend for the pitch rotation followed Phenomenon 2 characteristics. Finally, increasing or decreasing the shuttle width to 50 μm and 10 μm, respectively, did not significantly affect any of the metrics.

As the applied force was increased to 900 g's, more trends were discovered. Figure 6.26 provides the roll, pitch, yaw, and Z-displacement plots for the results of applying these forces while Table 6.3 displays the general findings of this test. The "F_{tr}" column lists the range of applied force containing F_{tr}, causing a Phenomenon 2 transition, if applicable. The "Pitch Trend" and "Z-disp Trend" columns state whether the model followed the general trends defined in the previous section. "Y" designates that the model followed both the Phenomenon 1 and Phenomenon 2 trends. The roll and yaw columns are excluded because a transition between phenomenon did not provide significant change to their magnitudes.

Increasing either the shuttle length or width caused an easier transition to Phenomenon 2. In contrast, decreasing the shuttle length or width caused the model to remain in the Phenomenon 1 condition longer (Figure 6.27). Each of the models followed the general trends defined for both phenomenon states with the exception of the small shuttle length model. An example of this non-conformity is shown in Figure 6.26(b). Here, the

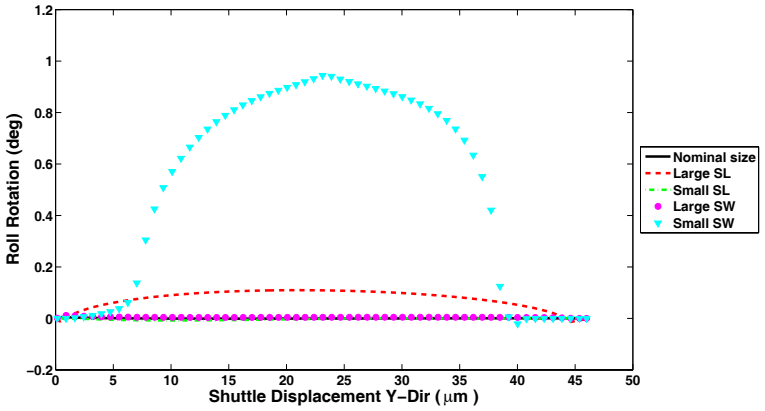

(a) Roll Rotation

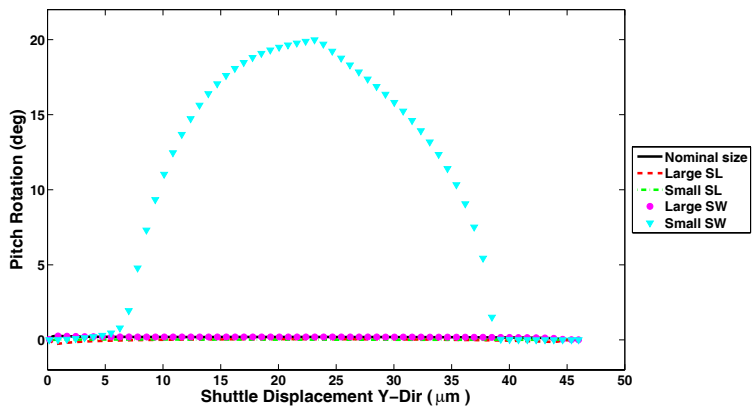

(b) Pitch Rotation

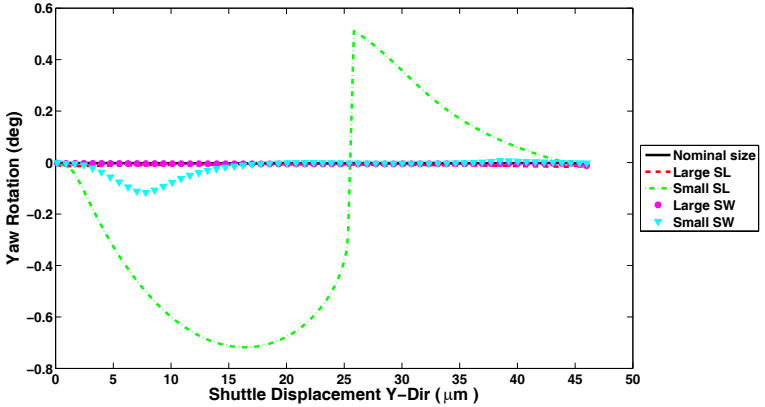

(c) Yaw Rotation

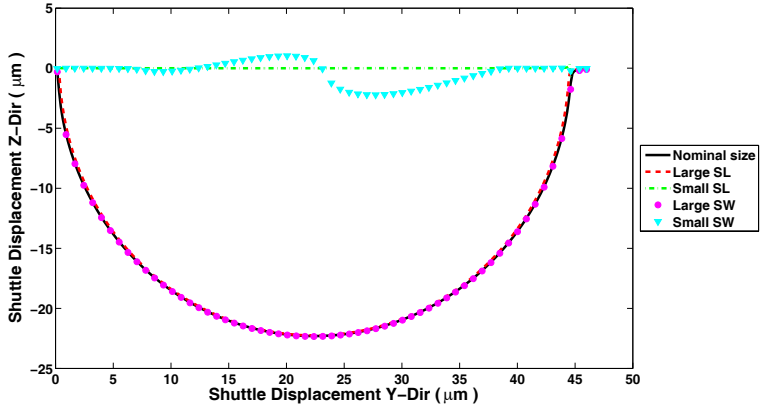

(d) Z-Disp of Shuttle

Figure 6.26: The rotation and Z-displacement plots generated by various shuttle designs when the back-side node was displaced, and a 800 g Z-direction off-axis force was applied to the center-top node.

Table 6.3: Effect of alternate shuttle dimensions.

Shuttle Dimensions	F_{tr} *(g's)*	*Pitch Trend*	*Z-Disp Trend*
NOMINAL	$750 < F_{tr} \leq 800$	Y	Y
LARGE SL	0	Y	Y
SMALL SL	$800 < F_{tr} \leq 1000$	N	Y
LARGE SW	$250 < F_{tr} \leq 500$	Y	Y
SMALL SW	N/A	Y	Y

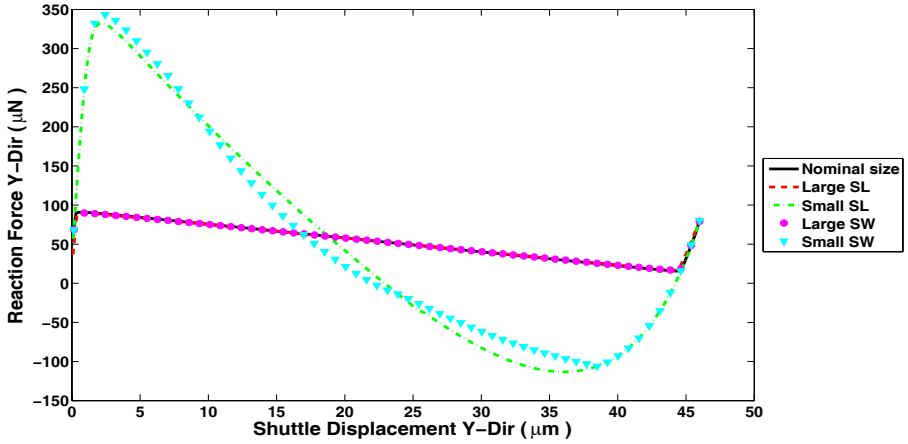

Figure 6.27: The force-displacement plots generated by various shuttle designs when the back-side node was displaced, and a 800 g Z-direction off-axis force was applied to the center-top node.

pitch angle of the "Small *SL*" model was expected to be near 20 °because it is exhibiting the Phenomenon 1 characteristics in every other metric. However, having nearly zero pitch, Phenomenon 2 characteristics were generated.

6.6.3 Thickness

The last test suite subset consisted of increasing the thickness (T) of the FCBM to understand how this may affect the three-dimensional behavior of the mechanisms. The thickness was increased from 3.5 μm to 7.0 μm. The results in Figure 6.28 show that when applying a 1 g force, doubling the thickness generated peak reaction forces that were nearly twice as large as those generated with the nominal thickness as expected. Both force-displacement plots generated Phenomenon 1 conditions. The roll, pitch, yaw, and Z-displacement plots for the same analysis are provided in Figure 6.29. The roll

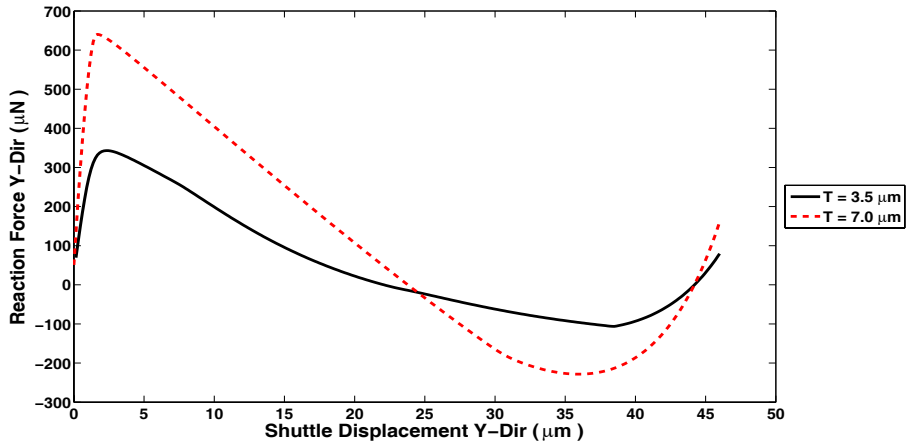

Figure 6.28: The force-displacement plot generated after increasing the thickness of the FCBM when the back-center node was displaced, and a 1 g Z-direction off-axis force was applied to the center-top node.

and yaw rotations were not affected significantly, and can still be approximated as zero. In contrast, the pitch rotation decreased significantly, producing Phenomenon 2 results. The Z-displacement plot also increased significantly, generating similar Phenomenon 2 results. Thus, increasing the thickness resulted in a well behaved Phenomenon 1 force-displacement curve, while unexpectedly generating Phenomenon 2 rotation and Z-displacement results.

The applied force was then increased to 900 g's, and the same plots were generated. Figure 6.30 shows that when applying larger forces, the large thickness model tended to continue producing Phenomenon 1 force-displacement plots when the smaller thickness model transitioned to Phenomenon 2. Thus, the thicker device is not as easily affected by applied off-axis forces. Once again, the roll and yaw rotations were not greatly affected. In addition, both the pitch rotation and Z-displacements were characteristic of Phenomenon 2 conditions even though the force-displacement plot was characteristic of Phenomenon 1. Also, as expected, the Z-displacements were smaller when the thickness was doubled because the out-of-plane stiffness increased (Figure H.9(d) in Appendix H).

Increasing the thickness of the FCBM helped to make the mechanism better behaved. The force-displacement plots tended to produce Phenomenon 1 characteristics even when larger forces were applied to the shuttle. The roll and yaw rotations were approx-

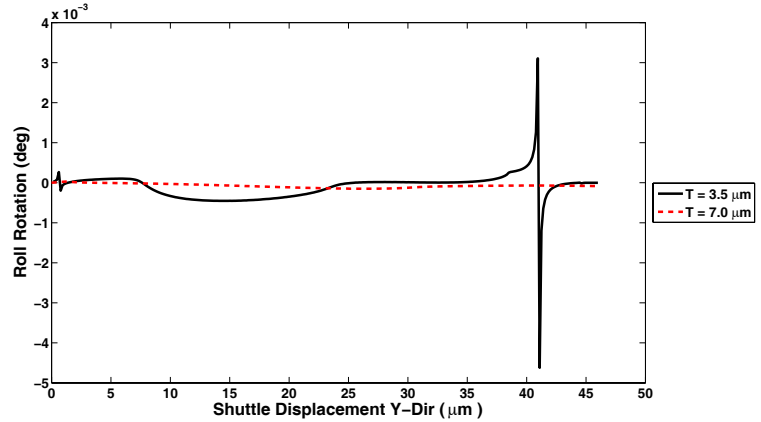

(a) Roll Rotation

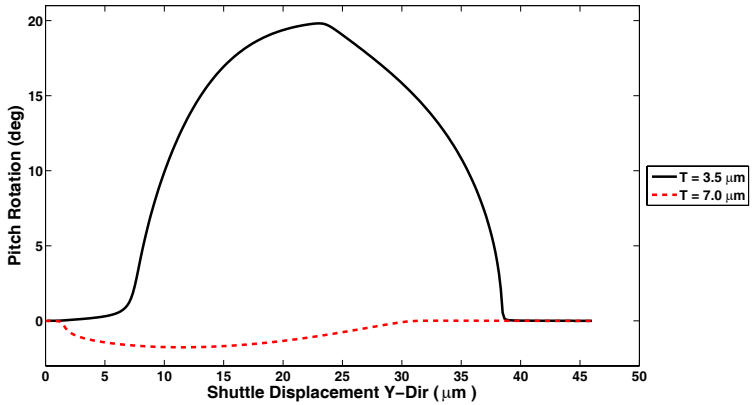

(b) Pitch Rotation

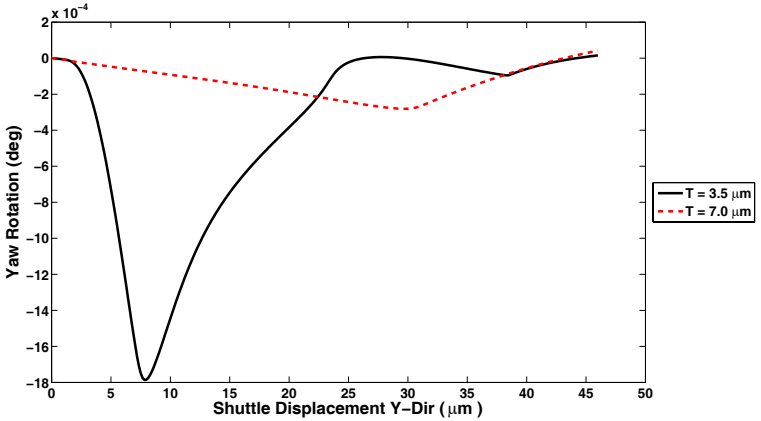

(c) Yaw Rotation

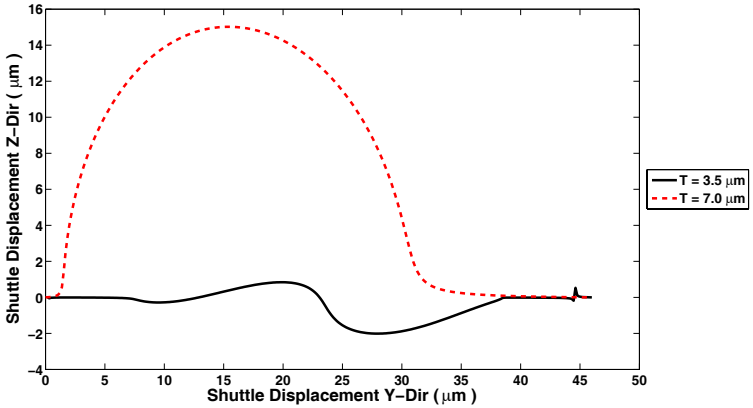

(d) Z-Disp of Shuttle

Figure 6.29: The rotation and Z-displacement plots generated when increasing the thickness when the back-center node was displaced, and a 1 g Z-direction off-axis force was applied to the center-top node.

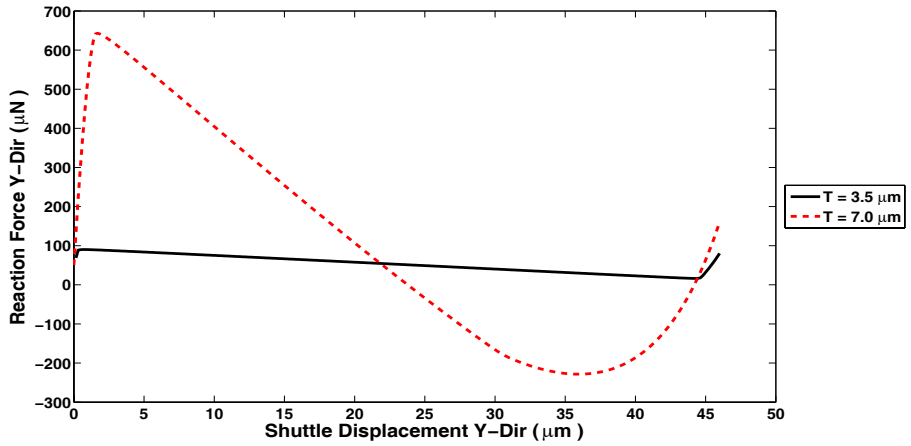

Figure 6.30: The force-displacement plot generated when increasing the thickness of the FCBM when the back-center node was displaced, and a 900 g Z-direction off-axis force was applied to the center-top node.

imately zero no matter what the magnitude of applied force. Finally, the pitch rotation and Z-displacement plots tended to produce Phenomenon 2 characteristics no matter what magnitude of applied force was applied. The characteristics of thicker FCBMs thus provide advantages that could benefit the application of an acceleration sensing array. The added stability and decreased reaction to applied forces could provide for more consistent sensors. Also, the force-displacement plots would tend to produce larger peak reaction forces. Thus, if the FCBMs were initially bistable, the probability that the force-displacement plot would transition to a Phenomenon 2 state, and possibly lose bistability, would decrease.

6.7 Mode Shapes

To gain further insight on the FCBM behavior, the mode shapes of the Bistable-A model were investigated. This helped to determine the natural or unforced behavior of the system, and see if the modes correlated with the phenomenon conditions. In summary, the general trends of displacement were repeated in the mode shape results. Figures 6.31 through 6.34 display the first four mode shapes. The first fifteen mode shapes were retrieved from the FEA model, but they are less likely to occur.

The first mode occurred at a frequency of 53.5 KHz, and the shuttle moved out-of-plane in the Z-direction. When this happens, the compliant legs undergo tension, and there

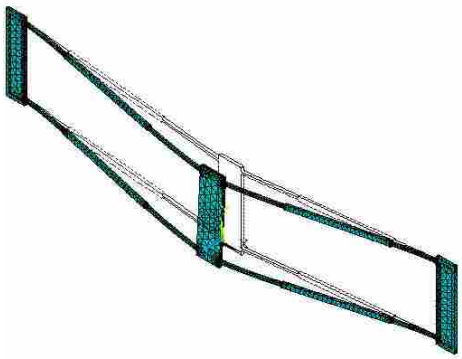

Figure 6.31: First mode of the Bistable-A model.

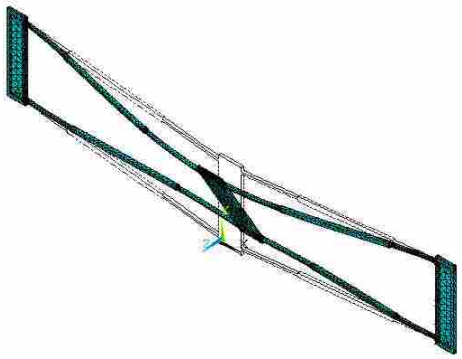

Figure 6.32: Second mode of the Bistable-A model.

is no shuttle movement in the X or Y-direction. This type of motion was seen in many of the Z-displacement plots for Phenomenon 2 motion.

Figure 6.32 displays the second mode, which occurred at 129.5 KHz. Here, the shuttle pitched about the X-axis. The shuttle's center of mass does not displace in either the X or Y direction. This motion resembles the pitch rotation generated during Phenomenon 1 motion.

Figure 6.33 shows that the third mode occurred at approximately 236.7 KHz. The shuttle displayed roll rotation with no displacement in the X, Y, or Z direction. Finally, the fourth mode was found to occur at 328.7 KHz (Figure 6.34). This mode showed the shuttle displacing in the positive Y-direction. There is no X or Z-direction shuttle displacement associated with this mode shape. This motion was seen in each of the test suite results because the shuttle is forced to displace in the Y-direction when moving to the second stable position.

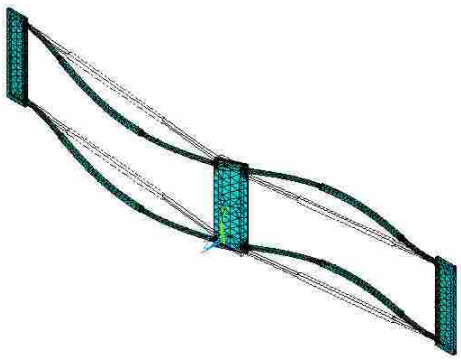

Figure 6.33: Third mode of the Bistable-A model.

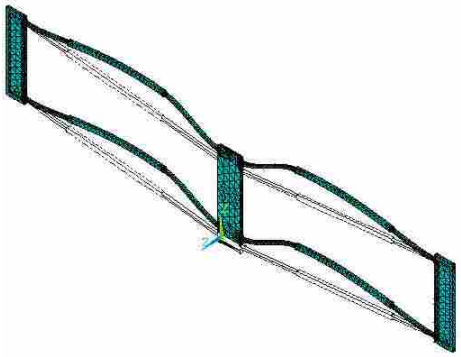

Figure 6.34: Fourth mode of the Bistable-A model.

6.8 Transition to Stable Position 1

The results have focused on moving the FCBM shuttle from the first stable equilibrium position to the second. However, there is value in understanding the FCBM's transition from a location beyond the second stable equilibrium position to the first. The 3-D solid element model was used to produce the results of this complex transition. The results of transitioning the mechanism from stable equilibrium position 1 to a location beyond stable equilibrium position 2 when displacing the back-center node and applying no off-axis force were used to preface the second half of the analysis. Once the mechanism had been displaced 46.0 μm in the Y-direction, the front-center node (Figure 5.5) was displaced to return the mechanism to its first stable equilibrium position. Figure 6.35 shows that when returning to stable position 1, the force-displacement plot generated Phenomenon 2 characteristics. The peak reaction forces were less than a third of the peak forces when moving

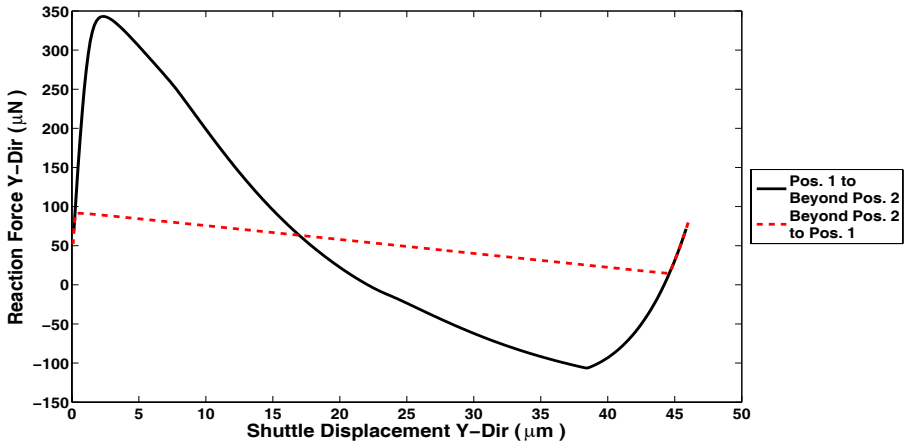

Figure 6.35: Force-displacement plot generated when transitioning the FCBM back to stable equilibrium position 1.

from stable equilibrium position 1 to 2. Thus, the direction of displacement may be another factor to consider when predicting reaction forces.

6.9 Additional Data

Several appendices provide additional data and plots supporting the work in this chapter. A portion of the results generated from prescribing displacement at the front-side, center-side, and back-side nodes are provided in Appendix F. Appendix G provides more detail regarding the similarities between the Bistable-A and Bistable-B designs. The roll, pitch, yaw, and Z-displacement results from when alternate shuttle geometries were analyzed are available in Figure H.8 (Appendix H). Also, some of the higher mode shapes retrieved from the FEA model are provided in Figure H.10 (Appendix H).

6.10 Conclusions

The three-dimensional behavior of the FCBMs are dependent on the method of displacement as well as the location, direction, and magnitude of off-axis applied forces. Phenomenon 1 and Phenomenon 2 characteristics were consistently produced, and were associated with specific motion trends. Phenomenon 1 tended to occur when either no off-axis forces were included or when the applied off-axis forces were small. In contrast,

Phenomenon 2 tended to occur when the off-axis forces increased in magnitude. Phenomenon 1 also tended to produce more consistent bistable mechanisms. The FCBMs were found to be far more sensitive to off-axis forces in the Z-direction (out-of-plane) than in the X-direction (in-plane). They were also better behaved when being pulled to their alternate stable equilibrium position rather than being pushed. Analyzing the Bistable-B design showed that similar trends were produced, suggesting that the trends are not restricted to a specific FCBM design. Increasing the out-of-plane thickness (T) of the FCBM facilitated Phenomenon 1 force-displacement relationships. Finally, increasing the shuttle length (SL) or shuttle width (SW) facilitated Phenomenon 2, while decreasing the same dimensions facilitated Phenomenon 1.

Chapter 7

Conclusions and Recommendations

The primary conclusions of this research are:

- The 3-D solid element and 3-D beam element models were capable of predicting the three-dimensional behavior of FCBMs.
- Including the geometric detail of fillets and anchors in the finite element models is important, and significantly affects the force-displacement relationship of FCBMs. Including residual stress had a similar but smaller effect, and because it is easy to apply, it is recommended that it be included.
- A chief discovery was the existence of Phenomenon 1 and Phenomenon 2 behavior characteristics. Each phenomenon was consistently associated with two different motion characteristics. Phenomenon 1 tended to occur when smaller off-axis forces were applied to the FCBM, while Phenomenon 2 tended to occur when larger off-axis forces were applied to the FCBM.
- The FCBMs are more sensitive to off-axis forces in the Z-direction (out-of-plane), and less sensitive to off-axis forces applied in the X-direction (in-plane).
- The FCBMs are better behaved when being pulled to their alternate stable equilibrium position as opposed to being pushed.
- To be used as an acceleration sensing array, it is recommended that one of two things should happen. Either a better understanding of Phenomenon 1 and Phenomenon 2 should occur, or the FCBMs should be designed to facilitate one of the two phenomenon conditions consistently.

These conclusions are described in more detail below.

Including fillets, residual stress, and anchors resulted in a model that could more accurately predict the force-displacement relationship of FCBMs. Including fillets increased the stiffness of the FCBM, resulting in larger peak reaction forces. Including residual stress in the model had a similar, but smaller effect. By including the geometric detail of anchors, the three-dimensional characteristic and critical reaction forces were altered. With these modifications, the 3-D solid element model was validated by comparison to experimental data. It matched the SUMMiT V results adequately, and also produced the two phenomenon characteristics discovered in the MUMPs testing.

The 3-D solid element model was able to predict the three-dimensional behavior of FCBMs experienced in laboratory testing. The solid element model can accurately retrieve the reaction forces, displacements of critical nodes, and the roll, pitch, yaw, and Z-displacement of the shuttle. It is recommended that the 3-D solid element model be used for analysis when highly accurate results are needed. The disadvantage of using this model, however, is longer computational time. The efficiencies of the 2-D models are still attractive for cases when they are applicable and when convergence time is critical, such as when many analysis iterations are required in optimizing performance for a particular application.

The test suite proved to be highly effective and beneficial, providing an understanding of the three-dimensional characteristics of FCBMs as well as a direction for future research. A chief discovery provided by this work was the existence of Phenomenon 1 and 2 characteristics. The Phenomenon 1 conditions tended to occur when either no applied forces were included in the model, or smaller applied forces were included. Phenomenon 1 trends produced larger pitch rotations and smaller shuttle Z-displacements than Phenomenon 2 trends. This phenomenon also tended to produce force-displacement plots with larger peak reaction forces, providing a more consistent bistable nature. On the other hand, the Phenomenon 2 condition tended to occur when larger off-axis applied forces were included in the model. Once this phenomenon surfaced, the FCBM tended to remain in this condition. Along with this phenomenon came reduced peak reaction forces, and a tendency of non-bistability. The pitch rotations decreased to nearly zero, and the Z-displacement of

the shuttle increased. Roll and yaw rotations correlated to each of the phenomenon characteristics, but were not affected as much as the pitch rotation and Z-displacement.

The FCBMs could experience much larger X-direction applied forces before transitioning to Phenomenon 2. In contrast, relatively small Z-direction forces caused the same transition. The FCBMs proved to be better behaved when a node on the back face of the shuttle was displaced to pull the shuttle rather than push it.

These findings suggest that several characteristics should be further researched before application of FCBMs in an acceleration sensing array. The primary challenge is that the transition from Phenomenon 1 to Phenomenon 2 provides inconsistency and possible non-bistability. This transition can be caused by relatively small Z-direction applied forces. If the FCBMs were to experience a shock or acceleration in the X-direction, they would be relatively unaffected. This was validated by the large magnitudes of applied force required to cause a Phenomenon 2 transition. Because the FCBMs proved to remain well behaved when displaced from the back-center or back-side nodes, it helps to understand that pulling the shuttle into the alternate stable position is preferred to pushing it.

To assure consistency as a sensor, either a better understanding of the two phenomenon conditions must be gained, or the device should be designed to be consistent with either Phenomenon 1 or Phenomenon 2. Both phenomenon conditions offer unique advantages. The Phenomenon 1 condition tends to generate well behaved bistable mechanisms more often. A shift in the force-displacement plot caused by geometry variance or manufacturing misalignment will not as readily affect the bistable nature of the device. Another advantage is that the peak reaction forces are larger than those associated with Phenomenon 2, allowing for greater non-volatile memory positioning. Once the mechanism is in either of the two stable equilibrium positions, a much larger force would be required to switch the mechanism to the alternate stable position, providing a more stable mechanism. Phenomenon 2 conditions also provide unique advantages. First, the peak reaction forces are smaller than those associated with Phenomenon 1. Past research [11] showed that using FCBMs in a sensing array may be difficult due to the large magnitudes of acceleration required to switch the mechanisms to their alternate stable position. FCBMs that provide Phenomenon 2 conditions could address this challenge. If both phenomenon con-

ditions were understood, it may be possible to design a mechanism that incorporates both phenomenon conditions, thus allowing greater control of the resulting three-dimensional behavior.

One successful method of providing more consistent Phenomenon 1 conditions was to increase the thickness of the FCBM. Transition to the Phenomenon 2 condition was delayed until much larger off-axis forces were applied to the mechanism. One cause of this effect was that the mechanism was more stiff, thus more readily resisting Z-displacement shuttle motion. Because the second phenomenon is associated with larger Z-displacement motion, this thick design resisted the tendency to transition, and continued producing Phenomenon 1 conditions longer. Additionally, decreasing the shuttle length and width proved to produce Phenomenon 1 results more consistently. Phenomenon 1 is associated with larger pitch rotation, allowing the shuttle to rotate more while moving to the alternate stable position rather than displace out-of-plane. By decreasing the shuttle length, pitch rotation is more likely to occur. Decreasing the shuttle width has the same affect.

Another possible solution that would help generate consistent phenomenon characteristics would be to construct a device that constrains the FCBM shuttle as it moves to its alternate stable position. To provide more consistent Phenomenon 1 conditions, a constraining structure could be included in the design that would prevent the FCBM shuttle from displacing out-of-plane. This could be accomplished by including a channel that constrains the motion of the FCBM shuttle as it displaces to its alternate stable position. Alternately, a structure could be included that forces large out-of-plane shuttle displacement, providing Phenomenon 2 conditions. This structure could be located between the FCBM shuttle and substrate, guiding the motion of the shuttle as it begins moving to its alternate stable position.

Further research must be conducted to understand how to prevent or control this phenomenon transition. A recommendation for future research is to discover what aspect ratio (AW/T) of the compliant legs is best to maximize the stability of the FCBM. A general sensitivity analysis could be made with these dimensions as well. This would help to understand the correlation between rotations and phenomenon transitions. Additionally, a slenderness ratio ($AL1/AW$, RAL/RAW, and AL/AW) could be researched to discover the

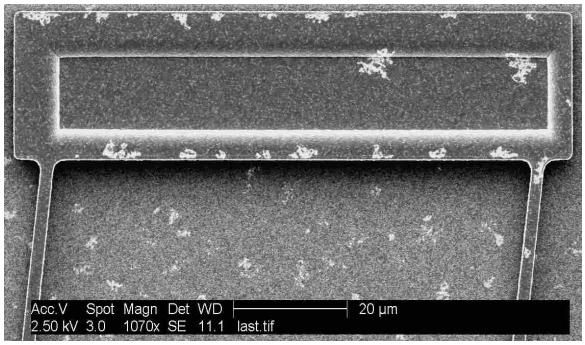

(a) Left Anchor

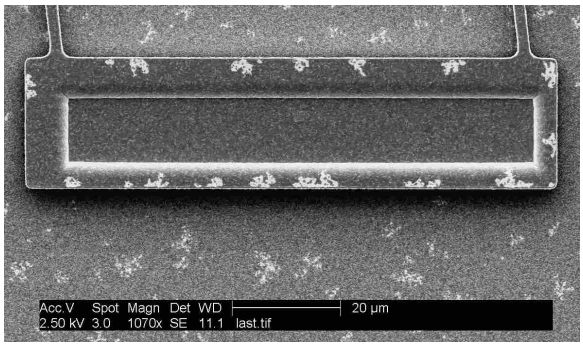

(b) Right Anchor

Figure 7.1: The left and right anchors of the Bistable-A MUMPs design (SEM).

same type of results. This research would be very time consuming, and parallel processing would be required to produce the amount of data required for analysis.

Similarly, researching the stiffness of the mechanism when altering the geometry could be of great benefit. It can realistically be assumed that the FCBM stiffness has a direct effect on the rotation of the mechanism as it moves to its alternate stable position, and thus an indirect effect on the phenomenon characteristic produced. Also, while observing the manufactured Bistable-A MUMPs design, it was discovered that the overhanging edge on the right and left anchors were not equal in length. Figure 7.1 shows that this difference can be as large as a few micrometers. This is caused from misalignment during the manufacturing process, and can be expected. This misalignment can cause a difference in the stiffness of the FCBM, and could be incorporated in future stiffness research.

Additional research that would be good to pursue is to alter the magnitude or location of loads applied to the FCBM while moving to its alternate stable position. The 3-D solid element model could include initially applied loads, then the loads could be removed

in the middle of the analysis. The reverse condition could also be tested; off-axis forces would initially be excluded, then applied in the middle of the analysis. This could help to better understand if the FCBM will change phenomenon characteristics once on a specified force-displacement curve. Understanding these additional characteristics may be used to purposefully apply a preload to an FCBM, forcing specified phenomenon characteristics to surface. The peak reaction forces, bistable nature, or Z-direction displacement could possibly be controlled to meet specific requirements.

Appendix A

2-D Plane Element ANSYS Batch Code

```
!=========================================================
/TITLE,Analysis of a Fully Compliant Bistable Mechanism
/CLEAR,NOSTART
/PREP7
PI=acos(-1)
!=========================================================
! INPUT PARAMETERS
!=========================================================
t = 2 !t
tr= 2 !t
L1 = 75.7 !al1
h1 = 2.5 !aw
theta1_deg = 6.4 !theta_degrees
theta1 = theta1_deg*(PI/180)
L2 = 57.3 !al2
h2 = 2.5 !aw
theta2_deg = 6.6 !alpha_degrees
theta2 = theta2_deg*(PI/180)
Lr = 126.3 !ral
hr = 5.2 !raw
thetar_deg = 5.6 !phi_degrees
thetar = thetar_deg*(PI/180)
swidth=30 !sw
sheight= 72 !sl
Wb= 2.989  !Width of the resistive beam
Lb= 16  !Length of the resistive beam
Ey = 164000 !ex
Pr = 0.22 !pr
NLegs=2
dY = -46 !ydisp
rho = 11.7e-8  !Resistivity (n-type Si)
p11=-102.2e-5
p12=53.4e-5
p44=-13.6e-5
Vs=1.5
Vg=0
/NOPR
ET,1,PLANE223,101
R,1,t
R,2,tr
MP,EX,1,Ey !*** Youngs Modulus ***
MP,PRXY,1,Pr !*** Poisson's Ratio ***
MP,RSVX,1,rho
TB,PZRS,1
TBDATA,1,P11,P12,P12
TBDATA,7,P12,P11,P12
TBDATA,13,P12,P12,P11
TBDATA,22,P44
Nonlinear = 1
Steps = 200
!=========================================================
! RELATIONAL PARAMETERS
!=========================================================
```

```
Lx=L1*cos(theta1)+Lr*cos(thetar)+L2*cos(theta2)
Ly=L1*sin(theta1)+Lr*sin(thetar)+L2*sin(theta2)
!=========================================================
! MODEL SETUP
!=========================================================
K,3,0,0,0
K,4,0,h1/(2*sin(PI/2-theta1)),0
K,5,0,-h1/(2*sin(PI/2-theta1)),0
K,8,L1*cos(theta1)-h1/2*sin(theta1),L1*sin(theta1)+h1/2*cos(theta1),0
K,9,L1*cos(theta1),L1*sin(theta1),0
K,10,L1*cos(theta1)+h1/2*sin(theta1),L1*sin(theta1)-h1/2*cos(theta1),0
K,11,L1*cos(theta1)-hr/2*sin(thetar),L1*sin(theta1)+hr/2*cos(thetar),0
K,12,L1*cos(theta1)+Lr*cos(thetar)-hr/2*sin(thetar),L1*sin(theta1)+Lr*sin(thetar)+hr/2*cos(thetar),0
K,13,L1*cos(theta1)+Lr*cos(thetar)-h2/2*sin(theta2),L1*sin(theta1)+Lr*sin(thetar)+h2/2*cos(theta2),0
K,14,L1*cos(theta1)+Lr*cos(thetar),L1*sin(theta1)+Lr*sin(thetar),0
K,15,L1*cos(theta1)+Lr*cos(thetar)+h2/2*sin(theta2),L1*sin(theta1)+Lr*sin(thetar)-h2/2*cos(theta2),0
K,16,L1*cos(theta1)+Lr*cos(thetar)+hr/2*sin(thetar),L1*sin(theta1)+Lr*sin(thetar)-hr/2*cos(thetar),0
K,17,L1*cos(theta1)+hr/2*sin(thetar),L1*sin(theta1)-hr/2*cos(thetar),0
K,18,Lx,Ly,0
K,19,Lx,Ly+h2/(2*sin(PI/2-theta2)),0
K,20,Lx,Ly+sheight/Nlegs/2,0
K,21,Lx+swidth/2,Ly+sheight/Nlegs/2,0
K,22,Lx+swidth/2,Ly-sheight/Nlegs/2,0
K,23,Lx,Ly-sheight/Nlegs/2,0
K,24,Lx,Ly-h2/(2*sin(PI/2-theta2)),0
L,4,8
L,8,11
L,11,12
L,12,13
L,13,19
L,19,20
L,20,21
L,21,22
L,22,23
L,23,24
L,24,15
L,15,16
L,16,17
L,17,10
L,10,5
L,5,4
AL,ALL
AGEN,Nlegs,1,1,1,0,-sheight/Nlegs,0,0,0,0
ARSYM,X,ALL,0,0,0
AGEN,2,Nlegs+1,2*Nlegs,1,Lx+swidth/2,0,0,0,0,1
AGEN,2,Nlegs+1,2*Nlegs,1,Lx+swidth/2,0,0,0,0,1
AADD,ALL
!*** MESH MECHANISMS ***
real,1
type,1
mat,1
AESIZE,5,h1/3
AMESH,5
ksel,s,kp,,21
nslk,s
*get,nkp1,node,0,num,max
nsel,all
ksel,all
!=========== Structural Boundary Constraints ===========
DL,16,,UX,0
DL,16,,UY,0
DL,32,,UX,0
DL,32,,UY,0
DL,48,,UX,0
DL,48,,UY,0
DL,64,,UX,0
DL,64,,UY,0
FINISH
```

```
!=========================================================
! SOLUTION STEPS
!=========================================================
/SOLU
NLGEOM,1 !***Nonlinear Analysis****
ANTYPE,0 !***Static Analysis Type***
!============ VERTICAL DISPLACEMENT =============
*DO,mm,1,Steps+1,1
DK,21, ,(mm-1)*dY/Steps, , , ,UY, , , , ,
lswrite,mm
*ENDDO
lssolve,1,Steps+1
FINISH
/POST1
!=========== RETRIEVE IMPORTANT DATA ===
*DIM,Ydis,TABLE,Steps+1
*DIM,Force,TABLE,Steps+1
*DO,n,1,Steps+1,1
Set,n
*GET,Ydis(n),NODE,nkp1,U,Y
*GET,Force(n),NODE,nkp1,RF,FY
*ENDDO
!Create Output File
/output, Configuration_D_results.txt
*VWRITE, Ydis(1), Force(1)
\%16.8G \%16.8G
/output
FINISH
```

Appendix B

2-D 8-Node Quad-Element ANSYS Batch Code

```
/batch
finish
/CLEAR,START
!CHANGE WORKING DIRECTORY
/cwd,'C:\Documents and Settings\Brian\Desktop\test_suite'
!Title (AFTER THE COMMA)
/title, 2D_PLANE82
!==================================
!             INPUT
!==================================
sw=30.0
sl=100.0
lta1=5.0
lta2=85.0
ral=126.3
raw=5.2
aw=2.5
al1=75.7
al2=57.3
theta_degrees=6.4
phi_degrees=5.6
alpha_degrees=6.6
t=3.5
ex=164
pr=0.22
loadsteps=300
ydisp=46.0
!CONVERT ANGLES TO RADIANS
pi = acos(-1)
theta = theta_degrees*pi/180
phi = phi_degrees*pi/180
alpha = alpha_degrees*pi/180
!ADD INTERNAL DIMENSIONS
ledge = (raw-aw)/2
al1_bottom = al1 + aw*tan(theta)
al2_bottom = al2 - aw*tan(alpha)
!================================
!            SETUP
!================================
!PRE-PROCESSOR MODE
/prep7
!CREATE MATERIAL PROPERTIES
mp,EX,1,ex
mp,PRXY,1,pr
!ELEMENT TYPE
et,1,plane82,,,3
r,1,t
!================================
!           GEOMETRY
!================================
!SHUTTLE (ORIGIN [0,0] AT LOWER LEFT OF SHUTTLE)
k,1,0,0,0
k,2,0,sl,0
```

```
k,3,sw,sl,0
k,4,sw,0,0
!ARM 1
k,5,sw,(sl-lta1),0
k,6,sw+al1*cos(theta),(sl-lta1)+al1*sin(theta),0
k,7,sw+al1*cos(theta)+aw*sin(phi),(sl-lta1)+al1*sin(theta)-aw*cos(phi),0
k,8,sw,(sl-lta1)-(aw/cos(theta)),0
!RIGID ARM
k,9,sw+al1*cos(theta)-ledge*sin(phi),(sl-lta1)+al1*sin(theta)+ledge*cos(phi),0
k,10,sw+al1*cos(theta)-ledge*sin(phi)+ral*cos(phi),(sl-lta1)+al1*sin(theta)+ledge*cos(phi) . . .
+ral*sin(phi),0
k,11,sw+al1*cos(theta)+aw*sin(phi)+ledge*sin(phi)+ral*cos(phi),(sl-lta1)+al1*sin(theta)- . . .
aw*cos(phi)-ledge*cos(phi+ral*sin(phi),0
k,12,sw+al1*cos(theta)+aw*sin(phi)+ledge*sin(phi),(sl-lta1)+al1*sin(theta)-aw*cos(phi)- . . .
ledge*cos(phi),0
!Arm 2
k,13,sw+al1*cos(theta)+ral*cos(phi),(sl-lta1)+al1*sin(theta)+ral*sin(phi),0
k,14,sw+al1*cos(theta)+ral*cos(phi)+al2*cos(alpha),(sl-lta1)+al1*sin(theta)+ral*sin(phi)+ . . .
al2*sin(alpha),0
k,15,sw+al1*cos(theta)+ral*cos(phi)+al2*cos(alpha),(sl-lta1)+al1*sin(theta)-aw*cos(phi)+ . . .
ral*sin(phi)+al2_bottom*sin(alpha),0
k,16,sw+al1*cos(theta)+aw*sin(phi)+ral*cos(phi),(sl-lta1)+al1*sin(theta)-aw*cos(phi)+ . . .
ral*sin(phi),0
!MIRROR THE UPPER RIGHT ARM AND POSITION CORRECTLY
ksymm,x,5,16,1,,1,0
kgen,1,17,28,1,sw,,,,,1
!CREATE AREAS FOR UPPER RIGHT ARM, AND GENERATE TO LOWER RIGHT ARM
l,5,6
l,6,7
l,7,8
l,8,5
al,1,2,3,4
l,9,10
l,10,11
l,11,12
l,12,9
al,5,6,7,8
l,13,14
l,14,15
l,15,16
l,16,13
al,9,10,11,12
agen,2,1,3,1,0,-lta2
!CREATE AREAS FOR UPPER LEFT ARM, AND GENERATE TO LOWER LEFT ARM
l,17,18
l,18,19
l,19,20
l,20,17
al,25,26,27,28
l,21,22
l,22,23
l,23,24
l,24,21
al,29,30,31,32
l,25,26
l,26,27
l,27,28
l,28,25
al,33,34,35,36
agen,2,7,9,1,0,-lta2
!CREATE AREA FOR SHUTTLE
l,1,2
l,2,3
l,3,4
l,4,1
al,49,50,51,52
!GLUE ALL AREAS TOGETHER
aglue,all
```

```
/replot
!=========================================================
!      MESH GEOMETRY AND WRITE NODAL AND ELEMENT DATA
!=========================================================
!MESH ALL GEOMETRY
allsel, all
smrtsize, 5
mshape, 1, 2d
mshkey, 0
amesh, all
!REFINE MESH FOR LEGS
asel, s, area,, 1
asel, a, area,, 3,4,1
asel, a, area,, 6,7,1
asel, a, area,, 9,10,1
asel, a, area,, 12
asel, a, area,, 14,17,1
esla,s
erefine, all,,, 1,3, clean
allsel, all
/replot
finish
!=========================================================
!                  Boundary Conditions
!=========================================================
!SOLUTION MODE
/solu
!ANALYSIS TYPE AND NON-LINEAR GEOMETRY SETTING:
antype, static
nlgeom, on
lsel, s, line,, 10, 10, 1
nsll, s, 1
lsel, a, line,, 22, 22, 1
nsll, a, 1
lsel, a, line,, 34, 34, 1
nsll, a, 1
lsel, a, line,, 46, 46, 1
nsll, a, 1
d, all, ux, 0
d, all, uy, 0
allsel,all
!DISPLACEMENT
*do,mm,1,loadsteps,1
lsel, s, line,, 52, 52, 1
nsll, s, 1
d, all, uy, mm*(ydisp/loadsteps)
outres,all
allsel,all
lswrite,mm
antype,static
nlgeom,on
solve
*ENDDO
/replot
finish
!=========================================================
!              Post Processing Data Retrieval
!=========================================================
!POST PROCESSING MODE
/post1
!CREATE EMPTY FILES FOR DATA TO BE WRITTEN TO
*dim, force_in_y, table,loadsteps
*dim, ydisp, table,loadsteps
*do, mm, 1, loadsteps, 1
allsel, all
!RETRIEVE THE REACTION FORCE SUM OF THE SHUTTLE FACE
set, mm
lsel, s, line,, 52, 52, 1
```

```
nsll, s, 1
fsum
*get, force_in, fsum, 0, item, fy
*set, force_in_y(mm), force_in
*set, force_in ,!ERASES FORCE_IN
!RETRIEVE THE NODE NUMBER OF ONE OF THE NODES ON THE SHUTTLE FACE
!RETRIEVE THE DISPLACEMENT OF THAT NODE
allsel, all
lsel, s, line,, 52, 52, 1
nsll, s, 1
nsel, r, loc, x, sw*(3/8), sw*(5/8), .001
*get, nkface, node,, num, max
*get, dispy, node, nkface, u, y
*set, ydisp(mm), dispy
*enddo
allsel, all
/output, temp_output.txt
*vwrite, force_in_y(1), ydisp(1)
%16.8G %16.8G
/output
finish
```

Appendix C

3-D Beam Element ANSYS Batch Code

```
/batch
finish
/clear, start
!CHANGE WORKING DIRECTORY
/cwd,'/tmp/bbc27'
!Title
/title, BEAM4_TRUSS_SHUTTLE
!=================================
!             INPUT
!=================================
!GLOBAL VARIABLES
pi = acos(-1) !PI
tpoly1 = 2 !POLY1 THICKNESS [um]
tpoly2 = 1.5 !POLY2 THICKNESS [um]
toxide = 2 !OXIDE THICKNESS [um]
var1 = 5 !VERTICAL DISTANCE FROM TOP OF ANCHOR TO TOP OF FIRST ARM [um]
is = -0.010 !PRESTRESS VALUE OF MAT (COMP)(mN/um^2) FOR F [mN]
grav = 9810000 !GRAVITY (um/s^2)
t = tpoly1+tpoly2 !OUT OF PLANE THICKNESS OF MECHANISM [um]
sw = 30 !SHUTTLE WIDTH [um]
sl = 100 !SHUTTLE LENGTH [um]
al1 = 75.7 !COMP ARM 1 LENGTH (BETWEEN SHUTTLE & RIGID ARM
al2 = 57.3 !COMP ARM 2 LENGTH (BETWEEN ANCHOR AND RIGID ARM
ral = 126.3 !RIGID ARM LENGTH [um]
aw = 2.5 !ARM WIDTH.  EACH ARM HAS THE SAME WIDTH [um]
raw = 5.2 !RIGID ARM WIDTH [um]
theta_degrees = 6.4 !ANGLE OF AL1 (FROM HORIZONTAL) [degrees]
phi_degrees = 5.6 !ANGLE OF RIGID ARM SECTION (FROM HORIZ) [degrees]
alpha_degrees = 6.6 !ANGLE OF AL2 (FROM HORIZONTAL) [degrees]
lta1 = 5 !VERT DIST TOP OF SHUTTLE TO TOP EDGE OF COMP ARM
ex = 164 !MODULUS OF ELASTICITY (mN/um^2) FOR FORCE [mN]
density = 2.33*(10**(-18)) !DENSITY (1000*kg/um^3) FOR FORCE [mN]
pr = 0.22 !POISSON'S RATIO
loadsteps = 500 !LOADSTEPS TO SOLVE SOLUTION
ydisp = 46.0 !Y-DIR DISPLACEMENT OF SHUTTLE [um]
!CALCULATED DIMENSIONS
forcegrav = density*sl*sw*t*grav !FORCE MAGNITUDE EQUAL TO 1 G OF ACCEL
gxy = ex/((1+pr)*2) !SHEAR MODULUS [uN/um^2] or [mN/um^2]
area_1 = aw*t !AREA FOR COMPLIANT ARM LEGS
area_2 = raw*t !AREA FOR RIGID ARM LEGS
area_3 = 2*area_2 !AREA FOR SHUTTLE MEMBERS
izz_1 = t*(aw**3)*(1/12) !Z-DIR MOMENT OF INERTIA FOR COMPLIANT ARM LEGS
izz_2 = t*(raw**3)*(1/12) !Z-DIRMOMENT OF INERTIA FOR RIGID ARM LEGS
izz_3 = 2*izz_2 !Z-DIR MOMENT OF INERTIA FOR SHUTTLE MEMBERS
iyy_1 = aw*(t**3)*(1/12) !Y-DIR MOMENT OF INERTIA FOR COMPLIANT ARM LEGS
iyy_2 = raw*(t**3)*(1/12) !Y-DIR MOMENT OF INERTIA FOR RIGID ARM LEGS
iyy_3 = 2*iyy_2 !Y-DIR MOMENT OF INERTIA FOR SHUTTLE MEMBERS
tkz = t !CROSS SECTIONAL HEIGHT OF COMP ARMS LEGS & RIGID ARM LEGS
tkz_3 = 2*tkz !CROSS SECTIONAL HEIGHT OF SHUTTLE MEMBERS
tky_1 = aw !CROSS SECTIONAL WIDTH OF COMPLIANT ARM LEGS
tky_2 = raw !CROSS SECTIONAL WIDTH OF RIGID ARM LEGS
tky_3 = 2*tky_2 !CROSS SECTIONAL WIDTH OF SHUTTLE MEMBERS
theta = theta_degrees*pi/180 !CONVERT DEGREES TO RADIANS FOR ARM1
```

```
phi = phi_degrees*pi/180 !CONVERT DEGREES TO RADIANS FOR RIGID-ARM
alpha = alpha_degrees*pi/180 !CONVERT DEGREES TO RADIANS FOR ARM2
lta2 = sl-2*lta1 !THE VERT DIST (INNER) BETWEEN THE 2 COMP LEGS
es_comp = 1000 !ELEMENT SIZE FOR COMPLIANT ARMS
es_rig = es_comp/2 !ELEMENT SIZE FOR RIGID ARMS
es_shut = es_comp/20 !ELEMENT SIZE FOR MIDDLE OF SHUTTLE
es_shut_edge = es_comp/200 !ELEMENT SIZE FOR TOP AND BOTTOM EDGE OF SHUTTLE
!================================
!            SETUP
!================================
!PRE-PROCESSOR MODE
/prep7
!MATERIAL PROPERTIES
mp, ex, 1, ex
mp, dens, 1, density
mp, gxy, 1, gxy
mp, damp, 1, 1.0
!ELEMENT TYPE 1
et, 1, beam4
keyopt, 1, 9, 9
r, 1, area_1, izz_1, iyy_1, tkz, tky_1, 0
r, 2, area_2, izz_2, iyy_2, tkz, tky_2, 0
r, 3, area_3, izz_3, iyy_3, 10*tkz, tky_3, 0
!================================
!           GEOMETRY
!================================
!BOTTOM OF SHUTTLE IS ORIGIN (0,0)
k,1,0,0,0
k,2,0,sl,0
k,3,sw,sl,0
k,4,sw,0,0
k,5,0,0,t
k,6,0,sl,t
k,7,sw,sl,t
k,8,sw,0,t
k,9,0,lta1,(t/2)
k,10,0,(lta1+lta2),(t/2)
k,11,sw,(lta1+lta2),(t/2)
k,12,sw,lta1,(t/2)
k,13,0,(sl/2),(t/2)
k,14,(sw/2),sl,(t/2)
k,15,sw,(sl/2),(t/2)
k,16,(sw/2),0,(t/2)
k,17,0,(sl/2),t
k,18,(sw/2),sl,t
k,19,sw,(sl/2),t
k,20,(sw/2),0,t
k,21,0,(sl/2),0
k,22,(sw/2),sl,0
k,23,sw,(sl/2),0
k,24,(sw/2),0,0
k,25,(sw/2),(sl/2),t
k,26,(sw/2),(sl/2),(t/2)
k,27,(sw/2),(sl/2),0
k,28,0,0,(t/2)
k,29,0,sl,(t/2)
k,30,sw,sl,(t/2)
k,31,sw,0,(t/2)
k,32,sw+al1*cos(theta),lta1+al1*sin(theta),(t/2)
k,33,sw+al1*cos(theta)+ral*cos(phi),lta1+al1*sin(theta)+ral*sin(phi),(t/2)
k,34,sw+al1*cos(theta)+ral*cos(phi)+al2*cos(alpha),lta1+al1*sin(theta)+. . .
ral*sin(phi)+al2*sin(alpha),(t/2)
k,35,-(al1*cos(theta)),lta1+al1*sin(theta),(t/2)
k,36,-(al1*cos(theta)+ral*cos(phi)),lta1+al1*sin(theta)+ral*sin(phi),(t/2)
k,37,(al1*cos(theta)+ral*cos(phi)+al2*cos(alpha)),lta1+al1*sin(theta)+. . .
ral*sin(phi)+al2*sin(alpha),(t/2)
k,38,sw+al1*cos(theta),lta1+lta2+al1*sin(theta),(t/2)
k,39,sw+al1*cos(theta)+ral*cos(phi),lta1+lta2+al1*sin(theta)+ral*sin(phi),(t/2)
```

```
k,40,sw+al1*cos(theta)+ral*cos(phi)+al2*cos(alpha),lta1+lta2+al1*sin(theta)+ral*sin(phi)+. . .
al2*sin(alpha),(t/2)
k,41,-(al1*cos(theta)),lta1+lta2+al1*sin(theta),(t/2)
k,42,-(al1*cos(theta)+ral*cos(phi)),lta1+lta2+al1*sin(theta)+ral*sin(phi),(t/2)
k,43,(al1*cos(theta)+ral*cos(phi)+al2*cos(alpha)),lta1+lta2+al1*sin(theta)+ral*sin(phi)+. . .
al2*sin(alpha),(t/2)
!LINES
!BOTTOM SURFACE OF SHUTTLE
l, 1, 21
l, 21, 2
l, 2, 22
l, 22, 3
l, 3, 23
l, 23, 4
l, 4, 24
l, 24, 1
!TOP SURFACE OF SHUTTLE
l, 5, 17
l, 17, 6
l, 6, 18
l, 18, 7
l, 7, 19
l, 19, 8
l, 8, 20
l, 20, 5
!CORNERS
l, 1, 28
l, 28, 5
l, 2, 29
l, 29, 6
l, 3, 30
l, 30, 7
l, 4, 31
l, 31, 8
!DIAGNALS ON BOTTOM SURFACE OF SHUTTLE
l, 1, 27
l, 2, 27
l, 3, 27
l, 4, 27
!DIAGNALS ON TOP SURFACE OF SHUTTLE
l, 5, 25
l, 6, 25
l, 7, 25
l, 8, 25
!DIAGNALS ON LEFT SIDE
l, 1, 13
l, 5, 13
l, 6, 13
l, 2, 13
!DIAGNALS ON TOP SIDE
l, 2, 14
l, 6, 14
l, 7, 14
l, 3, 14
!DIAGNALS ON RIGHT SIDE
l, 4, 15
l, 8, 15
l, 7, 15
l, 3, 15
!DIAGNALS ON RIGHT SIDE
l, 1, 16
l, 5, 16
l, 8, 16
l, 4, 16
!VERTICAL LINE ON LEFT SIDE
l, 21, 13
l, 13, 17
!VERTICAL LINE ON TOP SIDE
```

```
l, 22, 14
l, 14, 18
!VERTICAL LINE ON RIGHT SIDE
l, 23, 15
l, 15, 19
!VERTICAL LINE ON BOTTOM SIDE
l, 24, 16
l, 16, 20
!VERTICAL LINE IN MIDDLE
l, 27, 26
l, 26, 25
!DIAGNALS ON MIDDLE SURFACE
l, 28, 26
l, 29, 26
l, 30, 26
l, 31, 26
!SUPPORT MEMBERS ON BOTTOM FACE
l, 24, 27
l, 21, 27
l, 22, 27
l, 23, 27
!SUPPORT MEMBERS ON MIDDLE FACE
l, 16, 26
l, 13, 26
l, 14, 26
l, 15, 26
!SUPPORT MEMBERS ON TOP FACE
l, 20, 25
l, 17, 25
l, 18, 25
l, 19, 25
!BOTTOM LEFT LEG
l, 9, 35
l, 35, 36
l, 36, 37
!TOP LEFT LEG
l, 10, 41
l, 41, 42
l, 42, 43
!TOP RIGHT LEG
l, 11, 38
l, 38, 39
l, 39, 40
!BOTTOM RIGHT LEG
l, 12, 32
l, 32, 33
l, 33, 34
!SUPPORT BOTTOM LEFT LEG ATTACHMENT TO SHUTTLE
l, 1, 9
l, 5, 9
l, 13, 9
l, 26, 9
!SUPPORT TOP LEFT LEG ATTACHMENT TO SHUTTLE
l, 2, 10
l, 6, 10
l, 13, 10
l, 26, 10
!SUPPORT TOP RIGHT LEG ATTACHMENT TO SHUTTLE
l, 3, 11
l, 7, 11
l, 15, 11
l, 26, 11
!SUPPORT BOTTOM RIGHT LEG ATTACHMENT TO SHUTTLE
l, 4, 12
l, 8, 12
l, 15, 12
l, 26, 12
!GLUE ALL LINES TOGETHER
```

```
allsel, all
lglue, all
!=========================================================
!                     MESH GEOMETRY
!=========================================================
!LEFT INNER COMPLIANT LEGS
allsel, all
lsel, s, loc, x, 0-0.01, -(al1*cos(theta))
lsel, r, loc, z, (t/2)
latt, 1, 1, 1
!SPLIT THE COMPLIANT LEGS INTO A CERTAIN AMOUNT PER LINE
esize, 0, es_comp
lmesh, all
!RIGHT INNER COMPLIANT LEGS
allsel, all
lsel, s, loc, x, sw+0.01, sw+al1*cos(theta)
lsel, r, loc, z, (t/2)
latt, 1, 1, 1
!SPLIT THE COMPLIANT LEGS INTO A CERTAIN AMOUNT PER LINE
esize, 0, es_comp
lmesh, all
!LEFT OUTER COMPLIANT LEGS
allsel, all
lsel, s, loc, x, -(al1*cos(theta))-(ral*cos(phi))-0.01, -(al1*cos(theta))-. . .
(ral*cos(phi))-(al2*cos(alpha))
lsel, r, loc, z, (t/2)
latt, 1, 1, 1
!SPLIT THE COMPLIANT LEGS INTO A CERTAIN AMOUNT PER LINE
esize, 0, es_comp
lmesh, all
!RIGHT OUTER COMPLIANT LEGS
allsel, all
lsel, s, loc, x, sw+al1*cos(theta)+ral*cos(phi)+0.01, sw+al1*cos(theta)+. . .
ral*cos(phi)+al2*cos(alpha)
lsel, r, loc, z, (t/2)
latt, 1, 1, 1
!SPLIT THE COMPLIANT LEGS INTO A CERTAIN AMOUNT PER LINE
esize, 0, es_comp
lmesh, all
!LEFT RIGID LEGS
allsel, all
lsel, s, loc, x, -(al1*cos(theta)+0.01), -(al1*cos(theta)+ral*cos(phi))
latt, 1, 2, 1
esize, 0, es_rig
lmesh, all
!RIGHT RIGID LEGS
allsel, all
lsel, s, loc, x, sw+al1*cos(theta)+0.01, sw+al1*cos(theta)+ral*cos(phi)
latt, 1, 2, 1
esize, 0, es_rig
lmesh, all
!SHUTTLE SUPPORTS
allsel, all
lsel, s,,, 1, 2, 1
lsel, a,,, 5, 6, 1
lsel, a,,, 9, 10, 1
lsel, a,,, 13, 14, 1
lsel, a,,, 25, 36, 1
lsel, a,,, 41, 44, 1
lsel, a,,, 59, 63, 1
lsel, a,,, 65, 73, 2
lsel, a,,, 89, 101, 4
latt, 1, 3, 1
esize, 0, 25
lmesh, all
allsel, all
lsel, s,,, 3, 4, 1
lsel, a,,, 7, 8, 1
```

```
lsel, a,,, 11, 12, 1
lsel, a,,, 15, 16, 1
lsel, a,,, 37, 40, 1
lsel, a,,, 45, 48, 1
lsel, a,,, 64, 70, 2
latt, 1, 3, 1
esize, 0, 10
lmesh, all
allsel, all
lsel, s,,, 17, 24, 1
lsel, a,,, 49, 58, 1
latt, 1, 3, 1
esize, 0, 4
lmesh, all
allsel, all
lsel, s,,, 87, 88, 1
lsel, a,,, 91, 92, 1
lsel, a,,, 95, 96, 1
lsel, a,,, 99, 100, 1
latt, 1, 3, 1
esize, 0, 25
lmesh, all
allsel, all
lsel, s,,, 90, 102, 4
latt, 1, 3, 1
esize, 0, 50
lmesh, all
!COMPRESS THE NUMBERING SYSTEM
allsel, all
numcmp, all
!!!!!!!!!!!
!NAME NODES
!!!!!!!!!!!
!NAME FACENODE
allsel, all
nsel, s, loc, x, (sw/2)
nsel, r, loc, y, 0
nsel, r, loc, z, (t/2)
*get, facenode, node,, num, max
!NAME MIDNODE
allsel, all
nsel, s, loc, x, (sw/2)
nsel, r, loc, y, (sl/2)
nsel, r, loc, z, (t/2)
*get, midnode, node,, num, max
!NAME BACKNODE
allsel, all
nsel, s, loc, x, (sw/2)
nsel, r, loc, y, sl
nsel, r, loc, z, (t/2)
*get, backnode, node,, num, max
!NAME TOP LEFT SHUTTLE CORNER
allsel, all
nsel, s, loc, x, 0
nsel, r, loc, y, sl
nsel, r, loc, z, (t/2)
*get, tlnode, node,, num, max
!NAME TOP RIGHT SHUTTLE CORNER
allsel, all
nsel, s, loc, x, sw
nsel, r, loc, y, sl
nsel, r, loc, z, (t/2)
*get, trnode, node,, num, max
!NAME BOTTOM RIGHT SHUTTLE CORNER
allsel, all
nsel, s, loc, x, sw
nsel, r, loc, y, 0
nsel, r, loc, z, (t/2)
```

```
*get, brnode, node,, num, max
!NAME BOTTOM LEFT SHUTTLE CORNER
allsel, all
nsel, s, loc, x, 0
nsel, r, loc, y, 0
nsel, r, loc, z, (t/2)
*get, blnode, node,, num, max
!NAME N2 (SEE PAGE 28 OF NOTES)
allsel, all
nsel, s, loc, x, (sw/2)
nsel, r, loc, y, (sl/2)
nsel, r, loc, z, t
*get, n2, node,, num, max
!NAME N3 (SEE PAGE 28 OF NOTES)
allsel, all
nsel, s, loc, x, (sw/2)
nsel, r, loc, y, 0
nsel, r, loc, z, t
*get, n3, node,, num, max
!NAME N4 (SEE PAGE 28 OF NOTES)
allsel, all
nsel, s, loc, x, (sw/2)
nsel, r, loc, y, 0
nsel, r, loc, z, 0
*get, n4, node,, num, max
!NAME N5 (SEE PAGE 28 OF NOTES)
allsel, all
nsel, s, loc, x, (sw/2)
nsel, r, loc, y, sl
nsel, r, loc, z, t
*get, n5, node,, num, max
!NAME N7 (SEE PAGE 28 OF NOTES)
allsel, all
nsel, s, loc, x, (sw/2)
nsel, r, loc, y, sl
nsel, r, loc, z, 0
*get, n7, node,, num, max
!NAME N8 (SEE PAGE 28 OF NOTES)
allsel, all
nsel, s, loc, x, sw
nsel, r, loc, y, (sl/2)
nsel, r, loc, z, t
*get, n8, node,, num, max
!NAME N9 (SEE PAGE 28 OF NOTES)
allsel, all
nsel, s, loc, x, sw
nsel, r, loc, y, (sl/2)
nsel, r, loc, z, (t/2)
*get, n9, node,, num, max
!NAME N10 (SEE PAGE 28 OF NOTES)
allsel, all
nsel, s, loc, x, sw
nsel, r, loc, y, (sl/2)
nsel, r, loc, z, 0
*get, n10, node,, num, max
!NAME N11 (SEE PAGE 28 OF NOTES)
allsel, all
nsel, s, loc, x, sw
nsel, r, loc, y, 0
nsel, r, loc, z, (t/2)
*get, n11, node,, num, max
!NAME N12 (SEE PAGE 28 OF NOTES)
allsel, all
nsel, s, loc, x, sw
nsel, r, loc, y, sl
nsel, r, loc, z, (t/2)
*get, n12, node,, num, max
allsel, all
```

```
finish
!=========================================================
!                  Boundary Conditions
!=========================================================
!SOLUTION MODE
/solu
!ANALYSIS TYPE AND NON-LINEAR GEOMETRY SETTING
antype, static
nlgeom, on
!ZERO DISPLACEMENT BOUNDARY ON THE ANCHORS
allsel,all
ksel, s,,, 34
ksel, a,,, 37
ksel, a,,, 40
ksel, a,,, 43
nslk, s
d, all, all, 0.0
*do, mm, 1, loadsteps, 1
!PRESCRIBED DISPLACEMENT
allsel, all
d, backnode,, ydisp*(mm/loadsteps),,,, uy,,,,,
!INCLUDE ADDITIONAL PRESCRIBED FORCE ON SHUTTLE
allsel, all
f, n2, fz, -1*forcegrav
!SOLVE
allsel, all
outres, all
solve
*ENDDO
/replot
finish
!=========================================================
!              Post Processing Data Retrieval Post 1
!=========================================================
!POST PROCESSING MODE
/post1
!CREATE EMPTY FILES FOR DATA TO BE WRITTEN TO MID, FRONT AND BACK OF SHUTTLE
*dim, fsum_reaction, table, loadsteps
*dim, ux_mid, table, loadsteps
*dim, uy_mid, table, loadsteps
*dim, uz_mid, table, loadsteps
*dim, ux_face, table, loadsteps
*dim, uy_face, table, loadsteps
*dim, uz_face, table, loadsteps
*dim, ux_back, table, loadsteps
*dim, uy_back, table, loadsteps
*dim, uz_back, table, loadsteps
!TOP LEFT KEYPOINT DATA (SEE PAGE 21 OF NOTES)
*dim, ux_tl, table, loadsteps
*dim, uy_tl, table, loadsteps
*dim, uz_tl, table, loadsteps
!TOP RIGHT KEYPOINT DATA
*dim, ux_tr, table, loadsteps
*dim, uy_tr, table, loadsteps
*dim, uz_tr, table, loadsteps
!BOTTOM RIGHT KEYPOINT DATA
*dim, ux_br, table, loadsteps
*dim, uy_br, table, loadsteps
*dim, uz_br, table, loadsteps
!BOTTOM LEFT KEYPOINT DATA
*dim, ux_bl, table, loadsteps
*dim, uy_bl, table, loadsteps
*dim, uz_bl, table, loadsteps
*do, mm, 1, loadsteps, 1
!REACTION FORCE SUM OF THE SHUTTLE AT THE BACKNODE
allsel, all
set, mm
nsel, s,,, backnode
```

```
fsum
*get, force_in, fsum, 0, item, fy
*set, fsum_reaction(mm), force_in
!ERASE FORCE_IN
*set, force_in ,
!DISPLACEMENT OF MIDNODE
allsel, all
*get, xdisp_mid, node, midnode, u, x
*set, ux_mid(mm), xdisp_mid
*get, ydisp_mid, node, midnode, u, y
*set, uy_mid(mm), ydisp_mid
*get, zdisp_mid, node, midnode, u, z
*set, uz_mid(mm), zdisp_mid
!DISPLACEMENT OF FACENODE
allsel, all
*get, xdisp_face, node, facenode, u, x
*set, ux_face(mm), xdisp_face
*get, ydisp_face, node, facenode, u, y
*set, uy_face(mm), ydisp_face
*get, zdisp_face, node, facenode, u, z
*set, uz_face(mm), zdisp_face
!DISPLACEMENT OF BACKNODE
allsel, all
*get, nkface, node,, num, max
*get, xdisp_back, node, backnode, u, x
*set, ux_back(mm), xdisp_back
*get, ydisp_back, node, backnode, u, y
*set, uy_back(mm), ydisp_back
*get, zdisp_back, node, backnode, u, z
*set, uz_back(mm), zdisp_back
!DISPLACEMENT FOR TOP LEFT SHUTTLE NODE (SEE PAGE 21 OF NOTES)
allsel, all
*get, xdisp_tl, node, tlnode, u, x
*set, ux_tl(mm), xdisp_tl
*get, ydisp_tl, node, tlnode, u, y
*set, uy_tl(mm), ydisp_tl
*get, zdisp_tl, node, tlnode, u, z
*set, uz_tl(mm), zdisp_tl
!DISPLACEMENT FOR TOP RIGHT SHUTTLE NODE (SEE PAGE 21 OF NOTES)
allsel, all
*get, xdisp_tr, node, trnode, u, x
*set, ux_tr(mm), xdisp_tr
*get, ydisp_tr, node, trnode, u, y
*set, uy_tr(mm), ydisp_tr
*get, zdisp_tr, node, trnode, u, z
*set, uz_tr(mm), zdisp_tr
!DISPLACEMENT FOR BOTTOM RIGHT SHUTTLE NODE (SEE PAGE 21 OF NOTES)
allsel, all
*get, xdisp_br, node, brnode, u, x
*set, ux_br(mm), xdisp_br
*get, ydisp_br, node, brnode, u, y
*set, uy_br(mm), ydisp_br
*get, zdisp_br, node, brnode, u, z
*set, uz_br(mm), zdisp_br
!DISPLACEMENT FOR BOTTOM LEFT SHUTTLE NODE (SEE PAGE 21 OF NOTES)
allsel, all
*get, nkface, node,, num, max
*get, xdisp_bl, node, blnode, u, x
*set, ux_bl(mm), xdisp_bl
*get, ydisp_bl, node, blnode, u, y
*set, uy_bl(mm), ydisp_bl
*get, zdisp_bl, node, blnode, u, z
*set, uz_bl(mm), zdisp_bl
*enddo
allsel, all
/output, output_force_disp.txt
*vwrite, fsum_reaction(1), uy_back(1)
%16.8G %16.8G
```

```
/output
/output, output_shuttle_face_mid_back.txt
*vwrite, ux_face(1), uy_face(1), uz_face(1), ux_mid(1), uy_mid(1), uz_mid(1),. . .
 ux_back(1), uy_back(1), uz_back(1)
%16.8G %16.8G %16.8G %16.8G %16.8G %16.8G %16.8G %16.8G %16.8G
/output
/output, output_shuttle_corners.txt
*vwrite,ux_tl(1),uy_tl(1),uz_tl(1),ux_tr(1),uy_tr(1),uz_tr(1),ux_br(1),. . .
uy_br(1),uz_br(1),ux_bl(1),uy_bl(1),uz_bl(1)
%16.8G %16.8G %16.8G %16.8G %16.8G %16.8G %16.8G %16.8G %16.8G %16.8G %16.8G %16.8G
/output
finish
```

Appendix D

3-D Solid Element ANSYS Batch Code

```
/batch
finish
/clear, start
!CHANGE WORKING DIRECTORY
/cwd,'/tmp/bbc27'
!Title
/title, 3D_SOLID95_D_BACKNODE
!==================================
!             INPUT
!==================================
!GLOBAL VARIABLES
pi = acos(-1) !PI
tpoly1 = 2 !POLY1 THICKNESS [um]
tpoly2 = 1.5 !POLY2 THICKNESS [um]
toxide = 2 !OXIDE THICKNESS [um]
var1 = 5 !VERTICAL DISTANCE FROM TOP OF ANCHOR TO TOP OF FIRST ARM [um]
is = -0.010 !PRESTRESS VALUE OF MATERIAL (COMPRESSIVE)
grav = 9810000 !GRAVITY (um/s^2)
t = tpoly1+tpoly2 !OUT OF PLANE THICKNESS OF MECHANISM [um]
sw = 30 !SHUTTLE WIDTH [um]
sl = 100 !SHUTTLE LENGTH [um]
al1 = 75.7 !COMPLIANT ARM1 LENGTH (BETWEEN SHUTTLE AND RIGID ARM SECTION) [um]
al2 = 57.3 !COMPLIANT ARM 2 LENGTH (BETWEEN ANCHOR AND RIGID ARM SECTION) [um]
ral = 126.3 !RIGID ARM LENGTH [um]
aw = 2.5 !ARM WIDTH.  EACH ARM HAS THE SAME WIDTH [um]
raw = 5.2 !RIGID ARM WIDTH [um]
theta_degrees = 6.4 !ANGLE OF AL1 (FROM HORIZONTAL) [degrees]
phi_degrees = 5.6 !ANGLE OF RIGID ARM SECTION (FROM HORIZONTAL) [degrees]
alpha_degrees = 6.6 !ANGLE OF AL2 (FROM HORIZONTAL) [degrees]
lta1 = 5 !VERT DISTANCE FROM TOP OF SHUTTLE TO TOP EDGE OF COMPLIANT ARM[um]
fillrad = 1 !RADIUS OF FILLETS [um]
ex = 164 !MODULUS OF ELASTICITY (mN/um^2) FOR FORCE [mN]
density = 2.33*(10**(-18)) !DENSITY (1000*kg/um^3) FOR FORCE [mN]
pr = 0.22 !POISSON'S RATIO
loadsteps = 300 !LOADSTEPS TO SOLVE SOLUTION
ydisp = 46.0 !Y-DIR DISPLACEMENT OF SHUTTLE [um]
es_fillets = .6 !ELEMENT SIZE USED TO MESH FILLETS (VERY TOUCHY)
!CALCULATED DIMENSIONS
gxy = ex/((1+pr)*2) !SHEAR MODULUS [uN/um^2] or [mN/um^2]
forcegrav = density*sl*sw*t*grav !FORCE MAGNITUDE EQUAL TO 1 G OF ACC [mN]
theta = theta_degrees*pi/180 !CONVERT DEGREES TO RADIANS FOR ARM1
phi = phi_degrees*pi/180 !CONVERT DEGREES TO RADIANS FOR RIGID-ARM
alpha = alpha_degrees*pi/180 !CONVERT DEGREES TO RADIANS FOR ARM2
anx = 4 !CLEARANCE FROM POLY1 TO ANCHOR IN X DIR
any = 4 !CLEARANCE FROM POLY1 TO ANCHOR IN Y DIR
awy_anchor = aw/cos(alpha) !VERT DIST. OF ARM WHERE ARM AND ANCHOR INTERSECT
awy_shuttle = aw/cos(theta) !VERT DIST. OF ARM WHERE ARM AND SHUTTLE INTERSECT
lta2 = sl-2*lta1-2*awy_shuttle !THE VERT DIST BETWEEN THE TWO COMPLIANT LEGS
lanch = lta2+5*aw !ANCHOR LENGTH
wanch = lanch/4 !ANCHOR WIDTH
anxtemp = anx-tpoly1 !DIST FROM LEFT SIDE OF TOP ANCH VOL TO LEFT SIDE. . .
 OF MIDDLE ANCHOR VOLUME
anytemp = any-tpoly1 !DISTANCE FROM TOP OF TOP ANCHOR VOLUME TO TOP OF. . .
```

```
 MIDDLE ANCHOR VOLUME
fp2t = .01 !Z-DIR THICK OF THE MIDDLE VOLUME ON THE RIGHT ANCH
rigp =  .01 !RIGID-ARM PARTITION PERCENTAGE
ledge = (raw-aw)/2 !MEASURE OF THE LEDGE ON THE RIGID ARM (FROM AL1 OR AL2)
al1_bottom = al1 + aw*tan(theta)
al2_bottom = al2 - aw*tan(alpha)
loa = al1*cos(theta)+ral*cos(phi)+al2*cos(alpha)
es_fill_legs = aw*es_fillets !THE ELEMENT SIZE FILLETS
es_fill_sh_anch = aw*es_fillets !THE ELEMENT SIZE FILLETS
es_anchor = wanch*0.3 !THE ELEMENT SIZE OF THE ELEMENTS IN THE ANCHORS
es_shuttle = sw*0.3 !THE ELEMENT SIZE OF THE ELEMENTS IN THE SHUTTLE
es_rigarms = raw !THE ELEMENT SIZE OF THE ELEMENTS IN THE RIGID ARMS
es_comparms = aw*1.4 !THE ELEMENT SIZE OF THE ELEMENTS IN THE COMPLIANT ARMS
!================================
!            SETUP
!================================
!PRE-PROCESSOR MODE
/prep7
!CREATE MATERIAL PROPERTIES
mp, ex, 1, ex
mp, prxy, 1, pr
mp, gxy, 1, gxy
mp, dens, 1, density
!ELEMENT TYPE
et, 1, solid95
!================================
!           GEOMETRY
!================================
!SHUTTLE (ORIGIN [0,0] AT LOWER LEFT OF SHUTTLE)
k,1,0,0,0
k,2,0,sl,0
k,3,sw,sl,0
k,4,sw,0,0
k,5,0,0,t
k,6,0,sl,t
k,7,sw,sl,t
k,8,sw,0,t
!ARM 1 (TOP RIGHT ARM)
k,9,sw,(sl-lta1),0
k,10,sw+al1*cos(theta),(sl-lta1)+al1*sin(theta),0
k,11,sw+al1*cos(theta)+aw*sin(phi),(sl-lta1)+al1*sin(theta)-aw*cos(phi),0
k,12,sw,(sl-lta1)-(aw/cos(theta)),0
k,13,sw,(sl-lta1),t
k,14,sw+al1*cos(theta),(sl-lta1)+al1*sin(theta),t
k,15,sw+al1*cos(theta)+aw*sin(phi),(sl-lta1)+al1*sin(theta)-aw*cos(phi),t
k,16,sw,(sl-lta1)-(aw/cos(theta)),t
!RIGID ARM (TOP RIGHT ARM)
k,17,sw+al1*cos(theta)-ledge*sin(phi),(sl-lta1)+al1*sin(theta)+ledge*cos(phi),0
k,18,sw+al1*cos(theta)-ledge*sin(phi)+ral*cos(phi),(sl-lta1)+al1*sin(theta)+ . . .
ledge*cos(phi)+ral*sin(phi),0
k,19,sw+al1*cos(theta)+aw*sin(phi)+ledge*sin(phi)+ral*cos(phi),(sl-lta1)+ . . .
al1*sin(theta)-aw*cos(phi)-ledge*cos(phi)+ral*sin(phi),0
k,20,sw+al1*cos(theta)+aw*sin(phi)+ledge*sin(phi),(sl-lta1)+al1*sin(theta)- . . .
aw*cos(phi)-ledge*cos(phi),0
k,21,sw+al1*cos(theta)-ledge*sin(phi),(sl-lta1)+al1*sin(theta)+ledge*cos(phi),t
k,22,sw+al1*cos(theta)-ledge*sin(phi)+ral*cos(phi),(sl-lta1)+ . . .
al1*sin(theta)+ledge*cos(phi)+ral*sin(phi),t
k,23,sw+al1*cos(theta)+aw*sin(phi)+ledge*sin(phi)+ral*cos(phi),(sl-lta1)+ . . .
al1*sin(theta)-aw*cos(phi)-ledge*cos(phi)+ral*sin(phi),t
k,24,sw+al1*cos(theta)+aw*sin(phi)+ledge*sin(phi),(sl-lta1)+al1*sin(theta). . .
-aw*cos(phi)-ledge*cos(phi),t
!Arm 2 (TOP RIGHT ARM)
k,25,sw+al1*cos(theta)+ral*cos(phi),(sl-lta1)+al1*sin(theta)+ral*sin(phi),0
k,26,sw+al1*cos(theta)+ral*cos(phi)+al2*cos(alpha),(sl-lta1)+ . . .
al1*sin(theta)+ral*sin(phi)+al2*sin(alpha),0
k,27,sw+al1*cos(theta)+ral*cos(phi)+al2*cos(alpha),(sl-lta1)+ . . .
al1*sin(theta)+ral*sin(phi)+al2*sin(alpha)-awy_anchor,0
k,28,sw+al1*cos(theta)+aw*sin(phi)+ral*cos(phi),(sl-lta1)+al1*sin(theta)- . . .
```

```
aw*cos(phi)+ral*sin(phi),0
k,29,sw+al1*cos(theta)+ral*cos(phi),(sl-lta1)+al1*sin(theta)+ral*sin(phi),t
k,30,sw+al1*cos(theta)+ral*cos(phi)+al2*cos(alpha),(sl-lta1)+ . . .
al1*sin(theta)+ral*sin(phi)+al2*sin(alpha),t
k,31,sw+al1*cos(theta)+ral*cos(phi)+al2*cos(alpha),(sl-lta1)+ . . .
al1*sin(theta)+ral*sin(phi)+al2*sin(alpha)-awy_anchor,t
k,32,sw+al1*cos(theta)+aw*sin(phi)+ral*cos(phi),(sl-lta1)+al1*sin(theta)- . . .
aw*cos(phi)+ral*sin(phi),t

!KEYPOINTS FOR RIGHT ANCHOR (SEE PAGE 14 OF NOTEBOOK FOR NOTES)
k,33,sw+al1*cos(theta)+ral*cos(phi)+al2*cos(alpha),(sl-lta1)+ . . .
al1*sin(theta)+ral*sin(phi)+al2*sin(alpha)+var1,0
temp = -2*var1-2*awy_anchor-(sl-2*var1-2*awy_anchor)
k34y = (sl-lta1)+al1*sin(theta)+ral*sin(phi)+al2*sin(alpha)+var1+temp
k,34,sw+al1*cos(theta)+ral*cos(phi)+al2*cos(alpha),k34y,0
k,35,sw+al1*cos(theta)+ral*cos(phi)+al2*cos(alpha)+wanch,(sl-lta1)+ . . .
al1*sin(theta)+ral*sin(phi)+al2*sin(alpha)+var1,0
k,36,sw+al1*cos(theta)+ral*cos(phi)+al2*cos(alpha)+wanch,k34y,0
k,37,sw+al1*cos(theta)+ral*cos(phi)+al2*cos(alpha)+anx,(sl-lta1)+ . . .
al1*sin(theta)+ral*sin(phi)+al2*sin(alpha)+var1-any,t
k,38,sw+al1*cos(theta)+ral*cos(phi)+al2*cos(alpha)+wanch-anx,(sl-lta1)+ . . .
al1*sin(theta)+ral*sin(phi)+al2*sin(alpha)+var1-any,t
temp = -2*var1-2*awy_anchor-(sl-2*var1-2*awy_anchor)
k39y = (sl-lta1)+al1*sin(theta)+ral*sin(phi)+al2*sin(alpha)+var1+temp
k,39,sw+al1*cos(theta)+ral*cos(phi)+al2*cos(alpha)+anx,k39y+any,t
k,40,sw+al1*cos(theta)+ral*cos(phi)+al2*cos(alpha)+wanch-anx,k39y+any,t
k,41,sw+al1*cos(theta)+ral*cos(phi)+al2*cos(alpha),(sl-lta1)+ . . .
al1*sin(theta)+ral*sin(phi)+al2*sin(alpha)+var1,t
temp = -2*var1-2*awy_anchor-(sl-2*var1-2*awy_anchor)
k42y = (sl-lta1)+al1*sin(theta)+ral*sin(phi)+al2*sin(alpha)+var1+temp
k,42,sw+al1*cos(theta)+ral*cos(phi)+al2*cos(alpha),k42y,t
k,43,sw+al1*cos(theta)+ral*cos(phi)+al2*cos(alpha)+wanch,(sl-lta1)+ . . .
al1*sin(theta)+ral*sin(phi)+al2*sin(alpha)+var1,t
k,44,sw+al1*cos(theta)+ral*cos(phi)+al2*cos(alpha)+wanch,k34y,t
k,45,sw+al1*cos(theta)+ral*cos(phi)+al2*cos(alpha)+anx,(sl-lta1)+ . . .
al1*sin(theta)+ral*sin(phi)+al2*sin(alpha)+var1-any,t-toxide+fp2t
k,46,sw+al1*cos(theta)+ral*cos(phi)+al2*cos(alpha)+wanch-anx,(sl-lta1)+ . . .
al1*sin(theta)+ral*sin(phi)+al2*sin(alpha)+var1-any,t-toxide+fp2t
temp = -2*var1-2*awy_anchor-(sl-2*var1-2*awy_anchor)
k47y = (sl-lta1)+al1*sin(theta)+ral*sin(phi)+al2*sin(alpha)+var1+temp
k,47,sw+al1*cos(theta)+ral*cos(phi)+al2*cos(alpha)+anx,k47y+any,t-toxide+fp2t
k,48,sw+al1*cos(theta)+ral*cos(phi)+al2*cos(alpha)+wanch-anx,k39y+ . . .
any,t-toxide+fp2t
k,49,sw+al1*cos(theta)+ral*cos(phi)+al2*cos(alpha)+anxtemp,(sl-lta1)+ . . .
al1*sin(theta)+ral*sin(phi)+al2*sin(alpha)+var1-anytemp,0
k,50,sw+al1*cos(theta)+ral*cos(phi)+al2*cos(alpha)+wanch-anxtemp, . . .
(sl-lta1)+al1*sin(theta)+ral*sin(phi)+al2*sin(alpha)+var1-anytemp,0
k51x = sw+al1*cos(theta)+ral*cos(phi)+al2*cos(alpha)+wanch-anxtemp
temp = -2*var1-2*awy_anchor-(sl-2*var1-2*awy_anchor)+any
k51y = (sl-lta1)+al1*sin(theta)+ral*sin(phi)+al2*sin(alpha)+var1-anytemp+temp
k,51,k51x,k51y,0
k52x = sw+al1*cos(theta)+ral*cos(phi)+al2*cos(alpha)+anxtemp
temp = -2*var1-2*awy_anchor-(sl-2*var1-2*awy_anchor)+any
k52y = (sl-lta1)+al1*sin(theta)+ral*sin(phi)+al2*sin(alpha)+var1-anytemp+temp
k,52,k52x,k52y,0
k,53,sw+al1*cos(theta)+ral*cos(phi)+al2*cos(alpha)+anxtemp,(sl-lta1)+ . . .
al1*sin(theta)+ral*sin(phi)+al2*sin(alpha)+var1-anytemp,-toxide
k,54,sw+al1*cos(theta)+ral*cos(phi)+al2*cos(alpha)+wanch-anxtemp, . . .
(sl-lta1)+al1*sin(theta)+ral*sin(phi)+al2*sin(alpha)+var1-anytemp,-toxide
k55x = sw+al1*cos(theta)+ral*cos(phi)+al2*cos(alpha)+wanch-anxtemp
temp = -2*var1-2*awy_anchor-(sl-2*var1-2*awy_anchor)+any
k55y = (sl-lta1)+al1*sin(theta)+ral*sin(phi)+al2*sin(alpha)+var1-anytemp+temp
k,55,k55x,k55y,-toxide
k56x = sw+al1*cos(theta)+ral*cos(phi)+al2*cos(alpha)+anxtemp
temp = -2*var1-2*awy_anchor-(sl-2*var1-2*awy_anchor)+any
k56y = (sl-lta1)+al1*sin(theta)+ral*sin(phi)+al2*sin(alpha)+var1-anytemp+temp
k,56,k56x,k56y,-toxide
k,57,sw+al1*cos(theta)+ral*cos(phi)+al2*cos(alpha),k34y,t-toxide+fp2t
```

```
k,58,sw+al1*cos(theta)+ral*cos(phi)+al2*cos(alpha),(sl-lta1)+ . . .
al1*sin(theta)+ral*sin(phi)+al2*sin(alpha)+var1,t-toxide+fp2t
k,59,sw+al1*cos(theta)+ral*cos(phi)+al2*cos(alpha)+wanch,k34y,t-toxide+fp2t
k,60,sw+al1*cos(theta)+ral*cos(phi)+al2*cos(alpha)+wanch,(sl-lta1)+ . . .
al1*sin(theta)+ral*sin(phi)+al2*sin(alpha)+var1,t-toxide+fp2t
!!!!!!!!!!!!!!!
!DEFINE VOLUMES
!!!!!!!!!!!!!!!
!SHUTTLE VOLUME
v, 1, 2, 3, 4, 5, 6, 7, 8
!RIGHT ARM VOLUMES
!ARM 1 (TOP RIGHT ARM)
v, 9, 10, 11, 12, 13, 14, 15, 16
!RIGID ARM (TOP RIGHT ARM)
v, 17, 18, 19, 20, 21, 22, 23, 24
!ARM 2 (TOP RIGHT ARM)
v, 25, 26, 27, 28, 29, 30, 31, 32
!GENERATE LOWER RIGHT ARM FROM TOP RIGHT ARM
VSEL, s,,, 2, 4, 1
VGEN, 2, all,,, 0, -lta2-awy_shuttle,
!RIGHT ANCHOR VOLUMES
!TOP SURFACE (TOP VOLUME)
a, 41, 37, 39, 42
a, 41, 43, 38, 37
a, 43, 38, 40, 44
a, 42, 39, 40, 44
aadd, 43, 44, 45, 46
!SIDES SURFACES (TOP VOLUME)
a, 42, 57, 58, 41
a, 41, 43, 60, 58
a, 44, 43, 60, 59
a, 42, 44, 59, 57
a, 39, 37, 45, 47
a, 37, 38, 46, 45
a, 40, 38, 46, 48
a, 39, 40, 48, 47
!BOTTOM SURFACE (TOP VOLUME)
a, 57, 58, 45, 47
a, 58, 60, 46, 45
a, 60, 59, 48, 46
a, 57, 47, 48, 59
aadd, 52, 53, 54, 55
!TOP VOLUME FROM AREAS
va, 43, 44, 45, 46, 47, 48, 49, 50, 51, 56
!TOP SURFACE (MIDDLE VOLUME)
a,57, 58, 60, 59
!SIDE SURFACES (MIDDLE VOLUME)
a, 57, 58, 33, 34
a, 58, 60, 35, 33
a, 59, 60, 35, 36
a, 57, 59, 36, 34
!BOTTOM SURFACE (MIDDLE VOLUME)
a, 34, 33, 35, 36
!CREATE  MIDDLE VOLUME FROM AREAS
va, 52, 53, 54, 55, 57, 58
!TOP SURFACE (BOTTOM VOLUME)
a ,52, 49, 50, 51
!SIDE SURFACES (BOTTOM VOLUME)
a, 52, 49, 53, 56
a, 49, 50, 54, 53
a, 51, 50, 54, 55
a, 52, 51, 55, 56
!BOTTOM SURFACE (BOTTOM VOLUME)
a, 56, 53, 54, 55
!BOTTOM VOLUME FROM AREAS
va, 59, 60, 61, 62, 63, 64
!ADD THREE CREATED VOLUMES AS ONE
vadd, 8, 9, 10
```

```
!GLUE ALL VOLUMES TOGETHER
allsel, all
vglue, all
!ADD AREAS ON LEFT SIDE OF ANCHOR AS PRE-REQUISITE FOR FILLETS ON LEFT SIDE
aadd, 89, 90
aadd, 52, 56
aadd, 92, 93
aadd, 67, 68
aadd, 88, 91
!COMBINE LINES FOR ONE SHARED LINE
lcomb, 129, 132
lcomb, 130, 133
lcomb, 134, 137
lcomb, 135, 138
!!!!!!!!
!FILLETS
!!!!!!!!
!SHUTTLE/ARM1 INTERSECTIONS (TOP TO BOTTOM)
allsel, all
afillt, 8, 71, fillrad
a, 13, 96, 98
a, 9, 95, 97
va, 8, 18, 21, 33, 36
afillt, 10, 73, fillrad
a, 16, 100, 102
a, 12, 99, 101
va, 10, 31, 38, 43, 47
afillt, 26, 35, fillrad
a, 66, 104, 106
a, 61, 103, 105
va, 26, 35, 40, 67, 68
afillt, 28, 72, fillrad
a, 68, 108, 110
a, 64, 107, 109
va, 28, 56, 71, 89, 91
!ARM1/RIGID ARM INTERSECTIONS (TOP TO BOTTOM)
afillt, 17, 76, fillrad
a, 14, 112, 114
a, 10, 111, 113
va, 17, 73, 76, 93, 97
afillt, 22, 77, fillrad
a, 15, 116, 118
a, 11, 115, 117
va, 22, 77, 92, 100, 102
afillt, 39, 82, fillrad
a, 65, 120, 122
a, 62, 119, 121
va, 39, 82, 99, 105, 107
afillt, 53, 83, fillrad
a, 67, 124, 126
a, 63, 123, 125
va, 53, 83, 104, 110, 112
!RIGID ARM/ARM2 INTERSECTIONS (TOP TO BOTTOM)
afillt, 58, 78, fillrad
a, 29, 128, 130
a, 25, 127, 129
va, 58, 78, 109, 115, 118
afillt, 59, 79, fillrad
a, 32, 132, 134
a, 28, 131, 133
va, 59, 79, 114, 120, 123
afillt, 69, 84, fillrad
a, 82, 136, 138
a, 77, 135, 137
va, 69, 84, 119, 125, 128
afillt, 70, 85, fillrad
a, 84, 140, 142
a, 80, 139, 141
```

```
va, 70, 85, 124, 130, 133
!ARM2/RIGHT ANCHOR INTERSECTIONS (TOP TO BOTTOM)
afillt, 1, 108, fillrad
a, 30, 144, 146
a, 26, 93, 145
va, 1, 108, 129, 135, 137
afillt, 6, 113, fillrad
a, 31, 148, 150
a, 27, 147, 149
va, 6, 113, 134, 140, 142
afillt, 117, 132, fillrad
a, 81, 152, 154
a, 78, 151, 153
va, 117, 132, 139, 145, 147
afillt, 15, 122, fillrad
a, 83, 156, 158
a, 79, 94, 157
va, 15, 122, 144, 150, 152
!!!!!!!!!!!!!!!!!!!!!!!!!!!!!!!!!!!!!!!!!!!!!!!!
!PARTITION VOLUMES FOR REFINED MESHING VOLUMES
!!!!!!!!!!!!!!!!!!!!!!!!!!!!!!!!!!!!!!!!!!!!!!!!
!PARTITION SHUTTLE
wpstyle, 0.05 ,0.1, -100 ,100, 0.003, 0, 1,, 5
wpro,,, 90.000000
wpof,,, sw*0.1
!LEFT SIDE OF SHUTTLE
vsbw, 10
!RIGHT SIDE OF SHUTTLE
wpof,,, sw*0.8
vsbw, 26
!HORIZONTAL SHUTTLE PARTITIONS (TOP TO BOTTOM)
kwplan, -1, 98, 97, 102
wpro,, 90
vsbw, 25
vsbw, 27
kwplan, -1, 102, 101, 98
wpro,, 90
vsbw, 28
vsbw, 29
kwplan, -1, 106, 105, 110
wpro,, 90
vsbw, 27
vsbw, 31
kwplan, -1, 110, 109, 106
wpro,, 90
vsbw, 29
vsbw, 33
!SHUTTLE/ARM1 INTERSECTION PARTITIONS (TOP TO BOTTOM)
kwplan, -1, 96, 95, 100
vsbw, 2
kwplan, -1, 104, 103, 108
vsbw, 5
!LEFT ARM1/RIGID-ARM INTERSECTION PARTIONS (TOP TO BOTTOM)
kwplan, -1, 112, 111, 116
vsbw, 36
kwplan, -1, 120, 119, 124
vsbw, 37
!RIGHT ARM1/RIGID-ARM INTERSECTION PARTITIONS (TOP TO BOTTOM)
kwplan, -1, 17, 21, 24
wpof,,, ral*rigp
vsbw, 12
kwplan, -1, 69, 74, 76
wpof,,, ral*rigp
vsbw, 13
!LEFT RIGID-ARM/ARM2 INTERSECTION PARTITIONS (TOP TO BOTTOM)
kwplan, -1, 18, 22, 23
wpof,,, -ral*rigp
vsbw, 40
```

```
kwplan, -1, 70, 73, 75
wpof,,, -ral*rigp
vsbw, 41
!RIGHT RIGID-ARM/ARM2 INTERSECTION PARTITIONS (TOP TO BOTTOM)
kwplan, -1, 127, 128, 132
vsbw, 8
kwplan, -1, 135, 136, 140
vsbw, 9
!ARM2/ANCHOR INTERSECTION PARTITIONS (TOP TO BOTTOM)
kwplan, -1, 145, 146, 150
vsbw, 44
kwplan, -1, 151, 152, 158
vsbw, 45
!LEFT SIDE OF RIGHT ANCHOR PARTITIONS
!VERTICAL
kwplan, -1, 93, 144, 148
wpof,,, anxtemp/2
vsbw, 14
!HORIZONTAL (TOP TO BOTTOM)
kwplan, -1, 93, 144, 148
wpro,, 90
vsbw, 45
kwplan, -1, 148, 147, 93
wpro,, 90
vsbw, 49
kwplan, -1, 153, 154, 156
wpro,, 90
vsbw, 50
kwplan, -1, 156, 94, 153
wpro,, 90
vsbw, 51
vglue, all
!!!!!!!!!!!!!!!!!!!!!!!!!!!!!!
!ADD VOLUMES TO SIMPLIFY MODEL
!!!!!!!!!!!!!!!!!!!!!!!!!!!!!!
!SHUTTLE
vadd, 25, 10, 26, 32, 27, 31, 29
!SHUTTLE/ARM1 INTERSECTIONS (TOP TO BOTTOM)
vadd, 28, 1, 3, 33
vadd, 35, 2, 4, 6
!ARM1/RIGID-ARM INTERSECTION (TOP TO BOTTOM)
vadd, 5, 7, 11, 37
vadd, 36, 12, 15, 16
!RIGID-ARM/ARM2 INTERSECTION (TOP TO BOTTOM)
vadd, 42, 17, 18, 41
vadd, 43, 8, 19, 20
!ARM2/RIGHT ANCHOR INTERSECTION (TOP TO BOTTOM)
vadd, 9, 21, 22, 45
vadd, 23, 24, 44, 52
!RIGHT ANCHOR
vadd, 14, 48, 49, 50
!!!!!!!!!!!!!!!!!!!!!!!!!!!!!!
!ADD AREAS TO SIMPLIFY MODEL
!!!!!!!!!!!!!!!!!!!!!!!!!!!!!!
!SHUTTLE/ARM1 INTERSECTION (TOP-FRONT, TOP-BACK, BOTTOM-FRONT, BOTTOM-BACK)
aadd, 168, 8, 10, 188
aadd, 167, 21, 187, 38
aadd, 198, 26, 12, 28
aadd, 197, 35, 7, 71
!ARM1/RIGID-ARM INTERSECTION (TOP-FRONT, TOP-BACK, BOTTOM-FRONT, BOTTOM-BACK)
aadd, 212, 17, 30, 22
aadd, 211, 76, 25, 77
aadd, 217, 39, 200, 53
aadd, 81, 82, 199, 83
!RIGID-ARM/ARM2 INTERSECTION (TOP-FRONT, TOP-BACK, BOTTOM-FRONT, BOTTOM-BACK)
aadd, 226, 58, 219, 59
aadd, 225, 78, 218, 79
aadd, 231, 69, 24, 70
```

```
aadd, 230, 84, 19, 85
!ARM2/ANCHOR INTERSECTION (TOP-FRONT, TOP-BACK, BOTTOM-FRONT, BOTTOM-BACK)
aadd, 254, 1, 42, 6
aadd, 113, 246
aadd, 1, 108
aadd, 6, 37
aadd, 265, 117, 232, 15
aadd, 264, 132, 221, 122
!SHUTTLE FRONT
aadd, 157, 74, 148, 185, 163, 180, 170
!SHUTTLE BOTTOM (LOCATION OF DISPLACEMENT)
aadd, 153, 75, 161
!SHUTTLE TOP
aadd, 160, 5, 149
!SHUTTLE BACK
aadd, 2, 3, 156, 162, 184, 169, 179
!ANCHOR FRONT
aadd, 54, 251, 253, 257
aadd, 234, 248, 250, 243
aadd, 242, 249, 247, 235
aadd, 45, 55
!DELETE AREAS ON THE LEFT SIDE SO THE ENTIRE RIGHT SIDE CAN BE MIRRORED
vdele, 30,,, 1
vdele, 34,,, 1
!!!!!!!!!!!!!!!!!!!!!!!!!!
!MIRROR RIGHT SIDE TO LEFT
!!!!!!!!!!!!!!!!!!!!!!!!!!
!MIRROR ENRTIRE RIGHT SIDE TO LEFT
allsel, all
vsel, s,,, all
vsel, u,,, 51
vsymm, x, all
allsel,all
vsel, s,,, 9
vsel, a,,, 11, 12, 1
vsel, a,,, 14, 25, 1
vgen,1,all,,,sw,,,,,1
!GLUE ALL VOLUMES TOGETHER
allsel, all
vglue, all
!!!!!!!!!!!!!!!!!!!!!!!!!!!!!!!!!!!!!!!!!!!!!!!!!!!!!!!!!!!!!!!!!!!!!!!
!PARTITION SHUTTLE FURTHER FOR APPLICATION OF DISPLACEMENT AT SPECIFIC LOCATIONS
!!!!!!!!!!!!!!!!!!!!!!!!!!!!!!!!!!!!!!!!!!!!!!!!!!!!!!!!!!!!!!!!!!!!!!!!
!PARTITION THE SHUTTLE AT HALF THE THICKNESS
kwplan, -1, 6, 7, 8
wpof,,, t/2
vsbw, 26
!PARTITION THE SHUTTLE AT THE MIDPOINT OF Y/Z PLANE
kwplan, -1, 2, 5, 6
wpof,,, -sw/2
vsbw, 28
vsbw, 27
!PARTITION SHUTTLE AT THE MIDPOINT OF X/Z PLANE
kwplan, -1, 4, 5, 8
wpof,,, sl/2
vsbw, 26
vsbw, 28
vsbw, 29
vsbw, 30
!COMPRESS THE NUMBERING SYSTEM
numcmp, all

/replot
wpstyle,,,,,,,,0
!=========================================================
!                     MESH GEOMETRY
!=========================================================
!!!!!!!!!!!!!!!!!!!
```

```
!MESH COMPLIANT LEGS
!!!!!!!!!!!!!!!!!!!
allsel, all
vsel, s,,, 21, 22, 1
vsel, a,,, 24, 25, 1
vsel, a,,, 34, 35, 1
vsel, a,,, 37, 38, 1
esize, es_comparms
mshape, 1, 3d
mshkey, 0
vmesh, all
vimp, all
!!!!!!!!!!!!!!!
!MESH RIGID-ARMS
!!!!!!!!!!!!!!!
allsel, all
vsel, s,,, 13
vsel, a,,, 20, 23, 3
vsel, a,,, 36
esize, es_rigarms
mshape, 1, 3d
mshkey, 0
vmesh, all
vimp, all
!!!!!!!!!!!!!
!MESH SHUTTLE
!!!!!!!!!!!!!
allsel, all
vsel, s,,, 26, 33, 1
esize, es_shuttle
mshape, 1, 3d
mshkey, 0
lsel, s,,, 6, 8, 2
lsel, a,,, 24
lsel, a,,, 40
lsel, a,,, 43, 44, 1
lsel, a,,, 249
lsel, a,,, 282
lsel, a,,, 286
lsel, a,,, 295, 297, 1
lsel, a,,, 302
lsel, a,,, 311, 319, 4
lsel, a,,, 331, 334, 3
lsel, a,,, 498, 500, 2
lsel, a,,, 504, 505, 1
lsel, a,,, 542, 546, 4
lesize, all,,, 3,,,,, 1
lsel, s,,, 48, 49, 1
lsel, a,,, 299
lsel, a,,, 313, 316, 3
lsel, a,,, 333, 338, 5
lsel, a,,, 340, 341, 1
lsel, a,,, 501, 503, 2
lsel, a,,, 543
lesize, all,,, 2,,,,, 1
vmesh, all
vimp,all
!!!!!!!!!!!!!
!MESH ANCHORS
!!!!!!!!!!!!!
allsel, all
vsel, s,,, 8
vsel, a,,, 18
esize, es_anchor
mshape, 1, 3d
mshkey, 0
vmesh, all
! SELECT AREAS FOR REFINEMENT ON RIGHT ANCHOR
```

```
asel, s,,, 44, 46, 2
asel, a,,, 94, 95, 1
asel, a,,, 127
asel, a,,, 141, 143, 2
asel, a,,, 243, 244, 1
asel, a,,, 254, 255, 1
asel, a,,, 261
! SELECT AREAS FOR REFINEMENT ON LEFT ANCHOR
asel, a,,, 122, 123, 1
asel, a,,, 125
asel, a,,, 137
asel, a,,, 140, 142, 2
asel, a,,, 148, 149, 1
asel, a,,, 167, 169, 1
asel, a,,, 170
arefine, all,,, 1, 0, clean, on
vimp, all
!!!!!!!!!!!!!
!MESH FILLETS
!!!!!!!!!!!!!
!MESH AND REFINE FILLETS VOLUMES AT THE COMPLIANT LEG/SHUTTLE AND COMPLIANT LEG/ANCHOR
allsel, all
vsel, s,,, 1
vsel, a,,, 6, 7, 1
vsel, a,,, 9, 10, 1
vsel, a,,, 16, 17, 1
vsel, a,,, 19
esize,, es_fill_sh_anch
mshape, 1, 3d
mshkey, 0
vmesh, all
vimp, all
! REFINE THE MESH OF VOLUME 1
arefine, 40,,, 1, 0, clean, on
arefine, 56,,, 1, 0, clean, on
vimp, 1
! REFINE THE MESH OF VOLUME 6
arefine, 129,,, 1, 0, clean, on
arefine, 134,,, 1, 0, clean, on
vimp, 6
! REFINE THE MESH OF VOLUME 7
arefine, 139,,, 1, 0, clean, on
arefine, 144,,, 1, 0, clean, on
vimp, 7
! REFINE THE MESH OF VOLUME 9
arefine, 29,,, 1, 0, clean, on
arefine, 30,,, 1, 0, clean, on
vimp, 9
! REFINE THE MESH OF VOLUME 10
arefine, 18,,, 1, 0, clean, on
arefine, 31,,, 1, 0, clean, on
vimp, 10
! REFINE THE MESH OF VOLUME 16
arefine, 117,,, 1, 0, clean, on
arefine, 120,,, 1, 0, clean, on
vimp, 16
! REFINE THE MESH OF VOLUME 17
arefine, 132,,, 1, 0, clean, on
arefine, 135,,, 1, 0, clean, on
vimp, 17
! REFINE THE MESH OF VOLUME 19
arefine, 179,,, 1, 0, clean, on
arefine, 184,,, 1, 0, clean, on
vimp, 19
vimp, all
!MESH AND REFINE FILLET VOLUMES AT THE COMPLIANT-LEG/RIGID-LEG INTERSECTIONS
allsel, all
vsel, s,,, 2, 5, 1
```

```
vsel, a,,, 11, 12, 1
vsel, a,,, 14, 15, 1
esize, es_fill_legs
mshape, 1, 3d
mshkey, 0
vmesh, all
vimp, all
! REFINE THE MESH OF VOLUME 2 (LEFT SIDE OF TOP RIGHT ARM)
arefine, 73,,, 2, 0, clean, on
arefine, 92,,, 2, 0, clean, on
vimp, 2
! REFINE THE MESH OF VOLUME 3 (LEFT SIDE OF BOTTOM RIGHT ARM)
arefine, 99,,, 2, 0, clean, on
arefine, 104,,, 2, 0, clean, on
vimp, 3
! REFINE THE MESH OF VOLUME 4 (RIGHT SIDE OF TOP RIGHT ARM)
arefine, 109,,, 2, 0, clean, on
arefine, 114,,, 2, 0, clean, on
vimp, 4
! REFINE THE MESH OF VOLUME 5 (RIGHT SIDE OF BOTTOM RIGHT ARM)
arefine, 119,,, 2, 0, clean, on
arefine, 124,,, 2, 0, clean, on
vimp, 5
! REFINE THE MESH OF VOLUME 11 (RIGHT SIDE OF TOP LEFT ARM)
arefine, 41,,, 2, 0, clean, on
arefine, 42,,, 2, 0, clean, on
vimp, 11
! REFINE THE MESH OF VOLUME 12 (RIGHT SIDE OF BOTTOM LEFT ARM)
arefine, 59,,, 2, 0, clean, on
arefine, 74,,, 2, 0, clean, on
vimp, 12
! REFINE THE MESH OF VOLUME 14 (LEFT SIDE OF TOP LEFT ARM)
arefine, 78,,, 2, 0, clean, on
arefine, 81,,, 2, 0, clean, on
vimp, 14
! REFINE THE MESH OF VOLUME 15
arefine, 100,,, 2, 0, clean, on
arefine, 102,,, 2, 0, clean, on
vimp, 15
!REFINE THE MESH A COUPLE TIMES TO IMPROVE QUALITY
allsel, all
vimp, all
vimp, all
!NAME BACKNODE
allsel, all
nsel, s, loc, x, (sw/2)
nsel, r, loc, y, sl
nsel, r, loc, z, (t/2)
*get, backnode, node,, num, max
!REFINE ELEMENTS ON BACKNODE
allsel, all
nrefine, backnode,,, 1, 1, clean, on
!COMPRESS THE NUMBERING SYSTEM
allsel, all
numcmp, all
!!!!!!!!!!!
!NAME NODES
!!!!!!!!!!!
!NAME FACENODE
allsel, all
nsel, s, loc, x, (sw/2)
nsel, r, loc, y, 0
nsel, r, loc, z, (t/2)
*get, facenode, node,, num, max
!NAME MIDNODE
allsel, all
nsel, s, loc, x, (sw/2)
nsel, r, loc, y, (sl/2)
```

```
nsel, r, loc, z, (t/2)
*get, midnode, node,, num, max
!NAME BACKNODE
allsel, all
nsel, s, loc, x, (sw/2)
nsel, r, loc, y, sl
nsel, r, loc, z, (t/2)
*get, backnode, node,, num, max
!NAME TOP LEFT SHUTTLE CORNER
allsel, all
nsel, s, loc, x, 0
nsel, r, loc, y, sl
nsel, r, loc, z, (t/2)
*get, tlnode, node,, num, max
!NAME TOP RIGHT SHUTTLE CORNER
allsel, all
nsel, s, loc, x, sw
nsel, r, loc, y, sl
nsel, r, loc, z, (t/2)
*get, trnode, node,, num, max
!NAME BOTTOM RIGHT SHUTTLE CORNER
allsel, all
nsel, s, loc, x, sw
nsel, r, loc, y, 0
nsel, r, loc, z, (t/2)
*get, brnode, node,, num, max
!NAME BOTTOM LEFT SHUTTLE CORNER
allsel, all
nsel, s, loc, x, 0
nsel, r, loc, y, 0
nsel, r, loc, z, (t/2)
*get, blnode, node,, num, max
!NAME N2 (SEE PAGE 28 OF NOTES)
allsel, all
nsel, s, loc, x, (sw/2)
nsel, r, loc, y, (sl/2)
nsel, r, loc, z, t
*get, n2, node,, num, max
!NAME N3 (SEE PAGE 28 OF NOTES)
allsel, all
nsel, s, loc, x, (sw/2)
nsel, r, loc, y, 0
nsel, r, loc, z, t
*get, n3, node,, num, max
!NAME N4 (SEE PAGE 28 OF NOTES)
allsel, all
nsel, s, loc, x, (sw/2)
nsel, r, loc, y, 0
nsel, r, loc, z, 0
*get, n4, node,, num, max
!NAME N5 (SEE PAGE 28 OF NOTES)
allsel, all
nsel, s, loc, x, (sw/2)
nsel, r, loc, y, sl
nsel, r, loc, z, t
*get, n5, node,, num, max
!NAME N7 (SEE PAGE 28 OF NOTES)
allsel, all
nsel, s, loc, x, (sw/2)
nsel, r, loc, y, sl
nsel, r, loc, z, 0
*get, n7, node,, num, max
!NAME N8 (SEE PAGE 28 OF NOTES)
allsel, all
nsel, s, loc, x, sw
nsel, r, loc, y, (sl/2)
nsel, r, loc, z, t
*get, n8, node,, num, max
```

```
!NAME N9 (SEE PAGE 28 OF NOTES)
allsel, all
nsel, s, loc, x, sw
nsel, r, loc, y, (sl/2)
nsel, r, loc, z, (t/2)
*get, n9, node,, num, max
!NAME N10 (SEE PAGE 28 OF NOTES)
allsel, all
nsel, s, loc, x, sw
nsel, r, loc, y, (sl/2)
nsel, r, loc, z, 0
*get, n10, node,, num, max
!NAME N11 (SEE PAGE 28 OF NOTES)
allsel, all
nsel, s, loc, x, sw
nsel, r, loc, y, 0
nsel, r, loc, z, (t/2)
*get, n11, node,, num, max
!NAME N12 (SEE PAGE 28 OF NOTES)
allsel, all
nsel, s, loc, x, sw
nsel, r, loc, y, sl
nsel, r, loc, z, (t/2)
*get, n12, node,, num, max
allsel,all
finish
!=========================================================
!                  Boundary Conditions
!=========================================================
!SOLUTION MODE
/solu
!ANALYSIS TYPE AND NON-LINEAR GEOMETRY SETTING:
antype, static
nlgeom, on
nsubst
!TIGHTEN THE CONVERGENCE TOLERANCE FOR ACCURACY
cnvtol, u,, 0.000001,, 0.01
cnvtol, f,, 0.000001,, 0.01
!APPLY PRESTRESS (COMPRESSIVE) TO ALL MATERIAL IN ALL DIRECTIONS
istress, is, is, is
!ZERO DISPLACEMENT BOUNDARY ON THE ANCHORS
allsel,all
asel, s,,, 64
asel, a,,, 154
nsla, s, 1
d, all, ux, 0
d, all, uy, 0
d, all, uz, 0
!!!!!!!!!!!!!!!!!!!!!!!!!
!DISPLACEMENTS AND FORCES
!!!!!!!!!!!!!!!!!!!!!!!!!
*do, mm, 1, loadsteps, 1
!GRAVITY (OPPOSITE DIRECTION OF DESIRED DISPLACEMENT)
!allsel, all
!acel, 0, 0, 10*grav
!PRESCRIBED DISPLACEMENT AT NODE ON SHUTTLE BACK
!BRING IN VARIABLES FROM EXTERNAL FILE
d, backnode, uy, (mm/loadsteps)*ydisp
!INCLUDE ADDITIONAL PRESCRIBED FORCE ON SHUTTLE
!BRING IN VARIABLES FROM EXTERNAL FILE
!f, n2, fz, -1*forcegrav
!SOLVE
allsel, all
outres, all
solve
*ENDDO
/replot
finish
```

```
!=========================================================
!              Post Processing Data Retrieval Post 1
!=========================================================
!POST PROCESSING MODE
/post1
!CREATE EMPTY FILES FOR DATA TO BE WRITTEN TO MID, FRONT AND BACK OF SHUTTLE
*dim, fsum_reaction, table, loadsteps
*dim, ux_mid, table, loadsteps
*dim, uy_mid, table, loadsteps
*dim, uz_mid, table, loadsteps
*dim, ux_face, table, loadsteps
*dim, uy_face, table, loadsteps
*dim, uz_face, table, loadsteps
*dim, ux_back, table, loadsteps
*dim, uy_back, table, loadsteps
*dim, uz_back, table, loadsteps
!TOP LEFT KEYPOINT DATA (SEE PAGE 21 OF NOTES)
*dim, ux_tl, table, loadsteps
*dim, uy_tl, table, loadsteps
*dim, uz_tl, table, loadsteps
!TOP RIGHT KEYPOINT DATA
*dim, ux_tr, table, loadsteps
*dim, uy_tr, table, loadsteps
*dim, uz_tr, table, loadsteps
!BOTTOM RIGHT KEYPOINT DATA
*dim, ux_br, table, loadsteps
*dim, uy_br, table, loadsteps
*dim, uz_br, table, loadsteps
!BOTTOM LEFT KEYPOINT DATA
*dim, ux_bl, table, loadsteps
*dim, uy_bl, table, loadsteps
*dim, uz_bl, table, loadsteps
*do, mm, 1, loadsteps, 1
!REACTION FORCE SUM OF THE SHUTTLE AT THE BACKNODE
allsel, all
set, mm
nsel, s,,, backnode
fsum
*get, force_in, fsum, 0, item, fy
*set, fsum_reaction(mm), force_in
!ERASE FORCE_IN
*set, force_in ,
!DISPLACEMENT OF MIDNODE
allsel, all
*get, xdisp_mid, node, midnode, u, x
*set, ux_mid(mm), xdisp_mid
*get, ydisp_mid, node, midnode, u, y
*set, uy_mid(mm), ydisp_mid
*get, zdisp_mid, node, midnode, u, z
*set, uz_mid(mm), zdisp_mid
!DISPLACEMENT OF FACENODE
allsel, all
*get, xdisp_face, node, facenode, u, x
*set, ux_face(mm), xdisp_face
*get, ydisp_face, node, facenode, u, y
*set, uy_face(mm), ydisp_face
*get, zdisp_face, node, facenode, u, z
*set, uz_face(mm), zdisp_face
!DISPLACEMENT OF BACKNODE
allsel, all
*get, nkface, node,, num, max
*get, xdisp_back, node, backnode, u, x
*set, ux_back(mm), xdisp_back
*get, ydisp_back, node, backnode, u, y
*set, uy_back(mm), ydisp_back
*get, zdisp_back, node, backnode, u, z
*set, uz_back(mm), zdisp_back
!DISPLACEMENT FOR TOP LEFT SHUTTLE NODE (SEE PAGE 21 OF NOTES)
```

```
allsel, all
*get, xdisp_tl, node, tlnode, u, x
*set, ux_tl(mm), xdisp_tl
*get, ydisp_tl, node, tlnode, u, y
*set, uy_tl(mm), ydisp_tl
*get, zdisp_tl, node, tlnode, u, z
*set, uz_tl(mm), zdisp_tl
!DISPLACEMENT FOR TOP RIGHT SHUTTLE NODE (SEE PAGE 21 OF NOTES)
allsel, all
*get, xdisp_tr, node, trnode, u, x
*set, ux_tr(mm), xdisp_tr
*get, ydisp_tr, node, trnode, u, y
*set, uy_tr(mm), ydisp_tr
*get, zdisp_tr, node, trnode, u, z
*set, uz_tr(mm), zdisp_tr
!DISPLACEMENT FOR BOTTOM RIGHT SHUTTLE NODE (SEE PAGE 21 OF NOTES)
allsel, all
*get, xdisp_br, node, brnode, u, x
*set, ux_br(mm), xdisp_br
*get, ydisp_br, node, brnode, u, y
*set, uy_br(mm), ydisp_br
*get, zdisp_br, node, brnode, u, z
*set, uz_br(mm), zdisp_br
!DISPLACEMENT FOR BOTTOM LEFT SHUTTLE NODE (SEE PAGE 21 OF NOTES)
allsel, all
*get, nkface, node,, num, max
*get, xdisp_bl, node, blnode, u, x
*set, ux_bl(mm), xdisp_bl
*get, ydisp_bl, node, blnode, u, y
*set, uy_bl(mm), ydisp_bl
*get, zdisp_bl, node, blnode, u, z
*set, uz_bl(mm), zdisp_bl
*enddo
allsel, all
/output, output_force_disp.txt
*vwrite, fsum_reaction(1), uy_back(1)
%16.8G %16.8G
/output
/output, output_shuttle_face_mid_back.txt
*vwrite,ux_face(1),uy_face(1),uz_face(1),ux_mid(1),uy_mid(1),uz_mid(1),. . .
ux_back(1),uy_back(1),uz_back(1)
%16.8G %16.8G %16.8G %16.8G %16.8G %16.8G %16.8G %16.8G %16.8G
/output
/output, output_shuttle_corners.txt
*vwrite,ux_tl(1),uy_tl(1),uz_tl(1),ux_tr(1),uy_tr(1),uz_tr(1),ux_br(1),. . .
uy_br(1),uz_br(1),ux_bl(1),uy_bl(1),uz_bl(1)
%16.8G %16.8G %16.8G %16.8G %16.8G %16.8G %16.8G %16.8G %16.8G %16.8G %16.8G %16.8G
/output
finish
```

Appendix E

Mesh Optimization of 3-D Solid Element Model

To control the area and volume refinement around the fillets, partitioning was used. The edge of the fillet volume extended to the location where the curved fillet surface contacts the flat surface of the neighboring volume (Figure 2.10(a)). This technique solved the element shape warnings that occurred as elements attempted to fill an infinitely small tangent contact surface. In addition, the areas associated with the fillet volumes were added together so the elements did not have to adhere to multiple area interfaces. The fillet surfaces were then selected, and all elements associated with these areas were refined. Figures 2.10(a) and 2.10(b) display a fillet at the shuttle-compliant arm intersection, while Figure 2.10(c) displays an example of a compliant leg-rigid leg fillet. The fillets at the compliant leg-anchor intersections were treated in the same manner as the fillets at the shuttle-compliant leg intersection. By using this method of mesh refinement, the challenge of creating a refined mesh at critical fillet locations while maintaining a coarse mesh at non-critical locations was addressed.

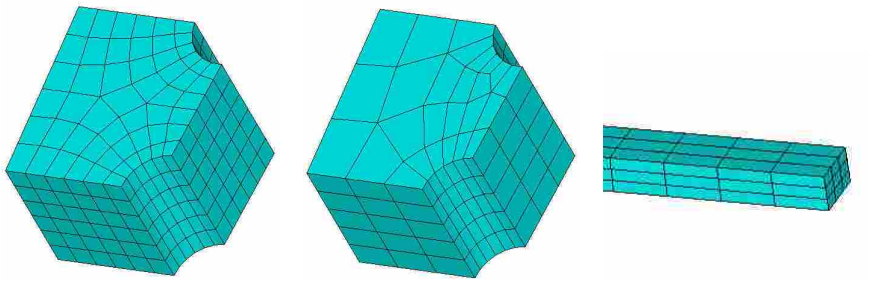

(a) (b) (c)

Figure E.1: Attempted hexahedral meshing of fillets and compliant arms.

An attempt was initially made to use the more reliable and accurate hexahedral shaped solid95 elements in the mesh. As an initial test, a fillet volume was meshed with the "sweep mesh" technique using two methods: six divisions on all edges (Figure E.1(a)), or three divisions on each straight edge and five divisions on each fillet edge (Figure E.1(b)). The compliant legs were meshed using a similar technique (Figure E.1(c)). However, it became apparent that the transition between tightly meshed fillet faces, moderately meshed volumes surrounding fillets, and loosely meshed compliant arms created poorly shaped elements in a critical region. Additionally, it is difficult to refine or improve hexahedral elements once they have been created, significantly limiting control over critical mesh regions such as the fillets. Thus, due to the anticipated poor element shape, and lack of tools for improving a hexahedral mesh, the tetrahedral shaped element was chosen to mesh this model.

Appendix F

Applied Forces: Displacements at the Front-side, Center-side, and Back-side Nodes

This appendix includes a portion of the results from testing the six applied force conditions while prescribing a displacement at the front-side, center-side, and back-side nodes. Table F.1 provides similar data to Table 6.2, but includes these additional results. It can be seen that the same general trends are found when displacement is applied at these nodes. The magnitude of applied force required for a Phenomenon 2 transition is much larger when forces are applied in the X-direction as compared to the Z-direction. Thus, it can be deduced that the FCBMs are less sensitive to X-direction accelerations during transition to the alternate stable position than when Z-direction accelerations are applied.

Some of the transition forces are not provided in Table F.1. This occurred when forces were applied to the back-center-top node. When this condition was analyzed, the model would not converge to a solution experiencing Phenomenon 2. The model would either produce Phenomenon 1 behavior, or not converge at all. In this case, the 3-D solid element model provides a hint that the system is not as well behaved when forces are applied at this location and direction.

Additionally, when the front-side node was displaced, the shape of the Phenomenon 1 and 2 force-displacement plots did not match the result when the back-center node was displaced. However, there still remained two distinct force-displacement shapes. Figure F.1 shows that the Phenomenon 1 force-displacement plot differs from what has been regularly seen. There are, however, similarities when comparing the characteristics of this plot to the traditional Phenomenon 1 plots. First, the largest peak reaction forces are associated with this phenomenon. Second, the plot is not linear. Finally, the plot does not shift or change magnitude significantly until a transition is made to the Phenomenon 2 characteristics. The largest difference is that the Phenomenon 1 plots are closer to being linear than any of the

Table F.1: F_{tr} magnitudes for Phenomenon 1 and 2 when displacing various nodes.

Displacement Location	*Force Location*	*Force Direction*	*Transition Force (F_{tr}) (g's)*
CENTER-SIDE	CENTER-TOP	-Z	$600 < F_{tr} \leq 700$
CENTER-SIDE	FRONT-CENTER-TOP	-Z	$550 < F_{tr} \leq 600$
CENTER-SIDE	BACK-CENTER-TOP	-Z	N/A
CENTER-SIDE	CENTER-SIDE	-X	$700{,}000 < F_{tr} \leq 750{,}000$
CENTER-SIDE	FRONT-SIDE	-X	$500{,}000 < F_{tr} \leq 550{,}000$
CENTER-SIDE	BACK-SIDE	-X	$550{,}000 < F_{tr} \leq 600{,}000$
FRONT-SIDE	CENTER-TOP	-Z	$350 < F_{tr} \leq 400$
FRONT-SIDE	FRONT-CENTER-TOP	-Z	$500 < F_{tr} \leq 600$
FRONT-SIDE	BACK-CENTER-TOP	-Z	$50 < F_{tr} \leq 75$
FRONT-SIDE	CENTER-SIDE	-X	$750{,}000 < F_{tr} \leq 850{,}000$
FRONT-SIDE	FRONT-SIDE	-X	$1{,}000{,}000 < F_{tr} \leq 1{,}250{,}000$
FRONT-SIDE	BACK-SIDE	-X	$600{,}000 < F_{tr} \leq 750{,}000$
BACK-SIDE	CENTER-TOP	-Z	$750 < F_{tr} \leq 775$
BACK-SIDE	FRONT-CENTER-TOP	-Z	$750 < F_{tr} \leq 775$
BACK-SIDE	BACK-CENTER-TOP	-Z	N/A
BACK-SIDE	CENTER-SIDE	-X	$1{,}000{,}000 < F_{tr} \leq 1{,}250{,}000$
BACK-SIDE	FRONT-SIDE	-X	$850{,}000 < F_{tr} \leq 900{,}000$
BACK-SIDE	BACK-SIDE	-X	$900{,}000 < F_{tr} \leq 950{,}000$

plots produced when displacement is applied at the back-center node, front-side node, or back-side node. The region near the peak reaction forces are also not smooth and rounded as before.

The Phenomenon 2 plot is similar to what has been seen before. The plot is linear, and the peak reaction forces decrease from the Phenomenon 1 values. The large difference in the two force-displacement shapes in Figure F.1 supports the fact that two distinct characteristics are present. Thus it was learned that Phenomenon 1 and Phenomenon 2 plots can generate different shapes, but still retain the same critical characteristics. Figure F.2 supports this idea as well.

Similar Phenomenon 1 characteristics are found when the back-side node is displaced, and forces are applied at the front-center-top, back-center-top, center-side, front-side, and back-side nodes. In these cases, however, the Phenomenon 2 plots sometimes generate a new characteristic. Figure F.3 shows that the magnitude of F_{max} is approximately the same in both phenomenon conditions. There is a spike in reaction force near

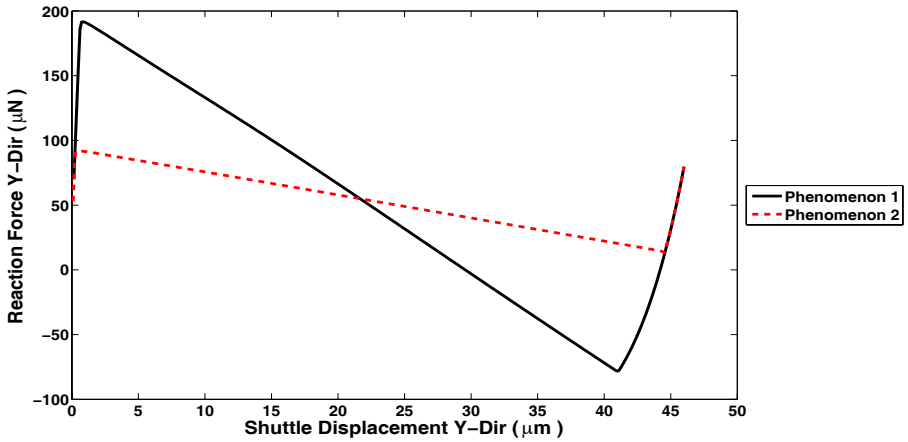

Figure F.1: Comparison of force-displacement plots when the front-side node was displaced, and a Z-direction off-axis force was applied to the center-top node.

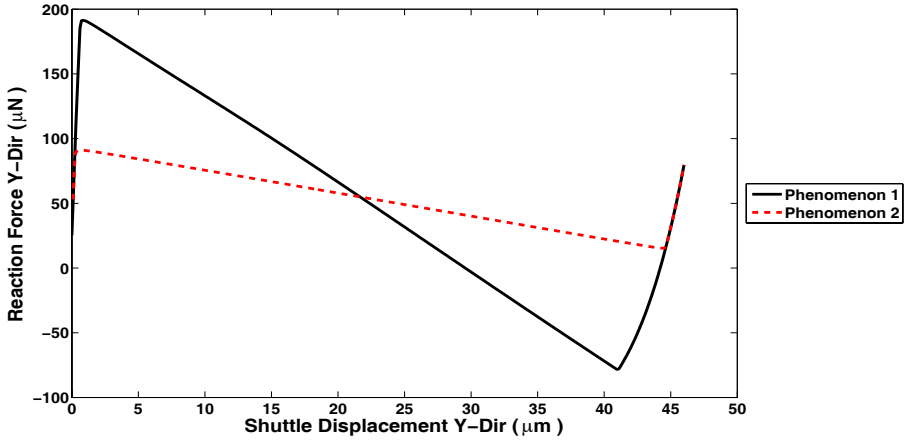

Figure F.2: Comparison of force-displacement plots when the front-side node was displaced, and a Z-direction off-axis force was applied to the front-center-top node.

F_{max} correlating with Phenomenon 2. Similar characteristics can be found in Figures F.4 and F.5.

Figure F.4 supports the idea that an unpredictable system will likely result if off-axis forces near F_{tr} are applied. In this case, an application of 750,000 and 1,000,000 g's both produce a Phenomenon 1 plot. In contrast, applying 850,000 g's to the FCBM produced a Phenomenon 2 plot. Usually, once the Phenomenon 2 plot has been produced, larger applied forces will continue to generate Phenomenon 2 results. This is not the case

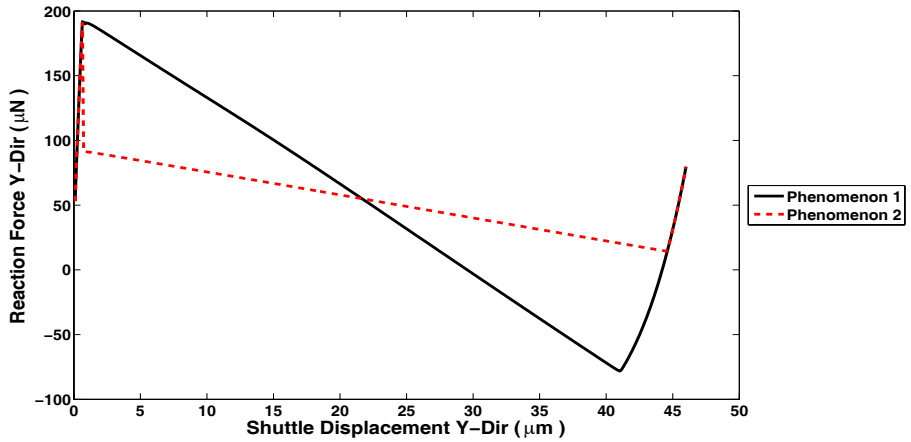

Figure F.3: Comparison of force-displacement plots when the front-side node was displaced, and a Z-direction off-axis force was applied to the back-center-top node.

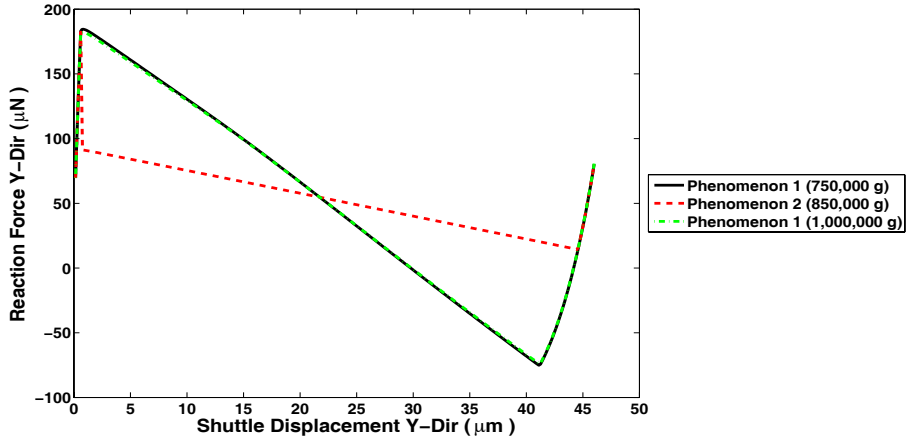

Figure F.4: Comparison of force-displacement plots when the front-side node was displaced, and a X-direction off-axis force was applied to the center-side node.

in this example. Since the applied forces were near the transition magnitude, the force-displacement plot is capable of producing either of the phenomenon shapes.

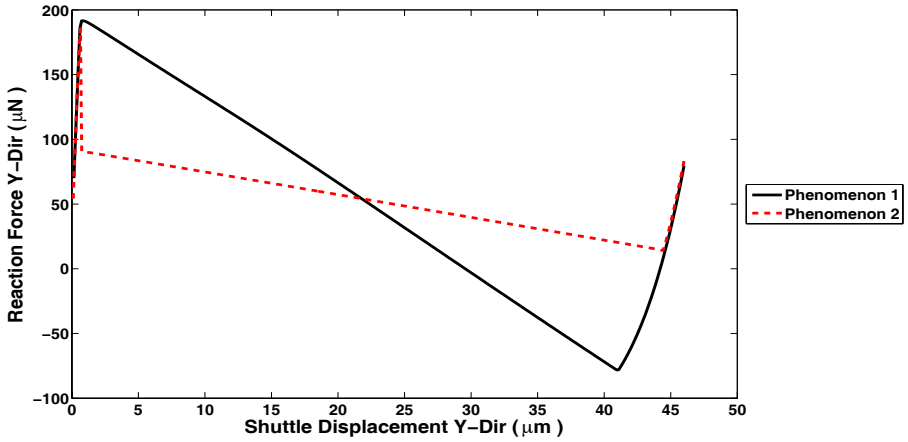

Figure F.5: Comparison of force-displacement plots when the front-side node was displaced, and a X-direction off-axis force was applied to the front-side node.

Appendix G

Bistable-A and Bistable-B Comparison

The results provided were generated by the 3-D solid element model, and the Bistable-B dimensions were used as the model design. The results from displacing the back-center node while applying a Z-direction force to the center-top node were used for comparison. The two figures provided display the results when a force of 500 and 900 g's was applied. The applied forces were increased in the same manner as they were in the Bistable-A model test suite.

Figure G.1 shows that many of the Bistable-A trends are repeated in the Bistable-B model. Most importantly, the Phenomenon 1 and 2 characteristics exist in the Bistable-B model. The magnitude of applied force required for a Phenomenon 2 transition changed, but this can be expected since the geometries of the two FCBMs are different. Figure G.2 shows that at higher applied forces, the trends of the two models were very similar. One important difference between the two models is that the pitch rotation trend did not always hold true. The Bistable-B model did not generate large pitch rotations when Phenomenon 1 occurred as expected. The pitch rotation was consistently near zero no matter what magnitude of force was applied. This discrepancy could be due to the geometry differences between the two models. The most important point of this comparison was to verify that the general trends discussed in the main text were not unique to the Bistable-A model. Though the trends associated with an FCBM are geometry dependent, this was accomplished.

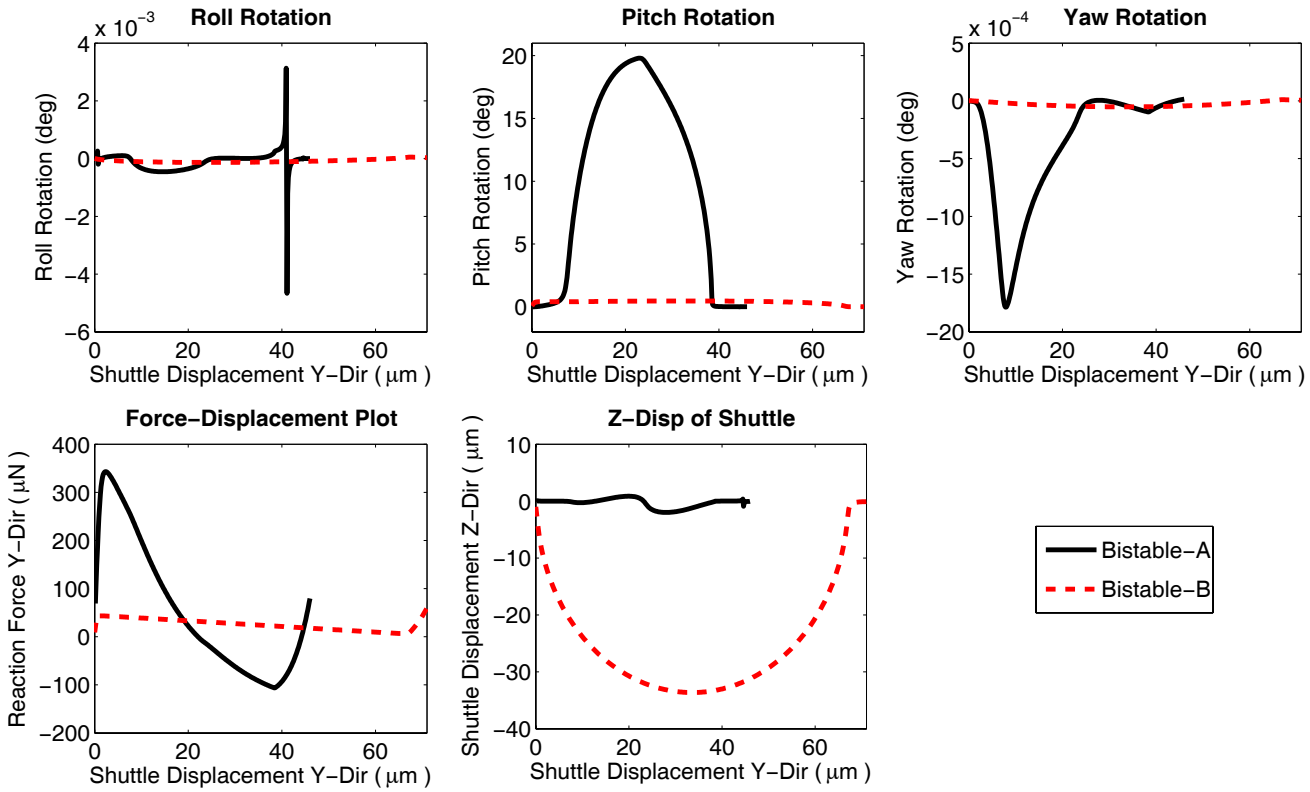

Figure G.1: Comparison of the Bistable-A and Bistable-B models when displacing the back-center node, while applying a 500 g Z-direction off-axis force to the center-top node.

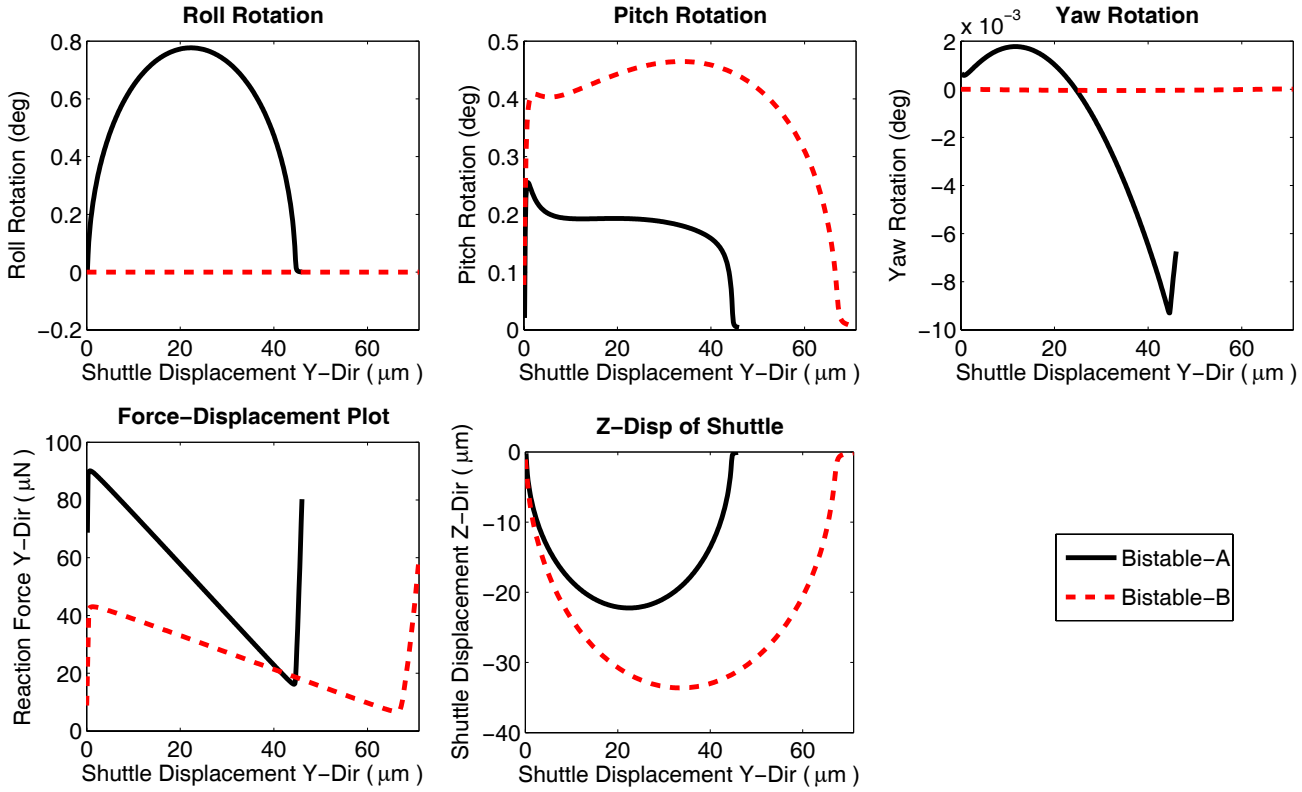

Figure G.2: Comparison of the Bistable-A and Bistable-B models when displacing the back-center node, while applying a 900 g Z-direction off-axis force to the center-top node.

Appendix H

Additional Plots

The experimental data for Figures H.1 through H.3 are from data collected during earlier research [1], [2].

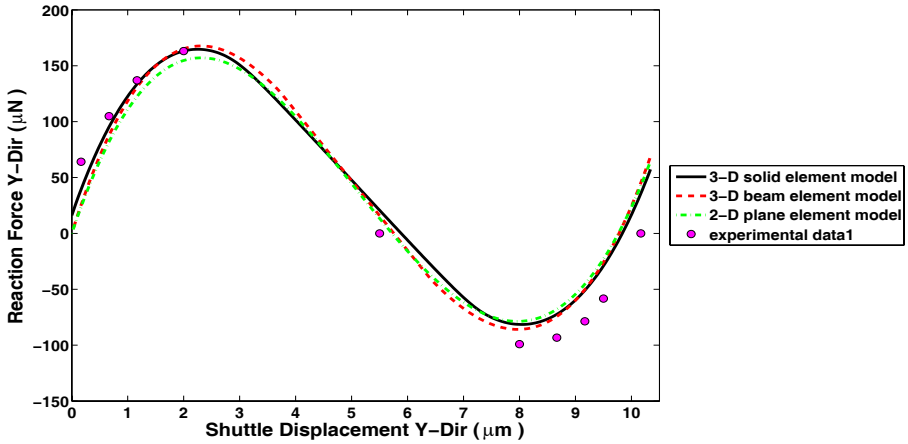

Figure H.1: Model comparison to experimental SUMMiT V data (set #1) for validation.

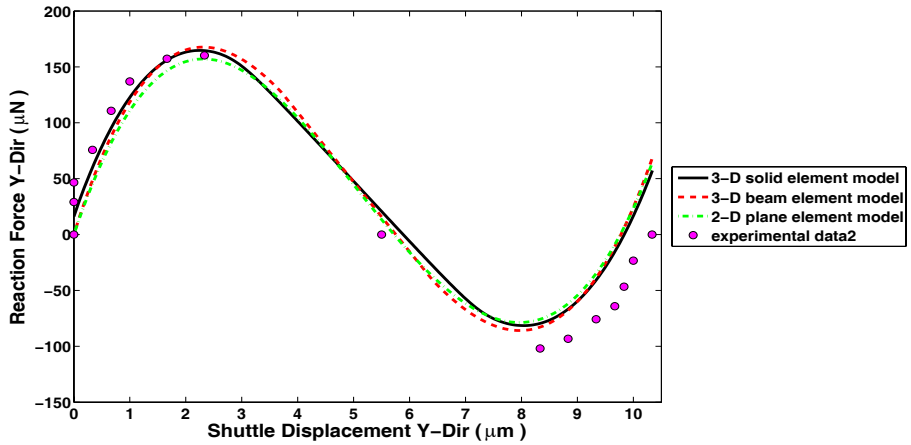

Figure H.2: Model comparison to experimental SUMMiT V data (set #2) for validation.

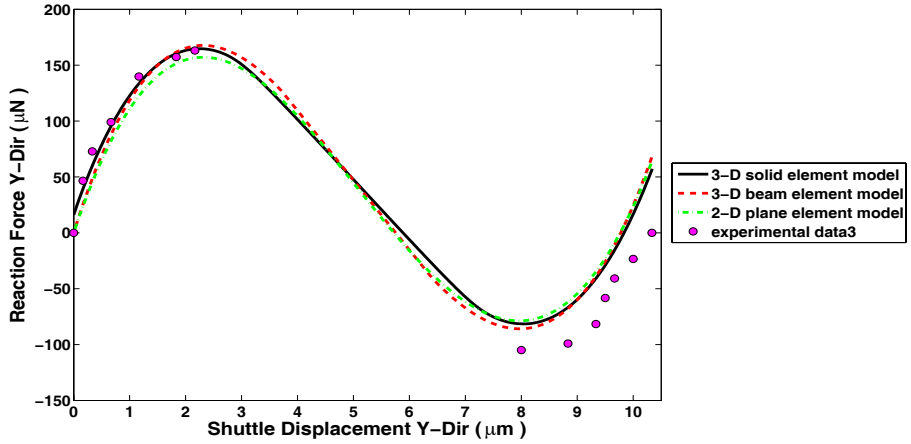

Figure H.3: Model comparison to experimental SUMMiT V data (set #3) for validation.

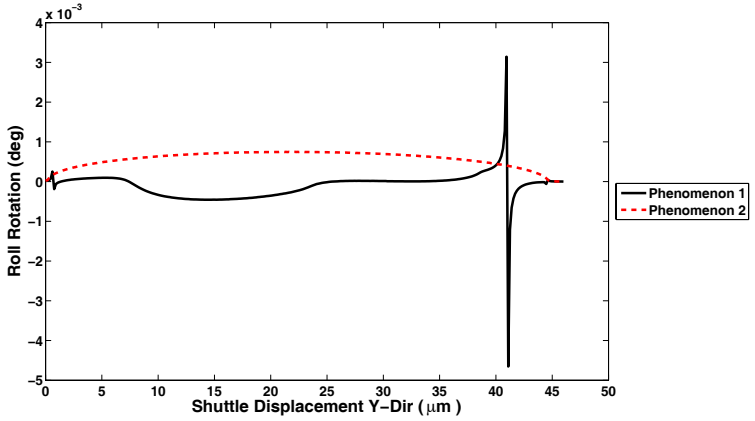

(a) Roll Rotation

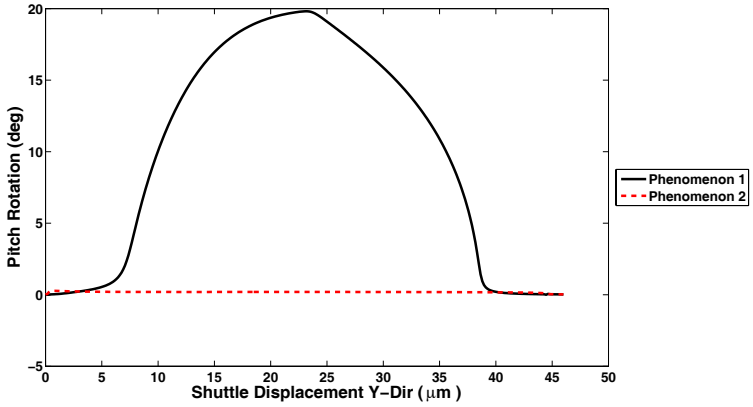

(b) Pitch Rotation

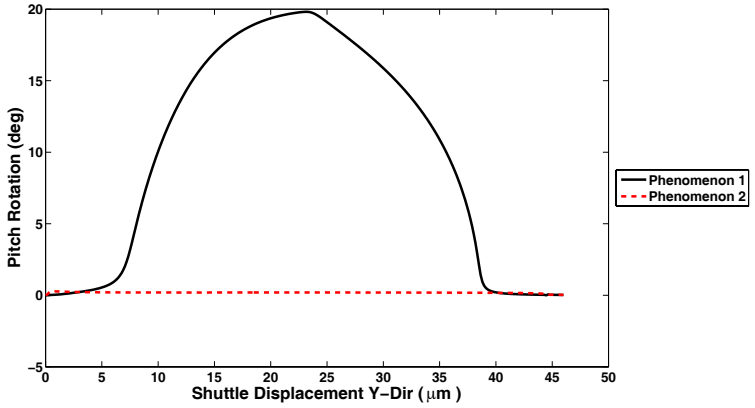

(c) Yaw Rotation

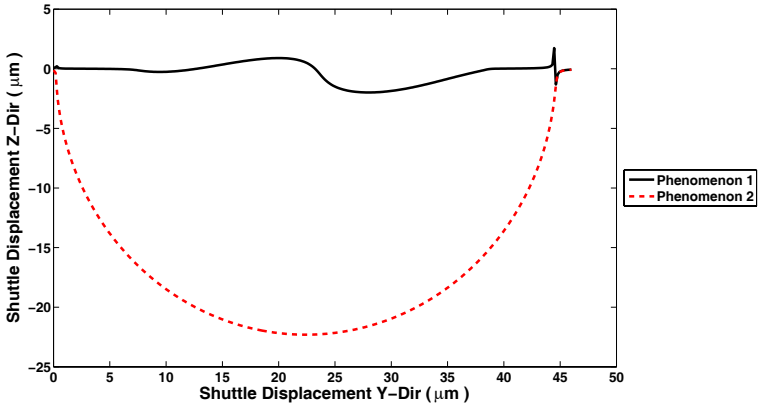

(d) Z-Disp of Shuttle

Figure H.4: The rotation and Z-displacement results when the back-center node was displaced, and a Z-direction off-axis force was applied to the front-center-top node.

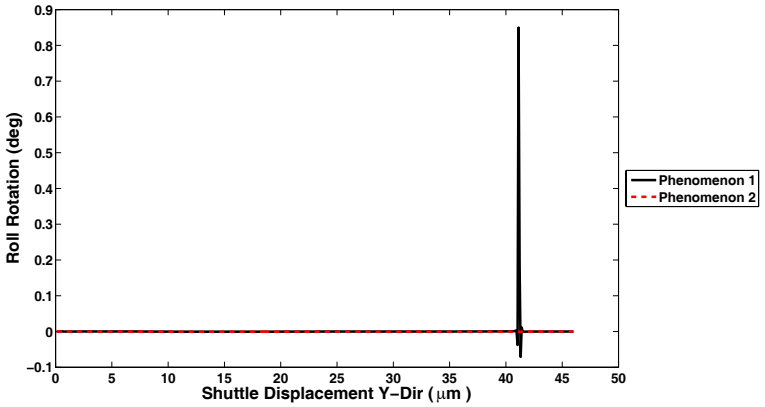

(a) Roll Rotation

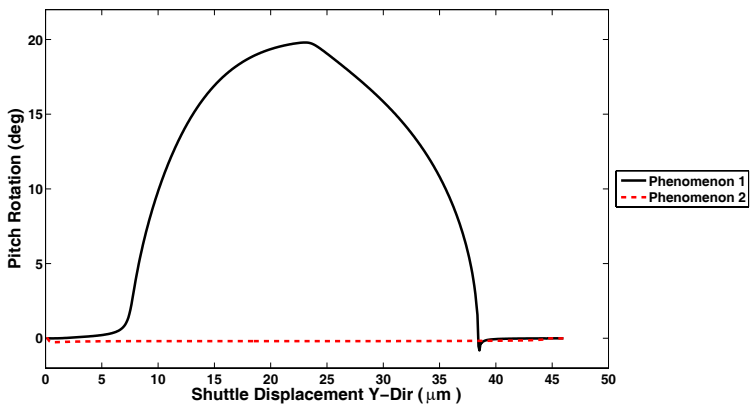

(b) Pitch Rotation

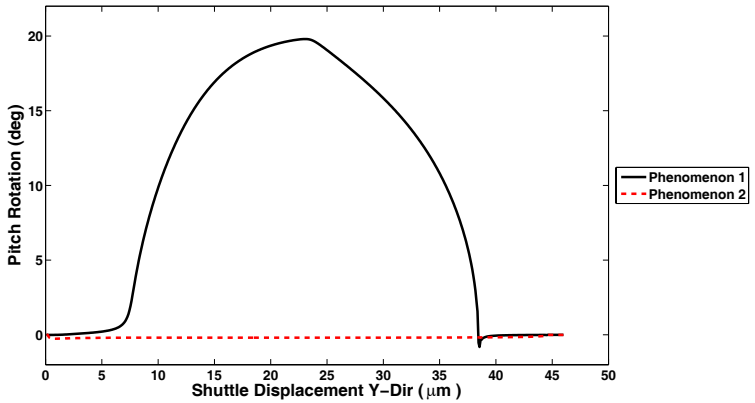

(c) Yaw Rotation

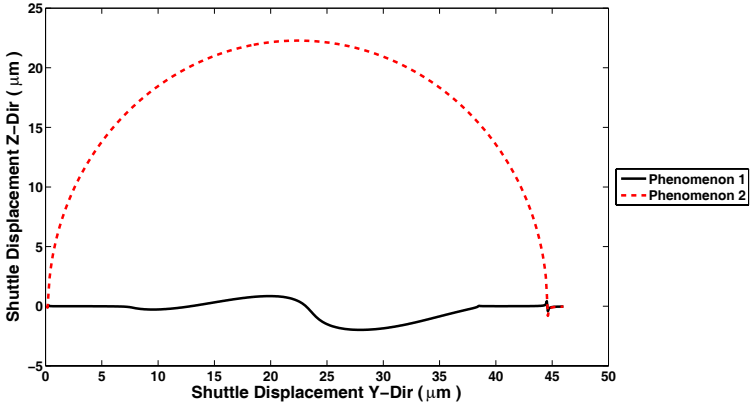

(d) Z-Disp of Shuttle

Figure H.5: The rotation and Z-displacement results when the back-center node was displaced, and a Z-direction off-axis force was applied to the back-center-top node.

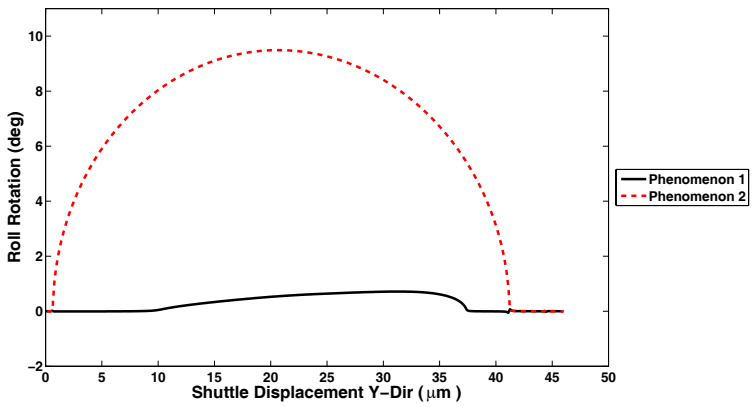

(a) Roll Rotation

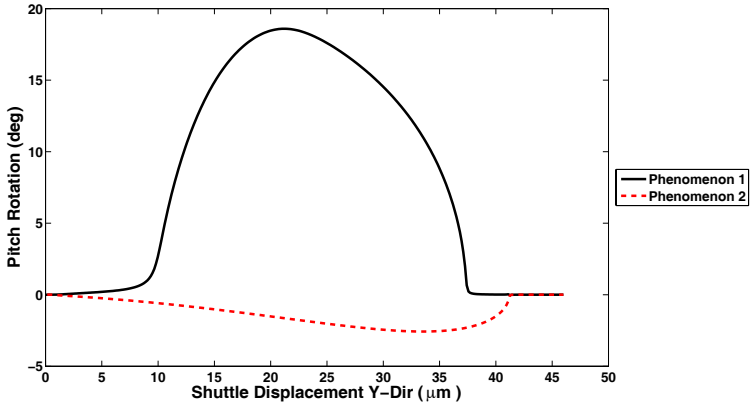

(b) Pitch Rotation

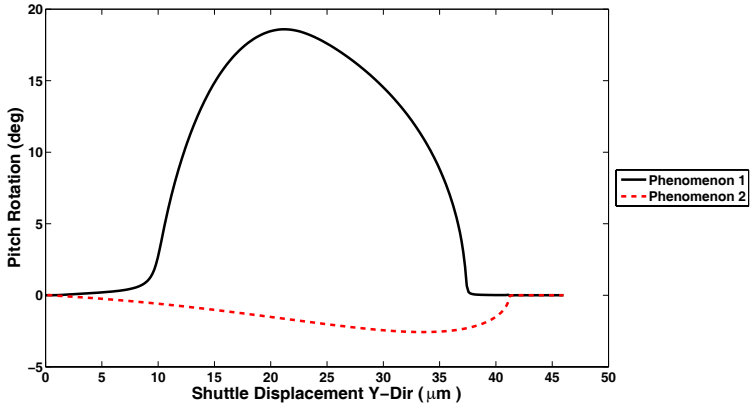

(c) Yaw Rotation

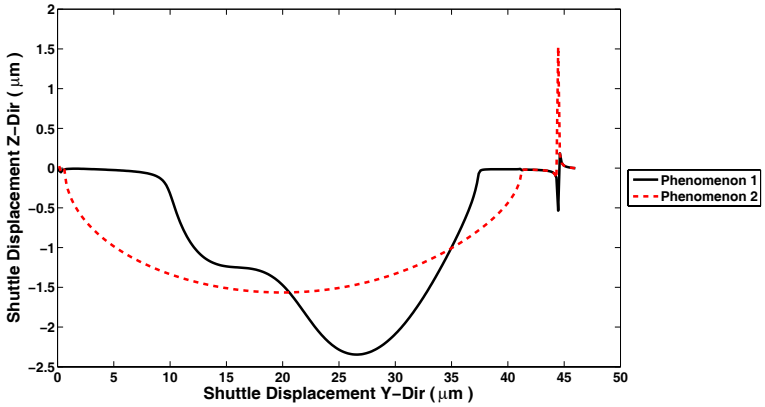

(d) Z-Disp of Shuttle

Figure H.6: The rotation and Z-displacement results when the back-center node was displaced, and a Z-direction off-axis force was applied to the front-side node.

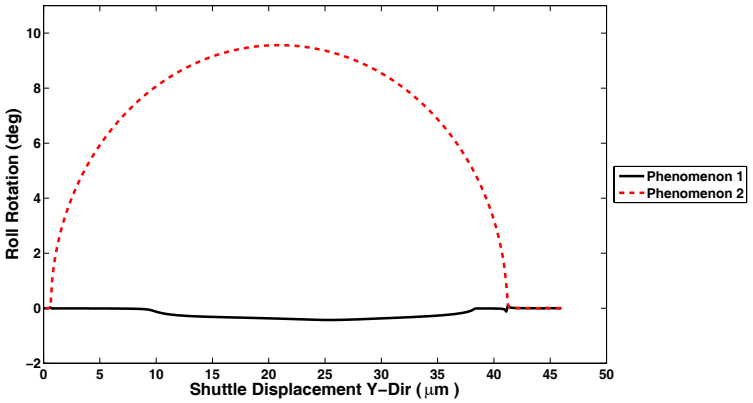

(a) Roll Rotation

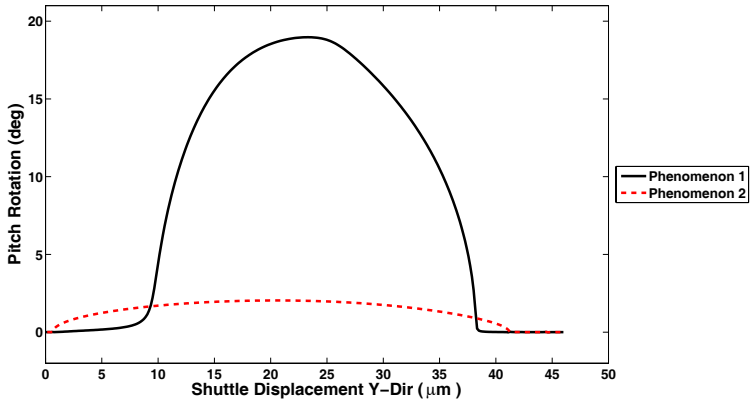

(b) Pitch Rotation

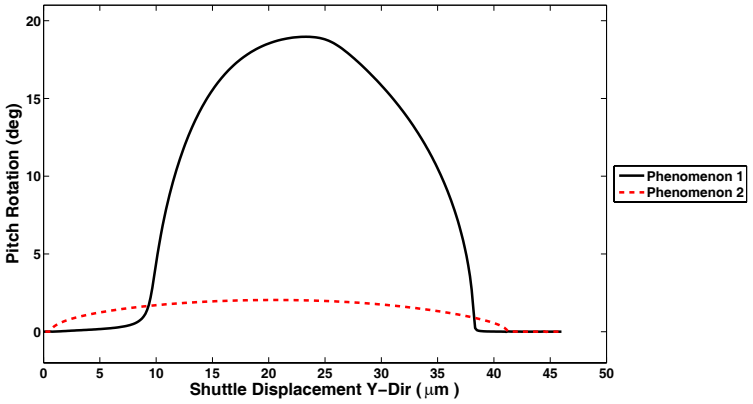

(c) Yaw Rotation

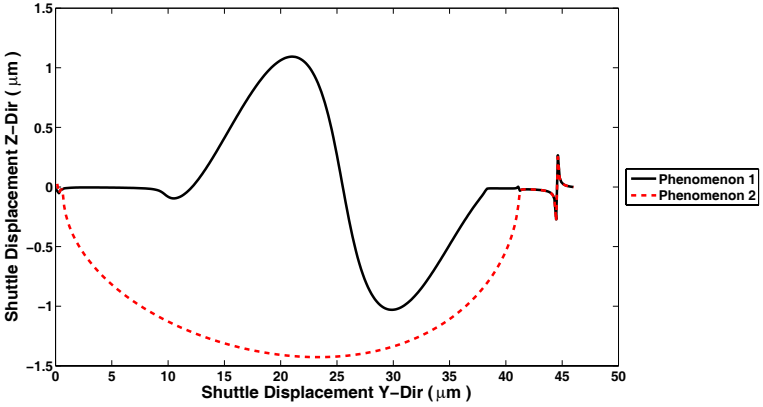

(d) Z-Disp of Shuttle

Figure H.7: The rotation and Z-displacement results when the back-center node was displaced, and a X-direction off-axis force was applied to the back-side node.

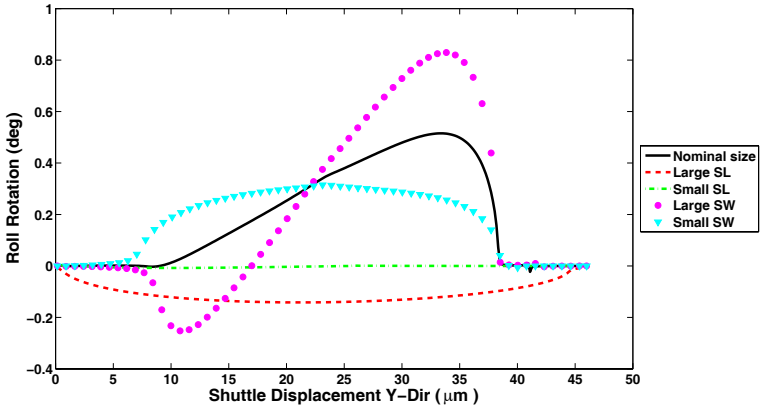

(a) Roll Rotation

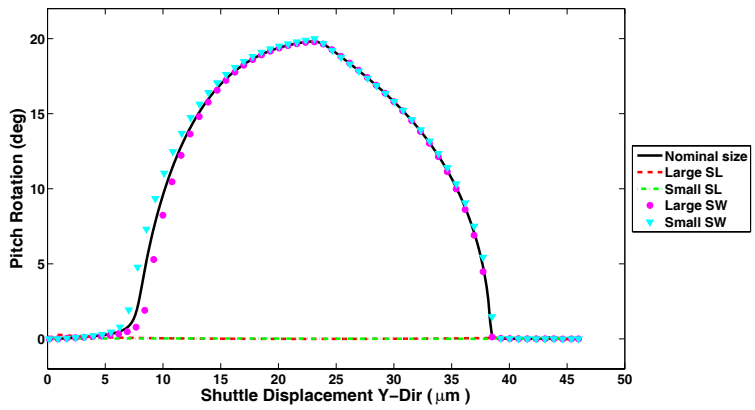

(b) Pitch Rotation

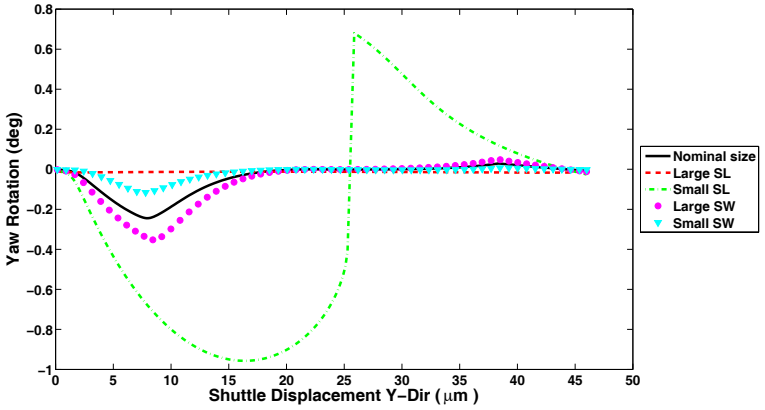

(c) Yaw Rotation

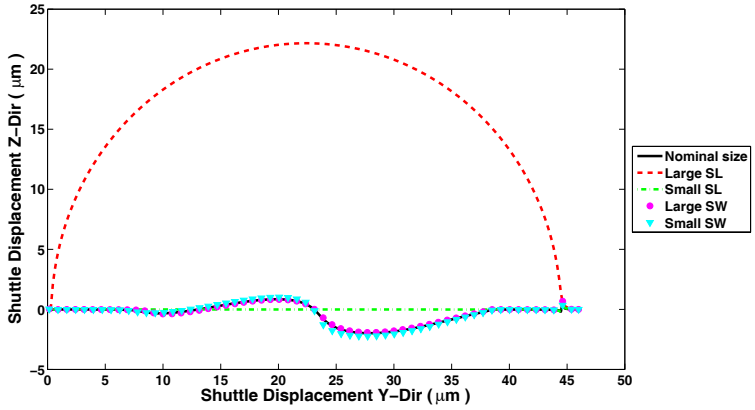

(d) Z-Disp of Shuttle

Figure H.8: The rotation and Z-displacement results generated by various shuttle designs when the back-side node was displaced, and no off-axis force was applied.

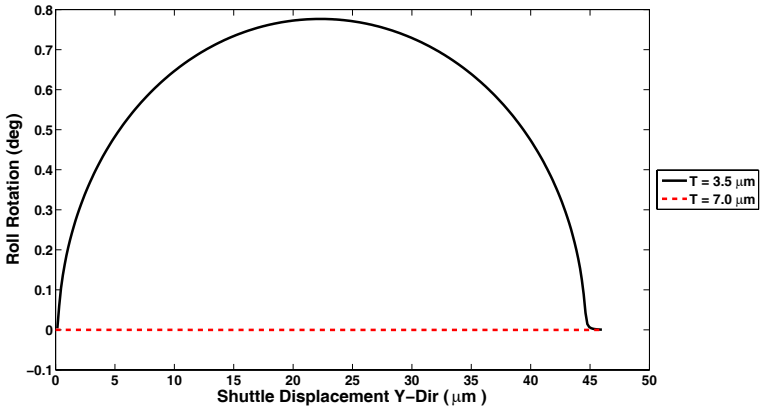

(a) Roll Rotation

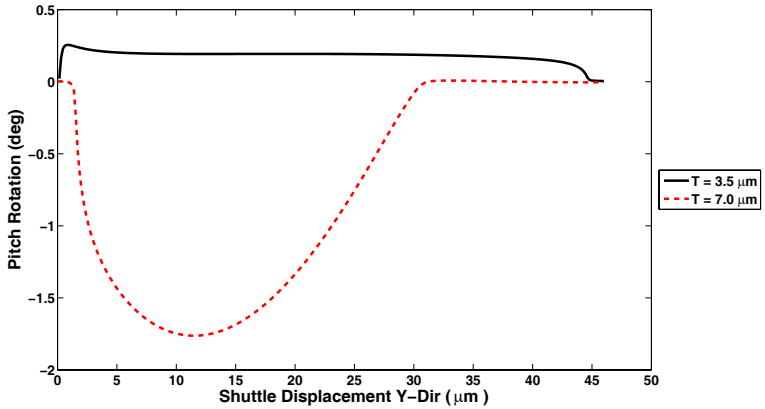

(b) Pitch Rotation

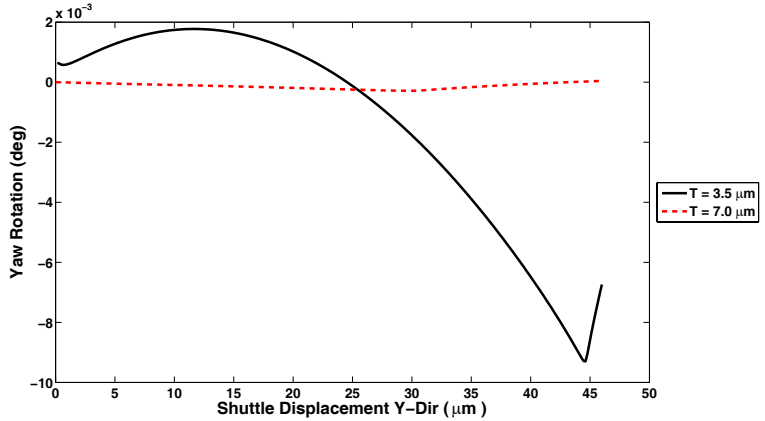

(c) Yaw Rotation

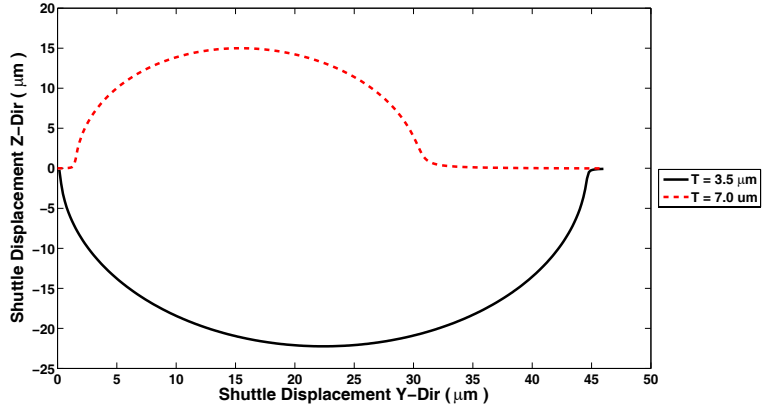

(d) Z-Disp of Shuttle

Figure H.9: The results of increasing the thickness of the FCBM when the back-center node was displaced, and a 900 g Z-direction off-axis force was applied to the center-top node.

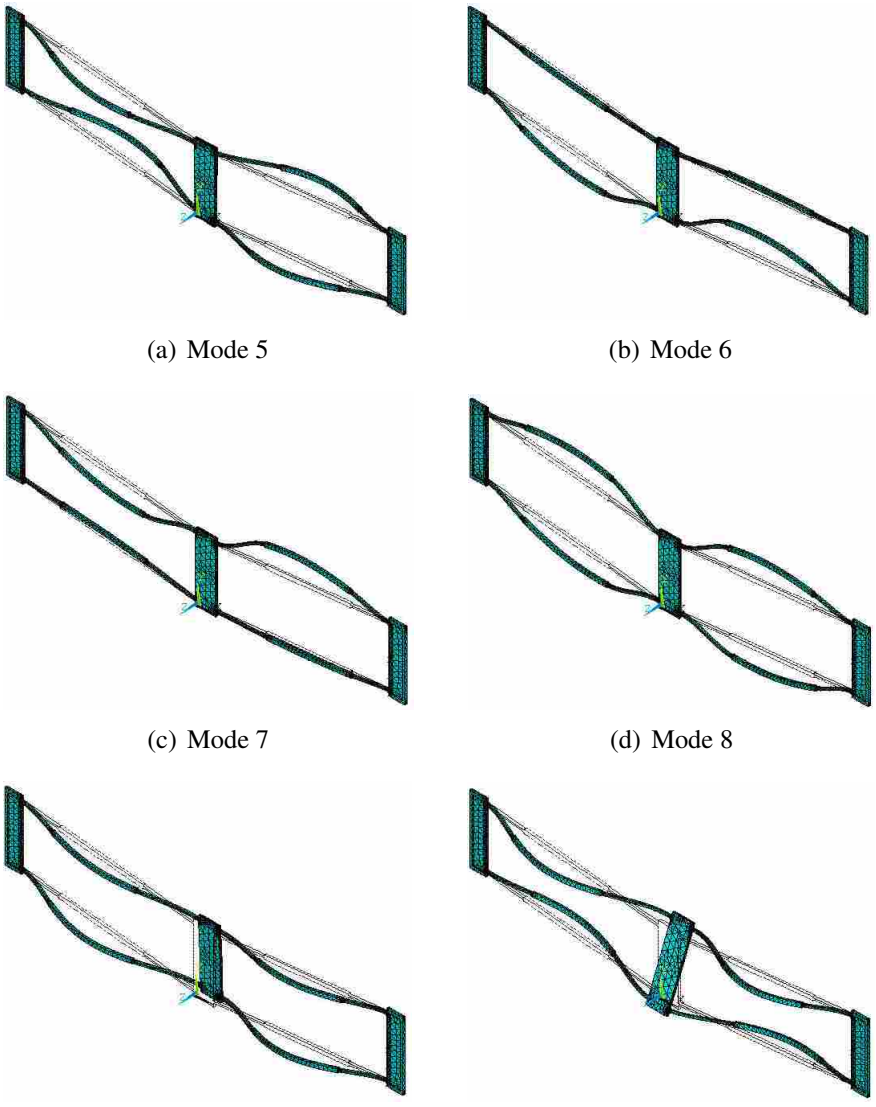

(a) Mode 5 (b) Mode 6

(c) Mode 7 (d) Mode 8

(e) Mode 9 (f) Mode 10

Figure H.10: Mode shapes 5 through 10 of the Bistable-A model.

Appendix I

Definition Connection to ANSYS Code and Archived Research

The definitions used in this paper have been simplified for the general audience. If future appended research is to be conducted, this appendix will assist with understanding the variable names as they are used in the ANSYS batch files and Matlab code. Table I.1 lists the variable definitions as they are presented in this thesis, and the variable name as they are used in ANSYS and the archived research.

Table I.1: Definition Conversions

Variable Definition in Thesis	*Variable Definition in ANSYS Batch Files*
BISTABLE-A	BISTABLE-01
BISTABLE-B	BISTABLE-14
BACK-CENTER NODE	BACKNODE
FRONT-CENTER NODE	FACENODE
CENTER-TOP NODE	NODE 2
FRONT-CENTER-TOP NODE	NODE 3
BACK-CENTER-TOP NODE	NODE 5
CENTER-SIDE NODE	NODE 9
FRONT-SIDE NODE	NODE 11
BACK-SIDE NODE	NODE 12
BACK-SIDE-L NODE	TL NODE
BACK-SIDE NODE	TR NODE
FRONT-SIDE-L NODE	BL NODE
FRONT-SIDE NODE	BR NODE
g	“forcegrav”

References

[1] J. Wittwer, "Simulation Based Design Under Uncertainty For Compliant Microelectromechanical Systems," Ph.D. dissertation, Brigham Young University, 2005.

[2] J. W. Wittwer, M. S. Baker, and L. L. Howell, "Robust Design and Model Validation of Nonlinear Compliant Micromechanisms," *Journal of Microelectromechanical Systems*, vol. 15, no. 1, pp. 33 – 41, 2006. [Online]. Available: http://dx.doi.org/10.1109/JMEMS.2005.859190

[3] D. Hyman and M. Mehregany, "Contact Physics of Gold Microcontacts for MEMS Switches," *IEEE Transactions on Components and Packaging Technologies*, vol. 22, no. 3, pp. 357 – 364, 1999. [Online]. Available: http://dx.doi.org/10.1109/6144.796533

[4] J. Qiu, J. Lang, A. Slocum, and C. MIT, "A Centrally-Clamped Parallel-Beam Bistable MEMS Mechanism," *The 14th IEEE International Conference on Micro Electro Mechanical Systems*, pp. 353–356, 2001.

[5] J. Qiu, "An Electrothermally-Actuated Bistable MEMS Relay for Power Applications," Ph.D. dissertation, Massachusetts Institute of Technology, 2003.

[6] T. Gomm, L. L. Howell, and R. H. Selfridge, "In-Plane Linear Displacement Bistable Microrelay," *Journal of Micromechanics and Microengineering*, vol. 12, no. 3, pp. 257 – 264, 2002. [Online]. Available: http://dx.doi.org/10.1088/0960-1317/12/3/310

[7] R. Luharuka and P. J. Hesketh, "Design of Fully Compliant, In-Plane Rotary, Bistable Micromechanisms for MEMS Applications," *Sensors and Actuators, A: Physical*, vol. 134, no. 1, pp. 231 – 238, 2007. [Online]. Available: http://dx.doi.org/10.1016/j.sna.2006.04.030

[8] U. Sonmez, "Compliant MEMS Crash Sensor Designs: The Preliminary Simulation Results," *Intelligent Vehicles Symposium*, pp. 303–308, 2007.

[9] I.-H. Hwang, Y.-S. Shim, and J.-H. Lee, "Modeling and Experimental Characterization of the Chevron-Type Bi-Stable Microactuator," *Journal of Micromechanics and Microengineering*, vol. 13, no. 6, pp. 948 – 954, 2003. [Online]. Available: http://dx.doi.org/10.1088/0960-1317/13/6/318

[10] J. Tsay, L.-Q. Su, and C.-K. Sung, "Design of a Linear Micro-Feeding System Featuring Bistable Mechanisms," *Journal of Micromechanics and Microengineering*, vol. 15, no. 1, pp. 63 – 70, 2005. [Online]. Available: http://dx.doi.org/10.1088/0960-1317/15/1/010

[11] J. K. Anderson, "Piezoresistive Sensing of Bistable Micro Mechanism State," Master's thesis, Brigham Young University, Provo, 2005.

[12] B. D. Jensen, M. B. Parkinson, K. Kurabayashi, L. L. Howell, and M. S. Baker, "Design Optimization of a Fully-Compliant Bistable Micro-Mechanism," vol. 2, New York, NY, United States, 2001, pp. 2931 – 2937.

[13] J. K. Anderson, L. L. Howell, J. W. Wittwer, and T. W. McLain, "Piezoresistive Sensing of Bistable Micro Mechanism State," *Journal of Micromechanics and Microengineering*, vol. 16, no. 5, pp. 943 – 950, 2006. [Online]. Available: http://dx.doi.org/10.1088/0960-1317/16/5/010

[14] H. Coleman, W. Steele *et al.*, *Experimentation and Uncertainty Analysis for Engineers*. Wiley-IEEE, 1999.

[15] A. Haldar and S. Mahadevan, *Reliability Assessment Using Stochastic Finite Element Analysis*. John Wiley & Sons New York, 2000.

[16] ——, *Probability, Reliability, and Statistical Methods in Engineering Design*. Wiley, 2000.

[17] W. Kuo *et al.*, *Optimal Reliability Design: Fundamentals and Applications*. Cambridge University Press, 2000.

[18] A. Parkinson, C. Sorensen, and N. Pourhassan, "General Approach for Robust Optimal Design," *Journal of Mechanical Design, Transactions Of the ASME*, vol. 115, no. 1, pp. 74 – 80, 1993.

[19] A. Saltelli, K. Chan, and E. Scott, *Sensitivity Analysis*. Wiley, 2000.

[20] J. Wittwer, L. Howell, S. Wait, and M. Cherry, "Predicting the Performance of a Bistable Micro Mechanism Using Design-Stage Uncertainty Analysis," *Proceedings of IMECE 2002, ASME International Mechanical Engineering Congress & Exposition*, pp. 17–22, 2002.

[21] C. Liu, *Foundations of MEMS*. Pearson/Prentice Hall, 2006.

[22] H. Fujita, "A Decade of MEMS and its Future," *Micro Electro Mechanical Systems*, vol. MEMS'97, Proceedings, IEEE.,, pp. 1–7, 1997.

[23] L. Howell, *Compliant Mechanisms*. Wiley-IEEE, 2001.

[24] C.-Y. Chong and S. P. Kumar, "Sensor Networks: Evolution, Opportunities, and Challenges," *Proceedings of the IEEE*, vol. 91, no. 8, pp. 1247 – 1256, 2003. [Online]. Available: http://dx.doi.org/10.1109/JPROC.2003.814918

[25] O. Port, "Ideas for the 21st Century," *Business Week*, vol. 30, pp. 78–167, 1999.

[26] D. L. Wilcox and L. L. Howell, "Fully Compliant Tensural Bistable Micromechanisms (FTBM)," *Journal of Microelectromechanical Systems*, vol. 14, no. 6, pp. 1223 – 1235, 2005. [Online]. Available: http://dx.doi.org/10.1109/JMEMS.2005.859089

[27] D. D. Wentzloff, B. H. Calhoun, R. Min, A. Wang, N. Ickes, and A. P. Chandrakasan, "Design Considerations for Next Generation Wireless Power-Aware Microsensor Nodes," vol. 17, Mumbai, India, 2004, pp. 361 – 367.

[28] A. Chandrakasan, R. Min, M. Bhardwaj, S. Cho, and A. Wang, "Power Aware Wireless Microsensor Systems," *Solid-State Device Research Conference*, pp. 37–44, Proceeding of the 32nd European, 2002.

[29] P. B. Koeneman, I. J. Busch-Vishniac, and K. L. Wood, "Feasibility of Micro Power Supplies for MEMS," *Journal of Microelectromechanical Systems*, vol. 6, no. 4, pp. 355 – 362, 1997. [Online]. Available: http://dx.doi.org/10.1109/84.650133

[30] iMEMS, "Analog Devices: iMEMS Accelerometers," http://www.analog.com/en/subCat/0,2879,764%255F800%255F0%255F%255F0%255F,00.html, 2007.

[31] *PolyMUMPs Design Handbook*, MEMSCAP Inc., 2005. [Online]. Available: www.memsrus.com/documents/PolyMUMPs.DR.v11.pdf

[32] R. Johnstone, D. Sameoto, and M. Parameswaran, "Non-Uniform Residual Stresses for Parallel Assembly of Out-of-Plane Surface-Micromachined Structures," *Journal of Micromechanics and Microengineering*, vol. 16, no. 11, pp. 17–22 –, 2006. [Online]. Available: http://dx.doi.org/10.1088/0960-1317/16/11/N01

[33] J.-N. Kuo, G.-B. Lee, and W.-F. Pan, "Stress-Induced Bending of Micromachined Bilayer Cantilever and its Optical Application," Shenyang, China, 2004, pp. 290 – 295.

[34] J. Wittwer and L. Howell, "Mitigating the Effects of Local Flexibility at the Built-In Ends of Cantilever Beams," *Journal of Applied Mechanics*, vol. 71, p. 748, 2004.

[35] *SUMMiT V - Five Level Surface Micromachining Technology Design Manual*, 1st ed., MEMS Device and Reliability Physics Department, Microelectronics Development Laboratory, Sandia National Laboratories, P.O. Box 5800, Albuquerque, NM 87185, 22 September 2005. [Online]. Available: www.sandia.gov/mstc/education/alliance/tools/SUMMiT_V_Dmanual_V1.3_MASTER_external.pdf

[36] J. W. Wittwer, T. Gomm, and L. L. Howell, "Surface Micromachined Force Gauges: Uncertainty and Reliability," *Journal of Micromechanics and Microengineering*, vol. 12, no. 1, pp. 13 – 20, 2002. [Online]. Available: http://dx.doi.org/10.1088/0960-1317/12/1/303